POLITECNICO
MILANO 1863

SCUOLA DI INGEGNERIA INDUSTRIALE
E DELL'INFORMAZIONE

Surface Functionalization for Electrical Detection of DNA

Tesi di Laurea Magistrale in
Materials Engineering and Nanotechnology -
Ingegneria dei Materiali e delle Nanotecnologie

Author: **Christian Fertitta**

Student ID: 996055
Advisor: Prof. Luca Magagnin
Co-advisor: Lillo Raia
Academic Year: 2023-24

Alla mia famiglia e agli amici di sempre.

Abstract

The rapid expansion of the biosensor market, particularly for DNA-based sensors, has driven significant advancements in developing platforms capable of highly specific and sensitive genetic material detection. This thesis focuses on the surface functionalization of silicon dioxide (SiO_2) using glycidyloxypropyltrimethoxysilane (GOPS) to create a stable interface for the subsequent grafting of oligonucleotides. Surface functionalization was performed using two silanization methods: Liquid Phase Deposition (LPD) and Vapor Phase Deposition (VPD). Characterization revealed that VPD outperformed LPD in terms of silane density, homogeneity, and functional group orientation. Contact angle measurements indicated higher values for VPD, suggesting a more effective silanization process. Among the solvents tested for LPD, toluene yielded the best results, achieving contact angles comparable to VPD. Both Atomic Force Microscopy (AFM) and Time-of-Flight Secondary Ion Mass Spectrometry (TOF-SIMS) analyses confirmed successful silanization, with VPD demonstrating superior performance. For DNA grafting, optimal conditions were identified by adjusting process parameters and pH. Fluorescence measurements validated successful oligonucleotide attachment. These results indicate that GOPS-functionalized SiO_2 surfaces are suitable for oligonucleotide grafting, paving the way for the development of a Solid-Phase Polymerase Chain Reaction (SP-PCR) sensor with potential applications in clinical diagnostics and environmental monitoring.

Keywords: GOPS, silanization, surface functionalization, grafting, biosensor

Abstract in lingua italiana

La rapida espansione del mercato dei biosensori, in particolare per i sensori basati sul DNA, ha guidato significativi progressi nello sviluppo di piattaforme capaci di rilevare materiale genetico con alta specificità e sensibilità. Questa tesi si concentra sulla funzionalizzazione superficiale del biossido di silicio (SiO_2) utilizzando il glicidiossipropiltrimetossisilano (GOPS) per creare un'interfaccia stabile per il successivo innesto di oligonucleotidi. La funzionalizzazione superficiale è stata eseguita utilizzando due metodi di silanizzazione: deposizione in fase liquida (LPD) e deposizione in fase vapore (VPD). La caratterizzazione ha rivelato che la VPD ha superato la LPD in termini di densità del silano, omogeneità e orientamento dei gruppi funzionali. Le misurazioni dell'angolo di contatto hanno indicato valori più alti per la VPD rispetto alla LPD, suggerendo un processo di silanizzazione più efficace. Tra i solventi testati per la LPD, il toluene ha dato i migliori risultati, raggiungendo angoli di contatto comparabili a quelli della VPD. Sia la Microscopia a Forza Atomica (AFM) che la Spettrometria di Massa a Tempo di Volo con Ioni Secondari (TOF-SIMS) hanno confermato la riuscita della silanizzazione, con la VPD che ha dimostrato una densità e omogeneità del silano superiori, oltre a un profilo chimico più favorevole dei frammenti ionici superficiali. Per l'innesto del DNA, sono state testate varie miscele e le condizioni ottimali sono state identificate regolando i parametri del processo e il pH della miscela di DNA. Le misurazioni della fluorescenza hanno confermato il successo dell'attacco degli oligonucleotidi. Questi risultati indicano che le superfici di SiO_2 funzionalizzate con GOPS sono altamente efficaci per l'innesto di oligonucleotidi, aprendo la strada allo sviluppo di un sensore per la Reazione a Catena della Polimerasi in Fase Solida (SP-PCR) con potenziali applicazioni nella diagnostica clinica e nel monitoraggio ambientale, offrendo una sensibilità e specificità migliorate nel rilevamento del materiale genetico.

Parole chiave: GOPS, silanizzazione, funzionalizzazione di superfici, grafting, biosensori

Contents

Introduction

Background and motivations

The development of advanced biosensors has gained substantial interest in recent years due to their potential applications in diagnostics, environmental monitoring, and biotechnology. Among these, DNA-based sensors are particularly valuable for their ability to provide highly specific and sensitive detection of genetic material, which is critical for various applications, including medical diagnostics and forensic analysis. The market for DNA-based biosensors is expanding rapidly, driven by the increasing demand for personalized medicine, early disease detection, and point-of-care testing. These devices are poised to revolutionize how we approach diagnostics, offering faster, more accurate, and more accessible options compared to traditional laboratory methods.

One promising approach in this field involves the surface functionalization of silicon dioxide (SiO_2), a widely used material in microelectronics and sensor platforms, with organosilane molecules like glycidyloxypropyltrimethoxysilane (GOPS). This functionalization forms a robust interface for the subsequent grafting of biomolecules, such as oligonucleotides, onto the surface. The immobilization of oligonucleotides is a crucial step in developing DNA sensors, as it enables the surface to interact specifically with target DNA sequences, facilitating detection through hybridization.

In particular, this research, conducted during my internship at the Silicon Biotech lab in STMicroelectronics, contributes to the development of a Solid-Phase Polymerase Chain Reaction (SP-PCR) sensor, capable of detecting grafted DNA through subsequent hybridization events. Such a sensor would not only enhance the sensitivity and specificity of DNA detection but also streamline the process, offering a practical solution for the growing demand in the biosensor market. The future implications of this research are significant, as the successful development of a reliable and efficient DNA sensor could pave the way for widespread adoption in clinical and environmental settings. This would mark a significant advancement in the field of molecular diagnostics, with the potential to impact various industries and improve public health outcomes globally.

Aim of the thesis

The primary aim of this thesis is to develop and optimize a protocol for the surface functionalization of silicon dioxide (SiO_2) using glycidyloxypropyltrimethoxysilane (GOPS) to facilitate the effective grafting of oligonucleotides, with the ultimate goal of creating a reliable platform for DNA-based biosensing.

To achieve this, the research begins with the development of a silanization protocol for GOPS, which involves evaluating the efficiency of various cleaning treatments and activation methods for the SiO_2 surface. Ensuring that the surface is properly prepared is crucial for successful silanization, as it directly affects the uniformity and density of the silane layer. Two silanization methods, LPD and VPD, were explored and optimized. For LPD, experiments were conducted to assess the effects of silanization time, annealing, concentration of the silane solution, and different solvents, aiming to identify the optimal conditions for uniform and stable surface coverage. VPD was similarly studied for its silanization time and annealing effects, providing a comparative analysis to determine the most effective method between LPD and VPD. Comprehensive surface characterization was performed using contact angle measurements, AFM and TOF-SIMS for both LPD and VPD methods. These analyses were essential in assessing the homogeneity, density, and chemical composition of the silane layers, which are critical for subsequent DNA grafting. Following surface functionalization, the research focused on developing a protocol for the preparation of DNA mixtures and their grafting onto the GOPS-functionalized surfaces. The grafting process was fine-tuned by adjusting various parameters, including time and temperature of the process, and the pH of the DNA mixture, to ensure successful attachment. Finally, the efficiency of DNA grafting was evaluated using fluorescence measurements. This step was crucial to confirm the presence and stability of grafted oligonucleotides, validating the effectiveness of the overall functionalization and grafting protocols.

This integrated approach aims to establish a robust method for creating DNA-functionalized surfaces, contributing to the advancement of biosensor technology.

Thesis structure

The thesis is structured into the following chapters, each building upon the previous to provide a comprehensive understanding of the work conducted:

1. *PCR*

   This chapter introduces the Polymerase Chain Reaction (PCR), which is essential for comprehending the final application of the research presented in this thesis. It provides the necessary background on the current processes and materials used in the field of DNA amplification and detection, setting the stage for the subsequent discussions and experiments.

2. *Electrical detection*

   This chapter explores the methods for electrical detection of DNA, with a particular focus on the current devices, such as Ion-Sensitive Field-Effect Transistors (ISFETs). It also reviews the literature on surface functionalization and the grafting of oligonucleotides, highlighting how these techniques are integrated into modern devices for electrical DNA detection.

3. *Materials and methods*

   This chapter details the materials and instruments used throughout the experiments. It provides explanations of the working principles of the key instruments employed, ensuring a clear understanding of how the experimental data was generated and the significance of the results obtained.

4. *Results*

   The core of the thesis, this chapter presents all the experiments conducted, focusing on the development of protocols for GOPS silanization and oligonucleotide grafting. The results are supported by thorough surface characterization, providing a detailed analysis that underscores the effectiveness of the developed methods.

5. *Conclusions and future developments*

   The final chapter offers a discussion of the results, drawing conclusions based on the findings presented. It also outlines potential future developments and directions for further research, suggesting how the work completed in this thesis could be expanded or applied in future studies.

1 | PCR

The Polymerase Chain Reaction (PCR) is a method extensively used in genetic testing and research for producing numerous copies of a specific DNA sequence. It was developed in the 1980s by Kary Mullis and his team at Cetus Corporation. Mullis was later awarded the Nobel Prize in Chemistry in 1993 for this groundbreaking work. Mullis himself said, *"PCR lets you pick the piece of DNA you're interested in and have as much of it as you want."*[28–30] This technology has significantly advanced various applications in the food, environmental, medical, and forensic sciences. One major advantage of PCR over previous DNA analysis methods is its ability to amplify DNA from only trace amounts. PCR relies on a straightforward enzymatic reaction in which DNA polymerase synthesizes a new strand of DNA that is complementary to the provided template strand. Therefore, if a sample contains a specific DNA sequence, PCR can amplify it, confirming its presence.[26]

Each PCR cycle requires the presence of several key components, which include:

- DNA template: This is the sample DNA containing the target sequence.
- Nucleotides: These are the four bases—adenine (A), thymine (T), cytosine (C), and guanine (G)—which serve as the building blocks used by DNA polymerase to synthesize the new DNA strands.
- DNA polymerase: This enzyme synthesizes new DNA strands complementary to the target sequence by assembling the nucleotides into a PCR product.
- Primers: These are short segments of single-stranded DNA that are complementary to the target DNA sequence. They provide a starting point for DNA polymerase to begin DNA synthesis.

1.1. PCR process

PCR is an efficient technique to amplify a specific DNA sequence and requires precise steps. To perform PCR, a reaction mix is prepared using a buffer solution with a small amount of target DNA. Essential components include the enzyme that carries the reaction,

DNA polymerase, the primers that create the starting and ending point for the sequence to be replicated and the building blocks for the reaction, the nucleotides. This mixture undergoes a series of steps within a thermocycler, a machine that precisely controls temperature changes across numerous cycles.[13, 16]

Each cycle typically consists of:

1. Denaturation: the double strands of the DNA helix are separated into single strands by heating to 94-96°C, which breaks the hydrogen bonds between nucleotide base pairs. The specific temperature and duration depend on the DNA sequence, with GC-rich sequences requiring a higher melting temperature than AT-rich ones. After this step, single-stranded DNA (ssDNA) containing the target sequence is produced.
2. Annealing: the temperature is lowered to 50-60°C, allowing the primers to bind to the ssDNA. Two sets of primers are used: forward primers that are complementary to the start of the target sequence on one strand, and reverse primers that are complementary to the end of the target sequence on the opposite strand.
3. Extension: the temperature is increased to 70-75°C to enable the DNA polymerase to synthesize new DNA strands. Starting from the annealed primers, the enzyme adds nucleotides from the mix to create a complete copy that is complementary to the target sequence.

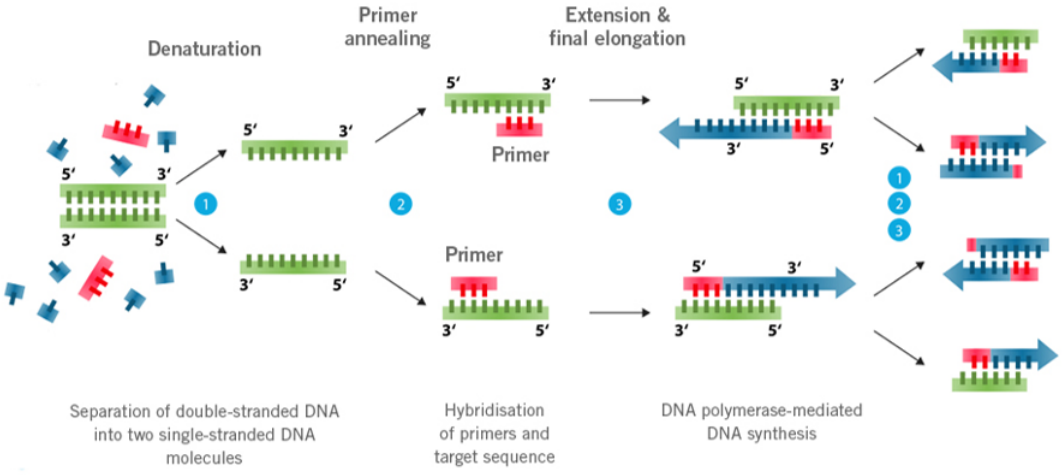

Figure 1.1: The three principal steps of a PCR process: denaturation, annealing and extension

These are the three steps that constitute a PCR cycle, as shown in Figure 1.1. This cycle is typically repeated approximately 25 to 40 times to achieve a sufficient quantity of the targeted DNA. PCR amplifies the targeted DNA sequence exponentially, which explains

the need for multiple cycles. Usually, before the first cycle, a longer initial denaturation step is performed to ensure the complete separation of the complex DNA template. At the end of all cycles, an additional extended extension step is carried out to finalize the synthesis of all new DNA products.[3]

1.2. Analysis of the PCR product

There are two main methods for analyzing PCR products:

1. Staining the amplified product with a chemical dye, such as ethidium bromide, which intercalates between the DNA strands and emits fluorescence[1] in the visible range when exposed to UV light.

2. Labeling the PCR primers or nucleotides with fluorescent dyes (fluorophores) before PCR amplification. This allows the labels to be incorporated directly into the PCR products.

The most widely used method for analyzing PCR products is agarose gel electrophoresis, which separates DNA fragments based on their size and charge. This technique can confirm the presence and estimate the size of the PCR product. The agarose gel electrophoresis set up is made of a box filled with an agarose gel and a salt-containing buffer that can conduct current and at the molecular level it's a matrix of agarose molecules that are held together by hydrogen bonds and form tiny pores. This box is composed by wells in one end that will contain the sample of DNA to be analyzed. One hand of the box is hooked to a positive electrode, while the other hand to a negative electrode. The end of the gel box with the wells is positioned towards the negative electrode, while the end without wells towards the positive electrodes.

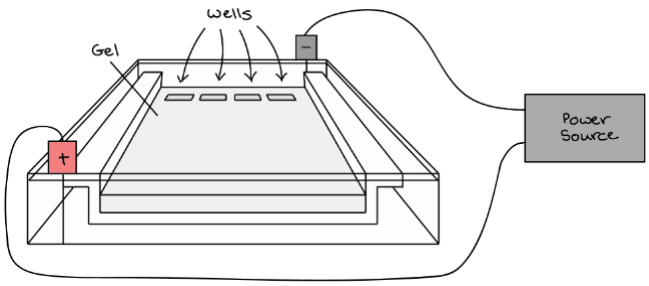

Figure 1.2: Scheme representation of an agarose gel electrophoresis

Whenever a sample of PCR products is analyzed, it is assumed that there is a great

[1]See Appendix A for the the working principles of fluorescence

quantity of DNA with fixed length, corresponding to the length of the target sequence. Furthermore, DNA intrinsically is negatively charged because of the phosphate groups in the backbone, so if a tension is applied between the two electrodes, then DNA will move through the gel box towards the positive electrode accordingly to their mass. Since DNA has a consistent charge-to-mass ratio, fragments are separated solely by size, allowing smaller fragments to move faster through the gel. A DNA ladder, a mixture of DNA fragments of known sizes, is run alongside the PCR products to serve as a reference for size determination. By comparing the migration patterns, the size of the PCR products can be inferred. After separation, the gel is stained with a DNA-binding dye and viewed under UV light, causing the DNA fragments to fluoresce and emit light. (see Figure 1.3).

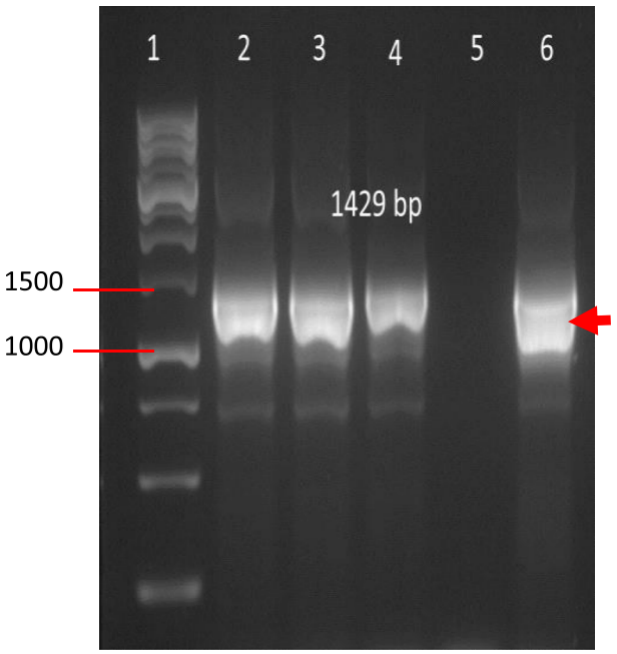

Figure 1.3: Agarose gel electrophoresis of PCR amplification of DNA products. Lane 1 contains the DNA ladder; lanes 2 to 6 show the analysis of different PCR product samples.[19]

1.3. PCR kinetics

If one were to extract a sample of the PCR product after each cycle and subject it to gel electrophoresis, the resulting bands could provide information on the progression of the reaction over time. By plotting the amount of DNA against the number of cycles, one can generate a curve that illustrates the reaction's progression.

The PCR process can be divided into four phases (see Figure 1.4):

1. Initial phase: during the initial cycles, there may be no apparent increase in DNA quantity due to the detection system's limitations.
2. Exponential phase: after several cycles, the DNA quantity increases exponentially as the detection system begins to register the accumulating DNA and sufficient reagents are still present.
3. Linear phase: following the exponential increase, the reaction enters a linear phase due to the depletion of reagents, which become the limiting factor.
4. Plateau phase: in the final cycles, the reaction reaches a plateau with a considerable amount of PCR products. Continuing the reaction at this stage is counterproductive because reagents are exhausted and the PCR products may start to degrade.

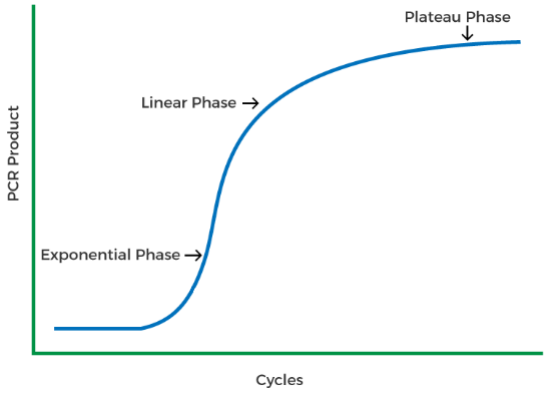

Figure 1.4: Relationship between the amount of DNA produced during a PCR process and the number of amplification cycles.

1.4. Real-Time PCR

The concept of measuring DNA quantity as a function of the number of PCR cycles can be incorporated into a technique known as Real-Time PCR or quantitative PCR (qPCR). Unlike conventional PCR, which qualitatively assesses DNA presence, qPCR tracks DNA concentration by measuring fluorescence during the reaction. This fluorescence correlates with the PCR product amount and is measured in real-time, as fluorescent markers are included in the initial mixture, thus negating the need for further analysis after the reaction. Real-Time PCR results, similar to those shown in Figure 1.5, mirror PCR kinetics discussed in Section 1.3. However, in qPCR, fluorescence readings take the place of DNA quantity, providing a direct correlation to the amount of DNA produced.

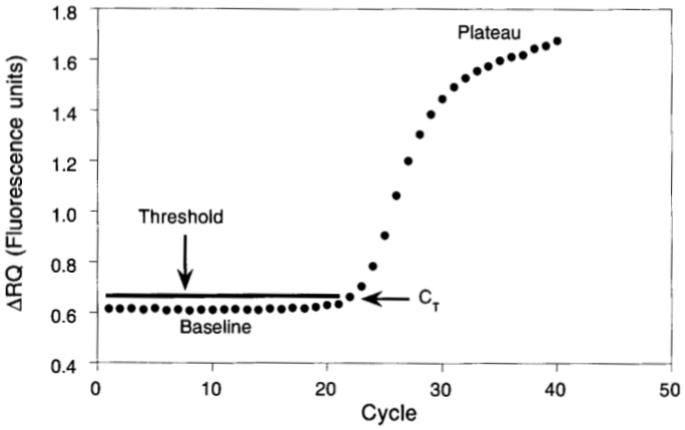

Figure 1.5: PCR product detection in real-time.

Figure 1.5 demonstrates the correlation between fluorescence output and cycle number in an qPCR process. The threshold cycle (C_T) is essential for precise quantification and is typically identified as the cycle number where the amplification curve intersects with a reference line. The latter one is based on a sample without any amplified product, representing the background fluorescence signal. It remains constant, approximating the initial cycle's background signal, and intersects at the start of the exponential phase. Fluorescence is measured after each cycle and is proportional to the amount of amplified DNA. As discussed in Section 1.3, the initial reaction phase may seem static when the signal is below the instrument's detection threshold. Adjusting the initial DNA template concentration can influence the C_T value, thereby shifting it according to the template concentration. Once the C_T threshold is crossed, the instrument's sensitivity threshold is surpassed, and the subsequent phases of DNA amplification become detectable. By integrating the measurement of PCR products into the amplification process, qPCR not only detects DNA but also quantifies the amount of a specific DNA sequence or gene present in the sample.[3]

There are two prevalent methods for detection and quantification of the product:

- Fluorescent dyes that non-specifically intercalate with double-stranded DNA.
- Sequence-specific DNA probes that include fluorescently labeled reporters.

1.4.1. DNA-binding dyes

This is the simplest yet most commonly used method to quantify DNA products in qPCR. Ideally, these molecules emit little to no fluorescence when free in solution. However, dur-

ing qPCR, they intercalate into the dsDNA, resulting in a significant increase in emitted fluorescence.[9] Ethidium bromide was initially described for use in real-time PCR due to its common use in agarose gel electrophoresis. However, its fluorescence enhancement upon intercalation with DNA is modest, leading to high background noise during measurements. Additionally, it is mutagenic and carcinogenic.[41] Subsequently, SYBR Green I (SG I) has become the most widely used DNA dye for real-time PCR applications due to its cost efficiency, lower toxicity, and ability to generically detect amplified DNA.[17]

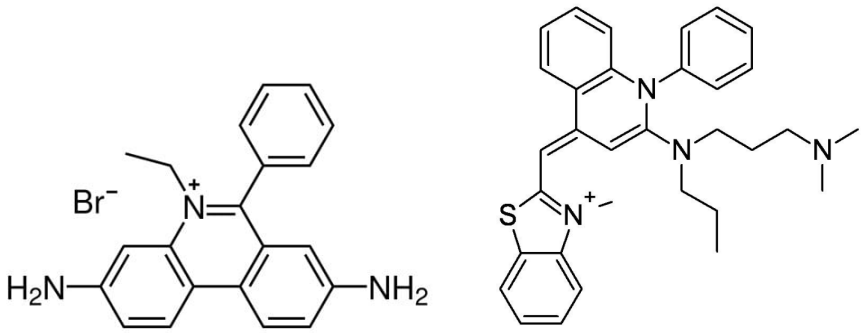

(a) Ethidium Bromide (b) SYBR Green I

Figure 1.6: Chemical formula of the two most used DNA-binding dyes.

SG I remains widely used despite numerous studies demonstrating its disadvantages such as PCR inhibition in a concentration-dependent manner,[31, 35] effects on DNA melting temperature[15, 35] and preferential binding to certain DNA sequences.[15]

During qPCR, fluorescence is continuously measured due to SG I binding with DNA in solution during each cycle, particularly during the annealing and extension steps. When exposed to blue light, SG I emits green light through fluorescence, with the intensity increasing in proportion to DNA product amplification as SG I binds to the accumulating DNA.[3] The SG I molecule (see Figure 1.8), which includes phenyl-quinolinium and benzo-thiazole aromatic systems along with propyl chains, contributes to the energy of the SG I/DNA complex formation through intercalation and electrostatic interaction. The tight fit of the aromatic groups between base pairs, van der Waals interactions with the bases, and electrostatic interactions between SG I and DNA, along with intercalation into the DNA's minor groove, significantly reduce the internal motion of SG I, resulting in enhanced fluorescence. The minor grooves of the DNA backbone, which are similar across different types of base pairs (see Figure 1.7), facilitate the intercalation of SG I in this region.

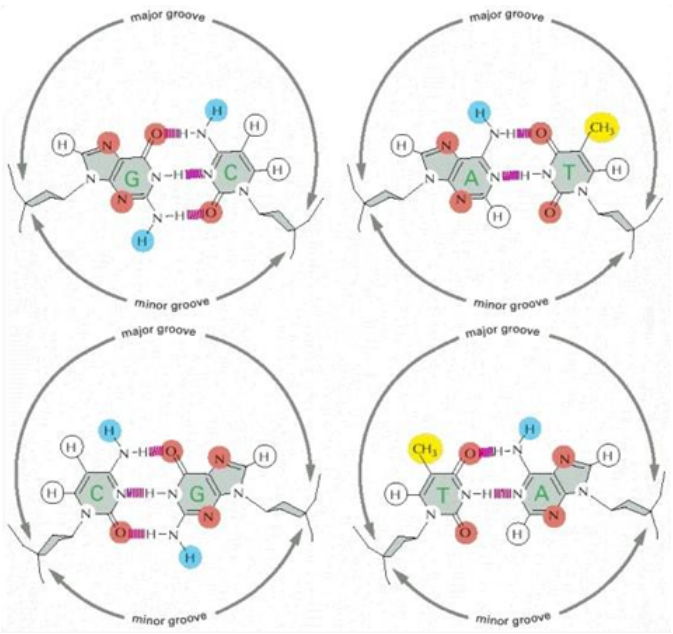

Figure 1.7: Chemical differences between major grooves and minor grooves for all base pairs.

The SG I/DNA complex is stabilized by charge-charge interactions formed between the positively charged thiazole group of SG I and the negatively charged phosphates of the DNA backbone. The quinolinium-thiazole system is effectively immobilized in a favorable conformational state through intercalation and Coulombic interactions, which lead to a dramatic enhancement of SG I fluorescence and a proportional increase in its lifetime.[9, 46]

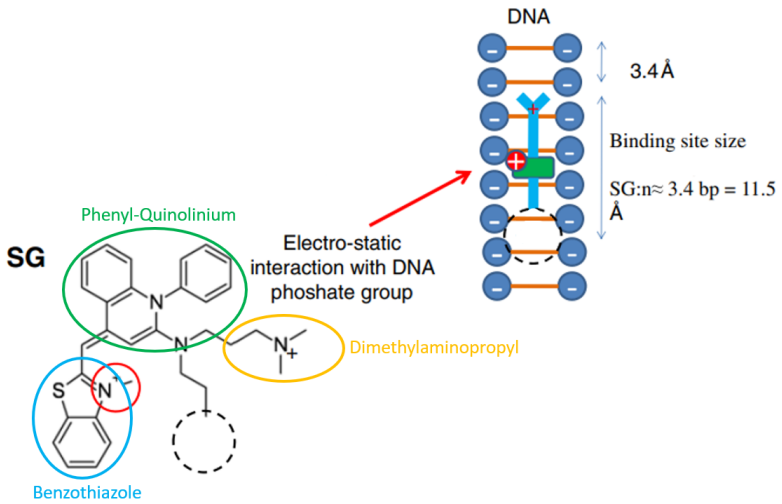

Figure 1.8: Representation of a molecule of SG I and its position inside the DNA backbone. The binding site size is approximately 3/4 base pairs.[9]

There is another variant of SYBR Green known as SG II. This molecule is slightly different and behaves similarly, but it performs better with ssDNA. The differences between SG I and SG II lie in the heteroatoms on the benzothiazole group and the linking arm of the molecules, as illustrated in Figure 1.9.

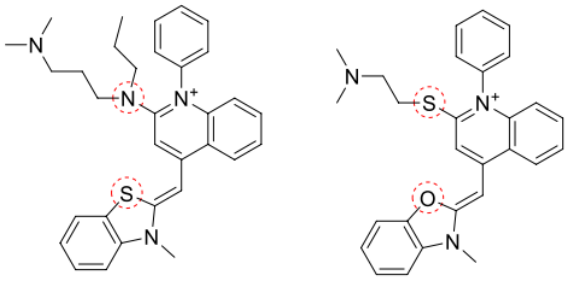

(a) SYBR Green I (b) SYBR Green II

Figure 1.9: Chemical difference between the two versions of SYBR Green.[36]

Although SG I generally exhibits higher brightness, SG II shows greater emission intensity when bound to ssDNA. This can be attributed to structural differences between the dyes, which lead to variations in binding affinity and the size of the binding site, thereby affecting their interactions with ssDNA. On average, a single molecule of SG I occupies 3.1 base pairs on the dsDNA lattice, whereas SG II requires only 2.8 base pairs.[20, 36]

1.4.2. Fluorescently labeled DNA probes

This method provides an alternative approach for detecting DNA products in qPCR. Fluorescent molecules, known as fluorophores, are incorporated into the ssDNA probe that is complementary to the target sequence. For each target sequence, two probes are designed: one with a fluorophore at the 5' end and the other at the 3' end. These fluorophores have partially overlapping spectra, with one's emission spectrum overlapping the other's absorption spectrum. When in close proximity, an energy transfer can occur between them. The probe with the 3' end fluorophore is called the donor. Upon illumination by the detection system, the donor absorbs light and transfers energy to the other probe, the acceptor, due to their overlapping spectra. The acceptor then emits light through fluorescence at a longer wavelength (and thus lower energy) than the light initially emitted by the detection system. This phenomenon is known as FRET (Fluorescence or Förster Resonance Energy Transfer).[3]

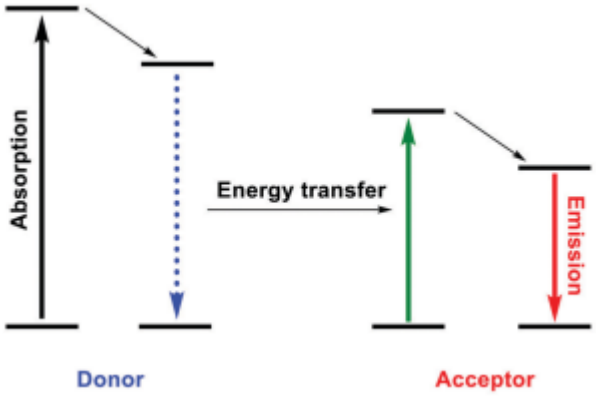

Figure 1.10: The energy transfer between acceptor and donor fluorophores occurs because their energy levels are compatible, allowing for efficient energy transfer. This process is facilitated when the emission spectrum of the donor overlaps with the absorption spectrum of the acceptor, enabling the transfer of energy through FRET.[44]

The two probes are specifically designed to bind to the target DNA sequence situated between the two primers. This design ensures that the fluorophores on the probes are in close proximity, facilitating energy transfer. The detection system then captures and quantifies the photons emitted through fluorescence from the acceptor fluorophores. These labeled probes possess a higher melting temperature than the primers, enabling stable binding to the DNA template during the annealing phase of the thermal cycling process. Consequently, the intensity of fluorescence emitted by the acceptor is directly proportional to the quantity of DNA products generated.

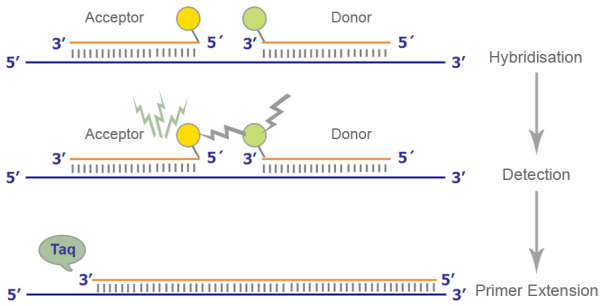

Figure 1.11: The donor and the acceptor bind to the DNA template during the annealing step and, due to spacial proximity, energy is transferred and the acceptor emits by fluorescence.

DNA polymerase inherently extends ssDNA from the 5' to 3' direction. To prevent the extension of the labeled probes, the probe with the acceptor fluorophore at the 5' end has a phosphate group at the 3' end, which inhibits extension by DNA polymerase. Similarly,

the donor probe cannot be extended because it is labeled with a fluorophore at the 3' end. Therefore, during each cycle, the two probes can be recycled without being elongated.[8]

1.4.3. Multiplex PCR

Multiplex PCR is a variation of PCR that enables the amplification of two or more target sequences by using multiple primer pairs in a single reaction. This technique can save considerable time and effort in the laboratory by allowing for the simultaneous detection of different target sequences. However, there are limitations to consider, such as reduced sensitivity and specificity, as well as the potential for preferential amplification of certain targets. To detect various target sequences, each is labeled with a specific fluorescent emission of a distinct wavelength by adding different donor-acceptor probe pairs to the reaction mix. Therefore, each pair of probes must be complementary to the specific target sequence to which they are designed, and if fluorescence corresponding to that wavelength is measured, then that sequence is present in the sample. This technique is more suitable for general screening of multiple targets. However, for accurate quantification, it is advisable to limit multiplexing to detecting two or three targets at most.

1.5. Solid Phase PCR

A typical PCR process is performed in a liquid medium, as discussed in Section 1. However, an intriguing alternative, which is the central topic of this thesis, involves DNA amplification on a solid surface. This method surpasses some of the limitations of conventional PCR, such as the ability to amplify multiple targets by using different primers at specific spots on the surface. While standard multiplex PCR can detect only 2-3 target sequences, solid-phase PCR (SP-PCR) has the potential to identify a greater number, limited only by the number of unique primer spots on the surface that match the target sequences.[42] Despite this significant advantage, SP-PCR has not been as widely adopted as it could be. The primary concern with SP-PCR is its lower amplification efficiency, which can result in significant challenges in nucleic acid-based analyses.[6]

1.5.1. Solid Phase Amplification

This innovative method involves attaching the 5' end of primers to a solid surface which facilitates amplification through two processes. The first process, interfacial amplification, captures a freely diffusing DNA target on the surface and copies it using a polymerase (see Figure 1.12).

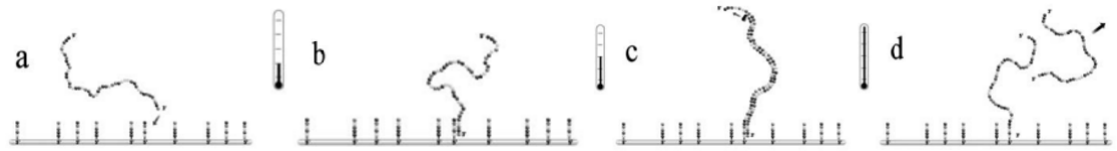

Figure 1.12: The representation of the solid-phase amplification process starts with the first cycle (a-b-c-d), where DNA replication occurs through interfacial amplification. The result is that one ssDNA molecule is now anchored to the surface via the primer. Subsequently, the solution is replaced with a new one that is devoid of DNA targets.

The newly synthesized DNA remains surface-bound, while the original DNA returns to the solution post-annealing. After several rounds of interfacial amplification, a second type of amplification can occur. In this phase, the free end of an attached DNA copy hybridizes with a surface-bound primer that is complementary to its sequence, initiating additional amplification (see Figure 1.13).

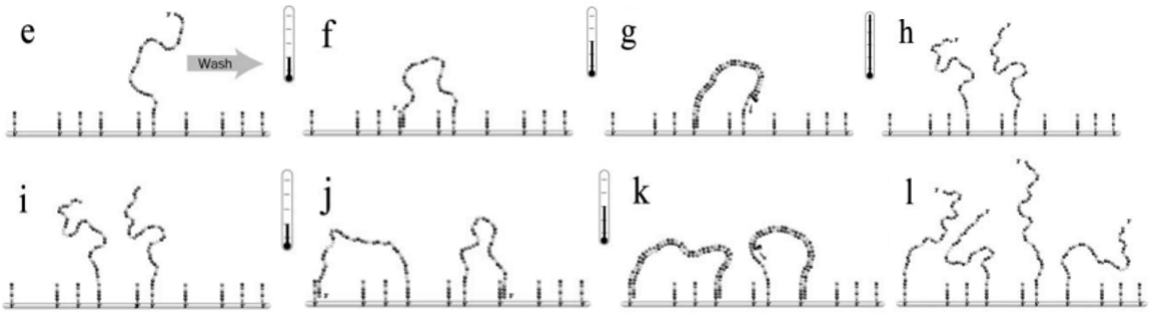

Figure 1.13: In subsequent cycles (e-f-g-h and i-j-k-l), only surface amplification occurs, resulting in the formation of a spatially localized DNA colony. Since each molecule synthesizes its complementary strand during a thermal cycle, both complementary strands will be present within the colony. Therefore, two different types of primers must be immobilized on the surface to accommodate the complementary sequences.

Both molecules remain attached to the surface, which is why it's called surface amplification. However, when both amplification processes are present, interfacial amplification tends to dominate. To promote surface amplification, the initial solution is replaced with one that is free of DNA targets, which allows surface amplification to proceed exclusively upon resuming the temperature cycles. Ideally, primers should stay fixed to the surface, but in practice, thermal cycling may cause some to detach.[1]

1.5.2. Limitations for the growth

When performing SP-PCR, it's crucial to consider several key factors. The density of the grafted chains is particularly critical as it significantly affects the probability of duplication within a specific cycle. Typically, higher densities of grafted chains result in a lower probability of duplication. If steric hindrance were the only factor, SP-PCR would lead to extremely high grafting densities.

However, additional factors also influence the duplication probability per cycle:

- Electrostatic forces: ssDNA carries a significant electric charge per unit length. High grafting densities can increase electrostatic repulsion between molecules, potentially causing them to extend away from the surface and hindering the free ends from reaching the surface, thus limiting surface amplification.[40]
- The finite number of primers: duplication occurs when a molecule comes into proximity with a surface-bound primer. Given that the number of primers is limited, the probability of duplication diminishes as the concentration of grafted molecules rises. Duplication ceases when all primers are utilized.
- Polymerase and nucleotide availability: the presence of a matching primer is just the initial step. Polymerase enzymes are essential for adding nucleotides and completing the formation of the double-stranded DNA molecule. Insufficient polymerase or nucleotides can significantly affect the process. The polymerase enzyme's size, similar to the persistence length of ssDNA, may also affect reaction efficiency.
- Incomplete molecules: if a thermal cycle ends before the polymerase fully replicates the complementary DNA strand, the resultant molecule is incomplete and unable to produce new copies, as its free end's DNA sequence doesn't align with the primer sequences on the surface. Nonetheless, this incomplete molecule occupies space, creating steric hindrance for adjacent molecules.
- Masking effect: given that the length of PCR amplicons is typically much greater than that of the primers, these longer DNA strands could obscure adjacent primers. As a result, these masked primers may be unable to participate in subsequent rounds of SP-PCR amplification.[6]
- DNA rigidity: dsDNA is approximately 10 times stiffer than ssDNA. Consequently, the rigidity of the molecule increases substantially once polymerase completes replication, forming the double-stranded molecule.

All these factors influence the SP-PCR growth process and are essential for a compre-

hensive understanding. They likely amplify the effects of steric interactions, making molecules at the center of a colony less likely to duplicate than those at the periphery, thereby limiting the maximum density within a colony.[25]

1.5.3. DNA microarray

The first step towards SPA involves DNA microarrays, which allow the detection of a vast number of targets, limited only by the number of spots available for analysis. This overcomes the limitations of traditional PCR, which can detect only a few targets. A DNA microarray, also known as a DNA chip or biochip, is a collection of microscopic DNA spots affixed to a solid surface. Each spot contains picomoles of a specific ssDNA sequence, known as probes, which are complementary to the DNA target of interest. Potentially, each spot corresponds to different DNA sequences to be detected. In typical applications, a DNA array is used to probe a solution containing a mixture of labeled DNA strands. The binding (hybridization) of these labeled "targets" to the "probes" on the array enables the detection of specific DNA sequences of interest.[5]

The typical steps required for a DNA microarray analysis are composed by:

1. Probe design and immobilization: initially, DNA probes that will be affixed to the microarray are selected and synthesized. These probes are short DNA sequences complementary to specific regions of the genes to be analyzed and are designed accordingly to the type of detection one want to perform. The probes are then immobilized at precise locations on a solid substrate, which can be glass, silicone, or plastic. This step is crucial because the physical location of each probe on the chip will correspond to a specific gene in the analysis process.

2. Extraction and labeling: DNA is extracted from the cells or tissues of interest and labeled with fluorescent dyes. There are various labeling methods, like direct incorporation of labeled DNA strands or post-hybridization labeling techniques.

3. Hybridization: the labeled sample is evenly distributed over the microarray to allow hybridization. The hybridization conditions, such as temperature and buffer composition, are optimized to encourage specific binding between the probes and the complementary sequences in the sample.

4. Removal of Excess: after a period of incubation, the microarray is washed to remove fragments of DNA that have not specifically bound to the probes. This phase is critical to reduce background noise and improve the specificity and reliability of the detected signals.

5. Detection: the microarray is then scanned by a device that excites the fluorophores and detects the emitted light. The intensity of the fluorescent signal, which corresponds to the amount of genetic material bound to each probe, is quantified and recorded.

6. Data analysis: the raw data are normalized to correct for technical and non-biological variations, such as differences in sample quantity or labeling efficiency. The data are then interpreted by comparing the signal intensities between different samples or with controls to identify which genes are expressed and to what extent.

2 | Electrical detection

Regarding the typical PCR technique discussed in Section 1, DNA detection is always performed using optical methods, where PCR products are analyzed by fluorescence. These systems are integrated with expensive optics that must interface with fluorophores, additional elements necessary for products detection. These components constitute the primary cost when developing a detection system. Therefore, this thesis aims to develop an alternative method to detect and analyze PCR products without using an optical detection system. For this purpose, DNA can also be detected electrically, leveraging its intrinsic negative charge. In a standard PCR process, the amount of DNA products correlates with fluorescence intensity. Similarly, the quantity of DNA products could be associated with their electrical charge, as an increase in PCR products should result in a rise in negative charge. The concept proposed here is to create a sensor that detects the presence of PCR products electrically by measuring the increase in electrical charge.

The advantages of this alternative detection method include:

- Lower costs for the detection system and the elimination of additional molecules for detection.
- More direct detection, as the electrical charge is inherent in the DNA backbone, whereas optical detection relies on fluorescence not emitted by the DNA itself but through added fluorophores.
- The potential for miniaturization is greater with an electrical system than with an optical one, as only a sensor is required for the detection.

However, there are potential limitations to consider:

- PCR efficiency might be compromised due to the limitations of surface amplification compared to amplification in a liquid medium. Indeed, electrical detection of DNA in a bulk medium, such as a liquid, is not feasible; the only way to detect it electrically is by performing surface amplification.
- The sensitivity of the sensor must be benchmarked against optical detection. The

sensitivity is indeed closely related to the distance between the sensor and the anchored DNA layer; a critical distance exists beyond which detection accuracy may diminish.

Electrical detection of DNA is possible due to the negative charge on its backbone, which arises from the presence of phosphate groups. These groups contain bonds between oxygen and phosphorus atoms that impart a negative charge. In the DNA structure, each phosphate group typically has one negatively charged oxygen atom, except at the 3' and 5' ends, where two negative oxygen atoms are present. This results in an overall negative charge for the entire DNA molecule.

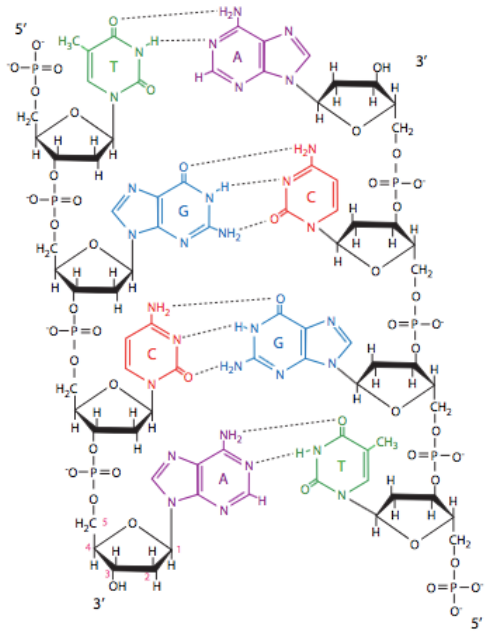

Figure 2.1: DNA is a polymer composed of nucleotide chains linked by 5' to 3' phosphodiester bonds, contributing to its negative electrical charge. Normally, DNA exists as two antiparallel, complementary strands held together by hydrogen bonds: adenine (A) pairs with thymine (T), and guanine (G) pairs with cytosine (C).

2.1. Ion-sensitive sensor

The negative charge of DNA can be detected using sensors that monitor variations in ion concentration. Such sensors are known as Ion Sensitive Field Effect Transistors (ISFET), which are a specific type of MOSFET. To fully comprehend how an ISFET functions, it's essential to first understand the operating principles of MOSFETs.

2.1.1. MOSFET

A Metal-Oxide-Semiconductor Field-Effect Transistor (MOSFET) is a particular type of FET that employs an electric field to modulate the current flow between its source (S) and drain (D) terminals. The conductivity of the device varies with the voltage applied to the gate (G), which facilitates the amplification or switching of electronic signals. Being unipolar, MOSFETs operate with only one type of charge carrier—either electrons or holes. Consequently, there are two varieties of MOSFETs: nMOS, which uses electrons as charge carriers, and pMOS, which relies on holes.

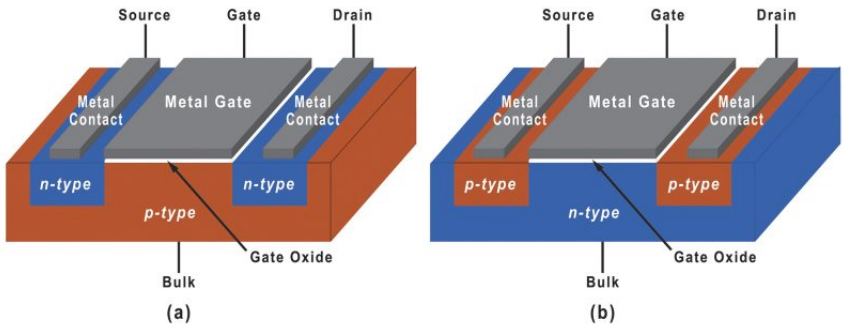

Figure 2.2: Comparison between the structures of a nMOS and a pMOS.

MOSFETs are three-electrode devices consisting of:

- Gate (G): this terminal is used to regulate the MOSFET. By applying voltage to the gate, you can control the current flow between the source and drain.
- Source (S): in an nMOS, this is the terminal where current enters, while in a pMOS, it is where current exits.
- Drain (D): for an nMOS, this terminal is where current exits, and for a pMOS, it is where current enters.

For an nMOS's operational principle, refer to Figure 2.3.

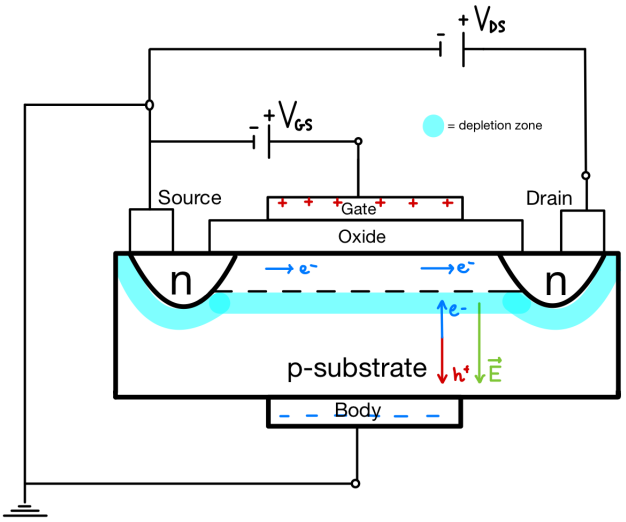

Figure 2.3: Scheme of the working principle of the formation of the channel between source and drain.

This type of device is composed by a p-doped substrate with two terminals which are instead n-doped. Tipically these regions are silicon based, doped with a pentavalent element for the n-type and a trivalent element for the p-type. At the interface between a n-type and a p-type region a depletion zone is formed, leading to the formation of a p-n junction[1]. The p-type substrate is connected with a terminal called body (B), while the two n-doped regions are connected respectively to the S and D terminals. An oxide layer, usually SiO_2, lies between S and D, topped by the gate (G) terminal. The B and S are connected internally grounded so that, since they are at the same potential, any current flow between B and S is prevented. Then a generator between D and S is connected, with the positive terminal connected to the D, so that a current between D and S can be generated. However, since there is no connection in the substrate between S and D, if we increase the voltage of the generator (V_{DS}) the depletion zone in the D terminal will increase because of the reversed bias. In order to create a connection between S and D, a small source generator is connected between G and B, with the positive terminal connected to the G. An higher voltage of this generator (V_{GS}) creates an electric field between the G and substrate. This moves the minority carriers (electrons) in the substrate towards the positive G (and the holes towards the body), but since the electrons can not reach the G because of the presence of the oxide layer it will form a sort of capacitor, leading to the formation of a channel between S and D. This closes the circuit and a current (I_{DS}) can be measured. The thickness of the channel can be controlled by changing the V_{GS}; there is a direct relationship between an increase or decrease of the voltage with

[1] see Appendix B for further details on p-n junctions.

respect to the thickness of the channel and the voltage at which the channel is formed is called threshold voltage (V_{TH}). As the channel is present, now the electrons can flow through the channel from S to D (while I_{DS} is conventionally flowing in the opposite direction, from D to S in the channel). By looking at a I_{DS} vs V_{DS} graph, when I_{DS} is measured, there is a first ohmic linear increase with V_{DS}, but, as said previously, as V_{DS} increases, the depletion zone will enlarge in the D due to the reversed bias. This fact, causes a shrinkage of the channel towards the D end and there is a critical value of the voltage where the channel is completely pinched off, as the name *pinch-off effect* suggests. However, in reality the channel isn't completely closed due to the large flow of electrons, but experimentally we will see a saturation of I_{DS}. A further increase of V_{DS} will not shrink anymore the channel leaving a constant saturation current. This problem can be solved by modulating appropriately the V_{GS}, with further increase of the channel leading to an higher saturation current.

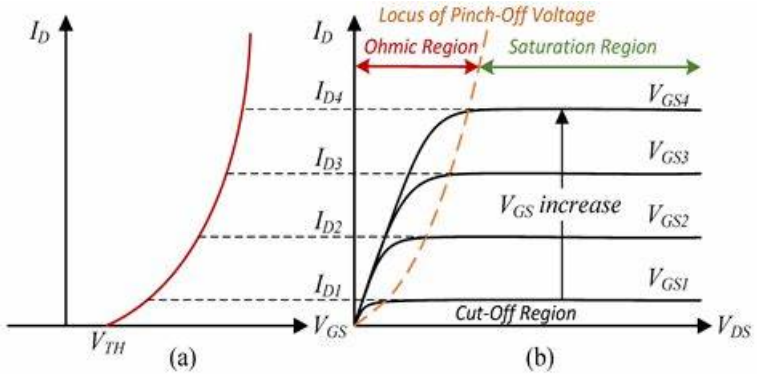

Figure 2.4: Drain characteristic and transfer characteristic of a nMOS. V_G controls the saturation current modulating the performance of the MOSFET.

Working regimes

The nMOS, described in the previous section, is working in accumulation regime, while there is another type of nMOS which instead works in depletion regime. It works basically in the same way, but the channel is formed originally during the doping of the substrate, so instead of enlarging the channel with a positive V_{GS}, a negative V_{GS} is applied thus reducing and closing the channel. This means that the depletion regime nMOS is normally ON and an application of a negative V_{GS} turns off the device.

Considering nMOS and pMOS there are four possible devices, depending on the working regimes:

- nMOS

  Accumulation regime: normally OFF ($V_{GS} > 0, V_{DS} > 0$)

  Depletion regime: normally ON ($V_{GS} < 0, V_{DS} > 0$)

- pMOS

  Accumulation regime: normally OFF ($V_{GS} < 0, V_{DS} < 0$)

  Depletion regime: normally ON ($V_{GS} > 0, V_{DS} < 0$)

Output characteristics

The pinch-off voltage divides the characteristic curves of a MOSFET into two distinct operating regimes: the linear regime and the saturation regime. In the saturation regime, the output current I_{DS} becomes independent of the drain-to-source voltage V_{DS}, while in the linear regime, the output current depends on both the gate voltage V_{GS} and V_{DS}. The pinch-off voltage, which signals the transition of the device into the saturation regime, is defined as the difference between the gate voltage V_{GS} at which the transistor begins to conduct and the threshold voltage V_{TH}:

$$V_{DS,\ pinch-off} = V_{GS} - V_{TH} \tag{2.1}$$

The threshold voltage can be calculated as:

$$V_{TH} = \frac{q * d * \rho_0}{C_{ox}} \tag{2.2}$$

Where q is the charge of the carriers, d is the thickness of the device, ρ_0 is the charge carrier density and C_{ox} is the gate capacitance per unit area ($C_{ox} = \frac{\epsilon_0 \epsilon_r}{t_{ox}}$, where t_{ox} is the thickness of the insulator). Depending on the regime we can calculate I_{DS} in two different ways. In the linear regime, I_{DS} will be equal to:

$$I_{DS} = \frac{W}{L} C_{ox} \mu \left[(V_{GS} - V_{TH}) V_{DS} - \frac{1}{2} V_{DS}^2 \right] \tag{2.3}$$

Where $\frac{W}{L}$ is the geometrical factor, which is the ratio between the channel width and length and μ is the carrier mobility. In the saturation regime, I_{DS} doesn't depend anymore on V_{DS}, so, by setting $V_{DS} = V_{GS} - V_{TH}$, I_{DS} can be calculated as:

$$I_{DS} = I_{SAT} = \frac{W}{2L} C_{ox} \mu (V_{GS} - V_{TH})^2 \tag{2.4}$$

The OFF current can be calculated by considering V_{GS} equal to zero:

$$I_{OFF} = \frac{W}{2L} C_{ox} \mu (V_{TH})^2 \tag{2.5}$$

2.1.2. ISFET

An ISFET is a variant of the MOSFET where the metal gate is replaced by an ion-sensitive membrane, an electrolyte solution in contact with the gate oxide, and a reference electrode submerged in the solution. The primary distinction between an ISFET and a MOSFET lies in the gate structure. Due to this similarity, ISFETs can be mass-produced using comparable techniques with straightforward modifications.

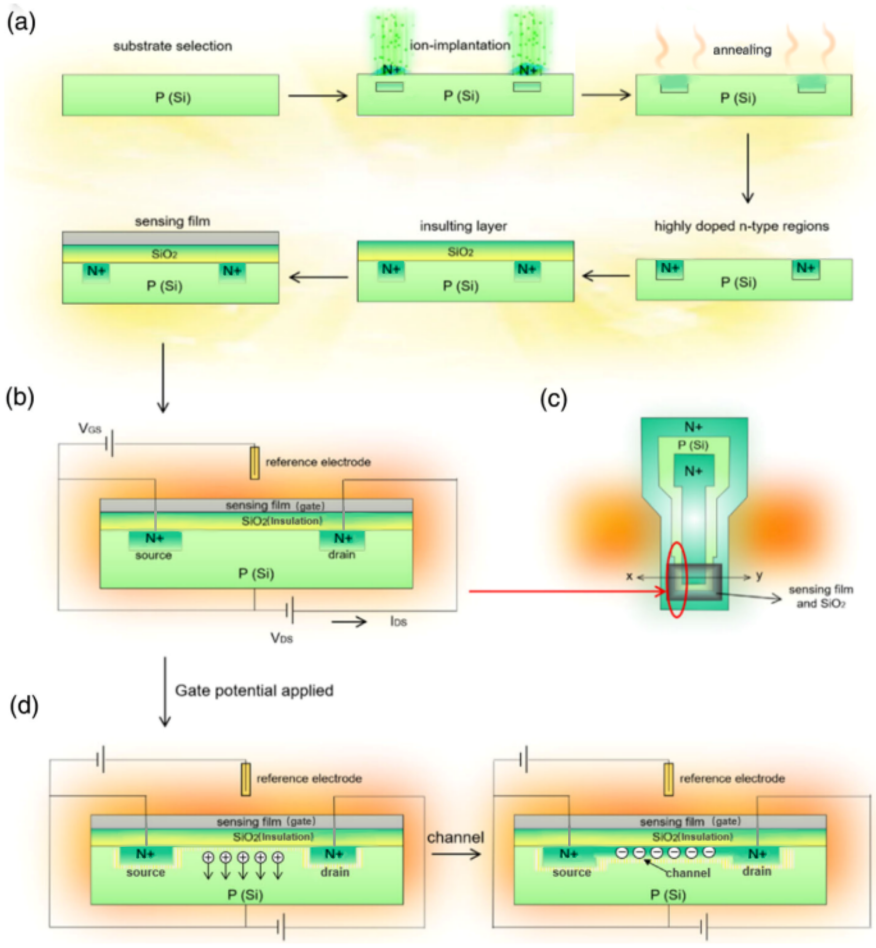

Figure 2.5: (a) The fabrication process, (b) the lateral view, and (c) the top view of a common ISFET. (d) The formation of conducting channel when the ISFET is working with the help of the gate potential (V_{GS}) applied.[2]

As depicted in Figure 2.5(a), the initial step is selecting the substrate material. Common

substrate materials include elemental semiconductors like silicon and germanium, as well as compound semiconductors such as gallium arsenide. Early semiconductor research focused on germanium and silicon, leading to advanced methods for creating smooth, thin layers, and considering production costs, these materials are often most suitable. Additionally, crystal orientation and electrical conductivity are crucial factors in substrate selection. For instance, when silicon is selected, a 100-crystal orientation and p-type substrate is usually adopted because of the highly efficient mobility of charged carriers, large drain current and large electrical output for a better performance of ISFET.

After selecting the substrate, the second step in ISFET fabrication involves diffusion techniques, such as ion-implantation, to prepare the source and drain electrodes. The ion-implantation technique is used to create two highly doped n-type regions, from which two metal electrodes are extended to serve as the source and drain. An annealing step is performed to diffuse the highly doped n-type region up to the surface, forming the two electrodes. Following this, an insulating layer (such as SiO_2) and a sensing film are deposited onto the electrodes using techniques like Chemical Vapor Deposition (CVD), magnetron sputtering, or radio frequency sputtering. The functions of the insulating layer and the sensing film in an ISFET are as follows:

1. The insulating layer acts as a dielectric between the sensing film and the substrate, forming a capacitor with these components. It also enables control of the gate voltage to form a conductive channel near the substrate's surface, ensuring separation between the channel and the sensing film.

2. The surface passivation of the insulating layer can prevent oxidation of the substrate, which enhances and stabilizes ISFET performance.

3. It offers waterproofing, preventing ion migration and penetration from the electrolyte to the substrate, crucial for the ISFET's stability.

4. The sensing film is responsible for ion recognition within the electrolyte, contributing to the ISFET sensor's sensitivity. Since a single type of sensing film may not fulfill all requirements, a layered structure with different materials may be necessary.

The ISFET requires additional packaging as it primarily operates in aqueous environments; thus, the device's encapsulation is crucial for enhancing its waterproof characteristics. A common approach is to use epoxy resin to encapsulate the entire ISFET, leaving only the ion-sensitive gate exposed to the electrolyte. The completed ISFET, as shown in Figure 2.5(b) and (c), along with the detailed operational processes, will be discussed in the following section.

Working principles

The fabricated ISFET can be utilized to convert biochemical signals into electrical signals for subsequent collection, analysis, and research. The structure of an ISFET is analogous to that of a MOSFET, with the metal gate replaced by a reference electrode (RE)/electrolyte/insulating gate assembly. Consequently, the signal transduction mechanism is similar, and the fundamental principle can be explained similarly. Specifically, when the ISFET is employed for ion detection, a gate voltage V_{GS} is applied through a RE via the electrolyte (Figure 2.5(d)). When V_{GS} is scanned from a low to a high value, holes in the ISFET substrate are repelled deeper into the material, and the accumulation of electrons begins to form a conductive channel between the source and drain electrodes. As V_{GS} reaches a certain level, which is V_{TH}, the electron density in the channel becomes sufficient to allow a current (I_{DS}) to flow with an applied voltage V_{DS} between the source and drain. Consequently, the concentration of ions in the analyte can be quantified directly by V_{TH}, which can be described by Equation 2.6:

$$V_{TH} = (E_{ref} - \varphi) + x - \varphi_{eo} - \left[\frac{Q_{ox}}{C_{ox}} - 2\emptyset_f + \frac{\emptyset_{si}}{q}\right] \tag{2.6}$$

where E_{ref} represents the potential of the reference electrode (RE); φ is the potential difference between the RE and the electrolyte; x, φ_{eo}, C_{ox}, and Q_{ox} denote the polarization potential, surface potential, capacitance per unit area, and charge density of the gate, respectively; $\emptyset_f$ and $\emptyset_{si}$ are the Fermi potential and work function of the silicon substrate; and q is the elementary charge. Therefore, V_{TH} is influenced solely by φ_{eo}, which is determined by the ion concentration. V_{TH} serves dual functions in an ISFET: it regulates the switching between the ON and OFF states and determines the ion concentration, enabling the conversion of chemical signals into electrical signals. However, in practice, V_{TH} cannot be measured directly; it is inferred from other parameters such as voltage (V_{GS} or V_{DS}), current (I_{DS}), or impedance. The relationship among I_{DS}, V_{GS}, V_{TH}, and V_{DS} is governed by the same equation used for MOSFETs (see Equation 2.3).

By fixing certain parameters of Equation 2.3, V_{TH} can be determined indirectly through other variables like I_{DS}, V_{GS}, and V_{DS}. Consequently, sensors can be categorized as either potentiometric or amperometric based on this relationship. Additionally, impedance can serve as an output, characterizing sensors as impedancemetric. Under potentiometric principles, if I_{DS} and V_{DS} remain constant, variations in V_{TH} due to ion concentration in the electrolyte are indicated by changes in V_{GS}. Alternatively, if I_{DS} and V_{GS} are constant, V_{TH} shifts are shown through V_{DS}. Generally, V_{GS} output is more commonly utilized than V_{DS} output. Under the amperometric principle, maintaining constant values

for V_{GS} and V_{DS} allows changes in V_{TH} to be indicated by variations in I_{DS}. In the case of the impedancemetric principle, with a fixed V_{DS}, V_{TH} alterations can be represented by changes in the transconductance ($g_m = \Delta I_{DS}/\Delta V_{GS}$) or by the impedance (Z) output of the ISFET. [2]

DNA detection

Accurate detection of DNA is crucial in various fields, including the diagnosis of genetic diseases, cancer genome screening, and the discovery of new medicines. Although existing methods offer high sensitivity and low detection limits, they have notable drawbacks such as complex measurement circuits, large and expensive instruments, time-consuming preparation, and the use of radioactive or poisonous labels. To address these issues, the ISFET method emerges as an excellent candidate due to its simple measurement circuit, compact sensing system, and straightforward fabrication and operation processes. Currently, there are two primary sensing mechanisms for ISFET-based DNA sensors. One mechanism involves enzymatic reactions using DNA polymerase to generate H^+ ions, which alter the surface charge distribution of the ISFET gate, thereby changing the gate surface potential. This change is detected as an electrical signal to identify DNA.[37] Similarly, the other mechanism is based on DNA strand hybridization, which generates negative charges. These negative charges influence the surface charge distribution of the ISFET gate, resulting in changes to the ISFET's electrical output.[22]

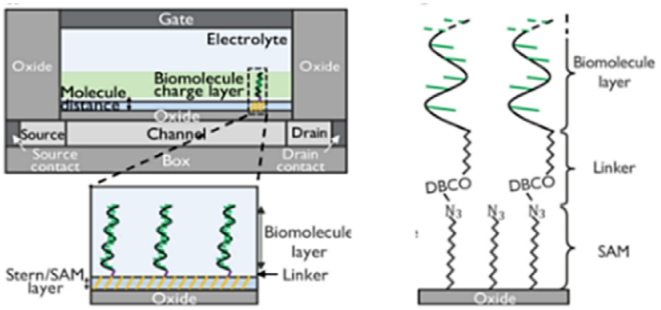

Figure 2.6: Scheme of an ISFET sensor used for DNA detection with the gate functionalized with the SAM, crosslinker and biomolecule.[37]

The combination of DNA and ISFET shows more advantages of fast detection speed, high sensitivity, low detection limit, good specificity, simple manufacturing process, and low cost. Based on the advantages, many studies of the ISFET-based DNA sensors have been developed these years. One of the most promising solutions is to functionalize the gate through silanization and then immobilize the DNA probes through the silane Self Assembled Monolayer (SAM), which will be described in Sections 2.2.3 and 2.2.5.

2.2. Silanization

Silicon sensor surfaces are commonly modified with silanes to provide a suitable interface between the silicon-based transducer and the biochemical environment. The homogeneity and surface morphology of silane films are crucial for controlling the structural order of immobilized single-stranded DNA (ssDNA) probes. In fact, the sensitivity and specificity of biosensors are determined by their arrangement. Before characterizing silanes, it is important to understand that silanes arrange on surfaces in a manner similar to SAMs. Therefore, a comprehensive explanation of SAMs is necessary first.

2.2.1. Self Assembled Monolayer

Self-assembled monolayers (SAMs) are thin organic coatings formed on substrates in an orderly manner. Typically, these are long alkyl chain surfactant molecules with a specific affinity for particular substrates, attached by chemisorption. SAMs provide a convenient, stable, and simple system to tailor the interfacial properties of metals, semiconductors, and metal oxides. They are organic assemblies formed by the adsorption of molecular constituents from solution or gas phase on solid surfaces or as regular arrays on liquid surfaces. The adsorbates spontaneously assemble into crystalline or semi-crystalline structures, held together by Van der Waals interactions.

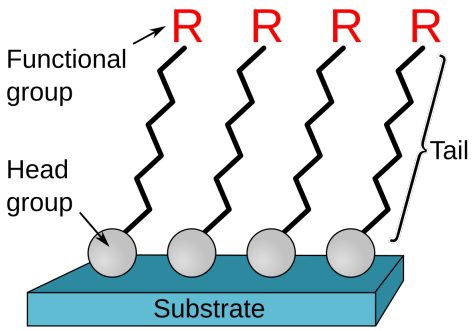

Figure 2.7: Schematic of a SAM on top of a generic substrate.

In Figure 2.7, it is evident that the molecules forming SAMs have a chemical functionality at one end, known as the headgroup, which has a specific chemical affinity for a particular substrate. The other end, connected to the headgroup via the tail, is the functional group, which determines the surface characteristics and the potential for further surface modification. The tail is typically an alkyl chain but can vary depending on the molecule used.

2.2.2. Kinetics

Two-dimensional (2D) molecular organization is crucial for the stability and function of SAMs. As adsorption progresses and surface coverage increases, the molecular order evolves. Initially, adsorption can be visualized as isolated, conformationally disordered molecules randomly distributed on the substrate. In the final stage, the film consists of closely packed adsorbate molecules with relatively uniform molecular orientation and conformation. While one might envision a continuous transition from the initial to the final structure, experimental evidence suggests a stepwise process. This process can be conceptualized as an isothermal path through a quasiequilibrium 2D-phase diagram, as schematically illustrated in Figure 2.8.

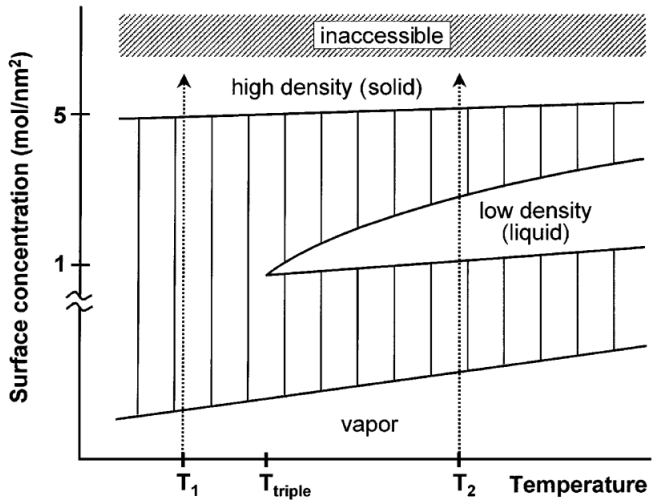

Figure 2.8: Quasi-equilibrium 2D-phase diagram for a generic SAM system. The dotted lines represent hypothetical isothermal paths of SAM growth at temperatures below (T_1) and above (T_2), the triple point (T_{triple}).

Possible states alluded to in this phase diagram include:

1. Low-density "vapor" phase: isolated, mobile adsorbate molecules are randomly deposited on the surface.
2. Intermediate-density phase:molecules are either conformationally disordered or lying flat on the surface.
3. High-density "solid" phase: molecules are conformationally ordered, closely packed, and standing approximately normal to the surface plane.

Two qualitatively different growth processes are suggested by the lines at temperatures T_1 and T_2 in Figure 2.8. If the temperature is lower than the triple point (e.g., temperature T_1), the growth sequence will be similar to the one shown in Figure 2.9A. Initially,

adsorbed molecules form a dilute 2D-vapor phase. At a relatively low surface concentration, the monolayer enters a coexistence region between the vapor and the high-density condensed (solid) phase. Domains (islands) of the solid phase nucleate and grow, surrounded by isolated adsorbate molecules in the vapor phase. Eventually, these domains grow to cover the entire substrate. This mechanism is analogous to the three-dimensional (3D) process of crystal nucleation and growth from a vapor phase precursor, and the 2D scenario is typical for epitaxial film growth from the vapor phase.

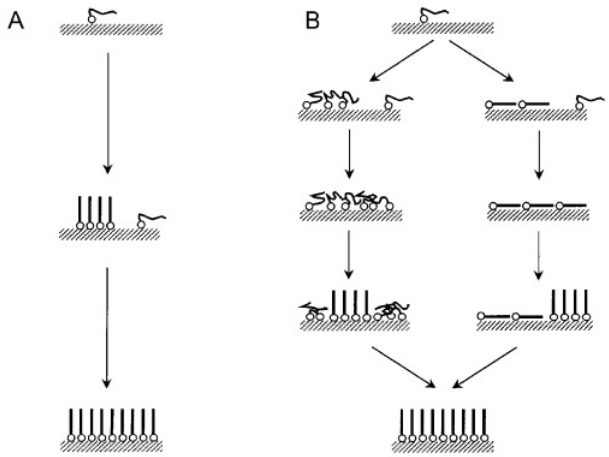

Figure 2.9: Typical sequences of a SAM structure during growth below (A) and above (B) a triple point like that shown in Figure 2.8. (A) $T_1 < T_{triple}$, growth proceeds from a 2D-vapor phase, through a solid-vapor coexistence region, to the solid phase. (B) $T_2 > T_{triple}$, the SAM must pass through three phases and two coexistence regions. The intermediate low-density phase may be a disordered (liquid) phase.

At a temperature above the triple point (e.g., T_2 in Figure 2.8), a more complicated progression occurs, as illustrated in Figure 2.9B. When the vapor phase reaches a certain surface concentration, islands of an intermediate, low-density condensed phase will nucleate and grow. This phase may be a disordered 2D-liquid phase or an ordered phase with lower density than the solid phase (e.g., a "lying-down" phase where the molecular axis is parallel to the surface plane). Eventually, the vapor phase is completely converted to the low-density condensed phase. As adsorption continues, a second transition occurs, involving the nucleation, growth, and coalescence of solid-phase islands surrounded by the low-density condensed phase. At any temperature, a snapshot of an incomplete film during growth will often show islands of one phase surrounded by another, particularly islands of the solid phase surrounded by either the liquid or vapor phase. It is important to recognize that the description in the previous paragraph is somewhat oversimplified. For instance, the adsorption rate will not always be much slower than other surface processes,

and as a result, partial monolayers may be quite far from equilibrium. If the nucleation and growth of condensed-phase domains do not keep up with the deposition rate, the less condensed phase will become "super concentrated" (i.e., it will have a density greater than the equilibrium coexistence concentration), causing its density to vary considerably during the growth of the more condensed phase. This behavior is well-known in vapor phase thin-film deposition, where the surface concentration of free adsorbate atoms is understood to vary during island nucleation and growth, and it is likely to occur during SAM growth as well. However, the surface concentration in the vapor phase will always be small and amount to a negligible fraction of the molecules on the surface. In the case of a 2D-liquid phase, the surface density is not negligible; in fact, the film thickness is directly related to the surface concentration. Therefore, variation of the surface density in a 2D liquid coexisting with solid-phase islands will significantly affect the appearance of the partial-monolayer film.[38]

2.2.3. Silane SAMs

The growth of silane-based SAMs is unique among SAM systems in that it involves an irreversible covalent cross-linking step. This is critical to the desirable properties of this class of SAMs, including their chemical and mechanical robustness on a variety of substrates. SAMs prepared on smooth surfaces like Si wafers exhibit extraordinary properties such as chemical homogeneity, ultra-low surface roughness and controlled wettability. The latter can be varied from hydrophilic to hydrophobic, depending on the end group of the silane. Silane layers in particular are mechanically robust, thermally stable up to at least 250°C and are not subject to swelling in the presence of solvents.[23]

Silane coupling agents

A silane compound is a monomeric, silicon-based molecule that contains four constituents. Silicon, like carbon, belongs to the same family on the periodic table and can form covalent bonds with four other atoms. However, silicon is less electronegative than carbon and undergoes unique reactions compared to typical organic compounds. Silanes that contain at least one bonded carbon atom are known as organosilanes. Organosilanes can also have hydrogen, oxygen, or halogen atoms directly attached to the silicon atom core. Some of these derivatives are highly reactive and can be used to form covalent linkages with other molecules or surfaces. The process of adding a silane coating (R_3Si–) to a particle or surface is known as silanization or sometimes silation. Tipically, organosilanes contain a functional organic component in addition to one or more silane-reactive groups. The organic portion may include a reactive group that allows the organosilane molecule

to conjugate with other organic compounds. Conversely, the silane-reactive groups are typically unreactive toward organic molecules but can covalently bond to certain inorganic substrates. This type of functional silane derivative is advantageous because it promotes the bonding of an organic molecule to an inorganic particle, surface, or substrate.

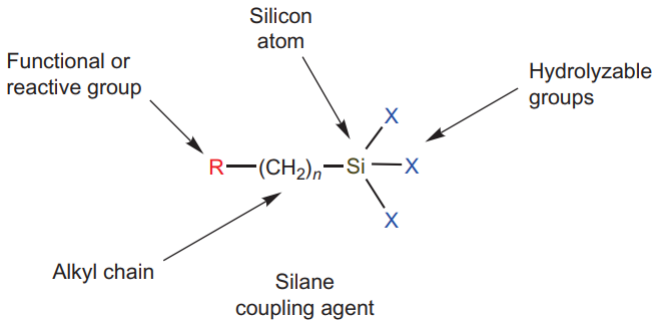

Figure 2.10: The general structure of a silane coupling agent includes a functional group or reactive group at the end of an organic spacer. This alkyl chain is attached to the central silicon atom, which also has up to three hydrolysable groups attached to it.

The general structure of a functional silane coupling agent, shown in Figure 2.10, consists of two parts:

- Organic Arm: This typically terminates in a functional group or reactive component, which facilitates covalent linkage to another organic molecule.
- Silane-Reactive Groups: These are attached directly to the silicon atom and can be of several types, including:
    - An hydrogen atom (silicon hydride).
    - An halogen–silicon derivative, such as a chlorine atom (chlorosilane).
    - An –OH group (silanol).
    - Groups containing methyl ether or ethyl ether organic constituents (methoxysilane or ethoxysilane, respectively).

The general reactions of silane coupling agents with inorganic substrates are illustrated in Figure 2.11. Unlike typical organic reactive groups, silane coupling agents (especially alkoxysilanes) often require hydrolysis to form a reactive intermediate. This hydrolysis converts alkoxysilanes into silanols, which are highly reactive and essential for coupling to inorganic surface hydroxyls.

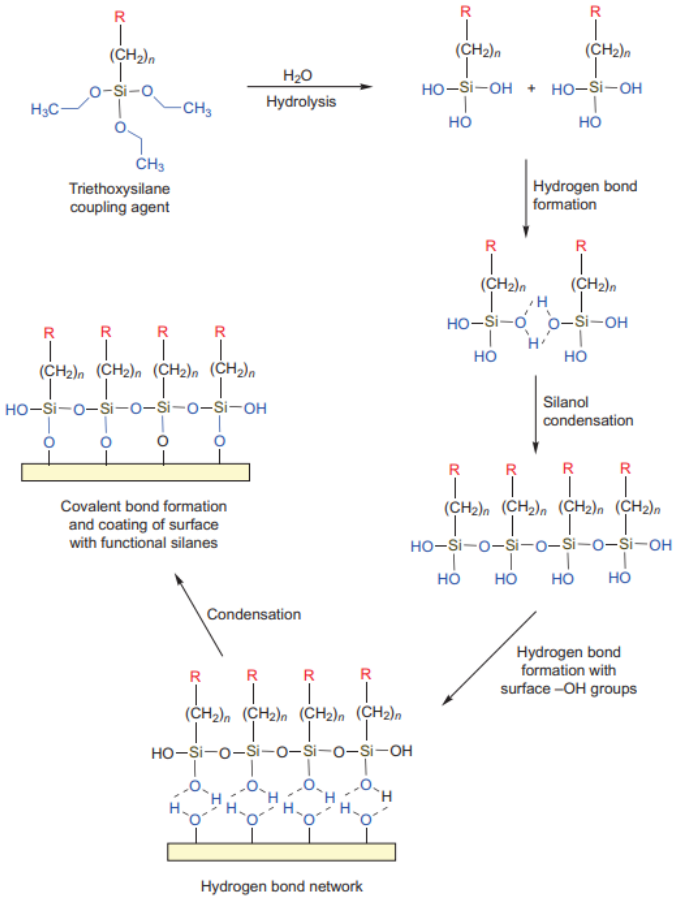

Figure 2.11: The reactions involved with the coupling of an organosilane compound to an inorganic surface with available –OH groups. The first step involves the hydrolysis of alkoxysilane groups to form highly reactive silanols. These silanols then undergo hydrogen bonding with other silanols in solution and on the substrate, creating a network of associated organosilane derivatives. A subsequent condensation reaction forms a polymerized coating of the organosilane on the surface of the substrate.

Initially, in solution or near an inorganic substrate, silane coupling agents condense to form a polymer matrix linked by –Si–O–Si– bonds. Simultaneously, the growing silane network interacts with the inorganic substrate through hydrogen bonding with surface –OH groups. A subsequent condensation reaction, usually facilitated by heat or vacuum to remove water, results in covalently linking the organosilane polymer to the surface, forming stable siloxane (or oxane) bonds. This process creates a thicker polymer layer rather than a monolayer, with reactive organic components extending from the surface. The thickness of the organo-siloxane layer depends on the concentration of the silane coupling agent and the amount of water in the solution. Alkoxysilanes are preferred for surface modification due to the instability of silanol derivatives, which tend to hydrogen bond and conjugate in solution. The alkoxy derivative stabilizes the silanol, prevent-

ing its polymerization. However, alkoxysilanes are generally unreactive with substrate hydroxyl groups at ambient temperatures. Ethoxysilanes are nearly unreactive with substrate –OH groups without prior hydrolysis, while methoxysilanes are more reactive but react very slowly at room temperature. Under appropriate conditions, both methoxy- and chlorosilane groups can directly couple with inorganic substrate functionalities without prior hydrolysis. For instance, adding a catalyst to the reaction can increase the hydrogen bonding capability of substrate hydroxyls, thereby accelerating the reaction rate for methoxysilanes. Additionally, chlorosilanes and methoxysilanes can be reacted in an organic solvent (e.g., tetrahydrofuran (THF), toluene, or hydrocarbon solvents) without the presence of water, if performed under refluxing conditions to drive the reaction to completion. In this case, a siloxane polymer network does not form in solution because no hydrolysis occurs to create silanols on the silane coupling agents. Therefore, instead of forming a thick polymer layer on the substrate as in aqueous reactions, a monolayer results where each organosilane is directly coupled to the substrate via a siloxane bond, as shown in Figure 2.12. The reactive organic components extend from this monolayer for eventual conjugation with biomolecules or other molecules.

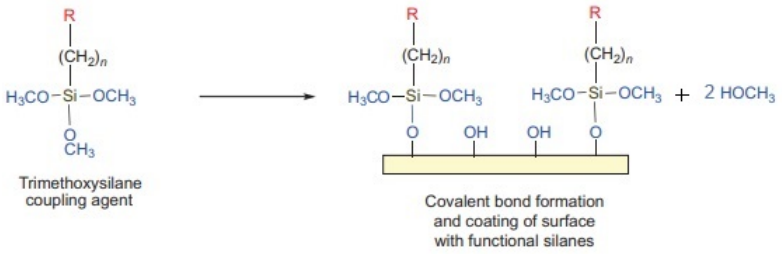

Figure 2.12: The reaction involved with the coupling of an organosilane compound to an inorganic surface without hydrolisis, due to the absence of water in the organic solution. In this scenario, each organosilane molecule reacts directly with the inorganic substrate. For methoxysilanes, this reaction produces methanol as a byproduct.

Common inorganic substrates used with silane coupling agents, listed in approximate order of efficiency and stability for modification, include silica, quartz, glass, and the oxides of aluminum, copper, tin, titanium, iron, chromium, zirconium, nickel, and zinc. All these substrates can have functional inorganic –OH groups on their surface that react with the silanols on the silane coupling agents to form siloxane bonds. Sometimes, the surfaces require prior treatment to form the –OH groups and remove contaminants that could interfere with the silanization process.[18]

2.2.4. Silanization techniques

The reaction techniques that can be used for functional silane coupling agents are varied and can be tailored to the specific needs of the substrate and the desired outcome. Here are some common deposition techniques:

- Aqueous/organic solvent deposition: this method uses a small amount of water at an acidic pH to facilitate the hydrolysis of the alkoxy groups on the silane, forming the reactive silanols necessary for coupling. The silane solution can be applied to the substrate by suspension stirring, dipping, spinning, or spraying.
- Organic solvent deposition: this method involves using an organic solvent without the addition of water, suitable for highly reactive silane derivatives such as chlorosilanes, aminosilanes, and methoxysilanes. This procedure is not effective for ethoxysilanes, as they are not reactive enough without prior hydrolysis to create silanols. This method is convenient for modifying silica particles and functionalizing metallic nanoparticles with the requisite –OH groups.
- Vapor-phase deposition: in this approach, many silane coupling agents can be applied to substrates by volatilization in an enclosed chamber under heat or vacuum. The substrate is placed within the chamber to allow vapor-phase molecules to access all areas to be derivatized. This method is commonly used for silanizing glass slides or substrates that are difficult to suspend in a silane solution. Slides are often placed in racks within the chamber, ensuring uniform modification with silane. Vapor deposition also uses a very small amount of organosilane compound compared to fully immersing a substrate device in solution.

These techniques can also be conducted at room temperature or under elevated temperature conditions. The choice of reaction strategy is often governed by the type of substrate being modified and the inorganic reactive groups on the silane. For instance, if the inorganic substrate can be treated by mixing or suspending it in a solution of functional silane, such as with particle coatings, this may be the simplest option for silanization. Another approach is to dip the substrate into the silane solution, as is sometimes done with glass slides and other small surfaces that can be handled in trays or baskets. Alternatively, complex surfaces, such as those often encountered with devices, may be treated in a chamber where the silane compound is volatilized by heating or placed under vacuum. This method usually results in the uniform modification of all surfaces with a thin layer of functionalized silane through vapor phase deposition.[18]

2.2.5. Functional silane compounds for bioconjugation

Functional silane compounds with organo-functional or organo-reactive arms can be used to conjugate biomolecules to inorganic substrates. By selecting the appropriate functional or reactive group, various biological entities such as proteins, oligonucleotides, whole cells, organelles, or tissue sections can be attached to substrates. Organosilanes for these applications include a variety of functional or reactive groups, such as hydroxyl, amino, aldehyde, epoxy, carboxylate, thiol, and alkyl groups, which can bind molecules through hydrophobic interactions. The two most commonly used organosilanes for DNA bioconjugation are APTS/APTMS and GPTMS/GPTES. However, many other organosilanes can be selected based on the specific application requirements.[18]

APTS/APTMS

3-Aminopropyltriethoxysilane (APTS) and 3-Aminopropyltrimethoxysilane (APTMS) are among the most popular silane coupling agents used to create a functional group on an inorganic surface or particle. Both reagents contain a short organic 3-aminopropyl group that terminates in a primary amine. The only difference between these compounds, as shown in Figure 2.13, is the silane-reactive portion, which contains either a triethoxy group or a trimethoxy group. This difference leads to variations in their reactivity toward substrate –OH groups, based on the relative reactivity of the alkoxysilane functionalities.

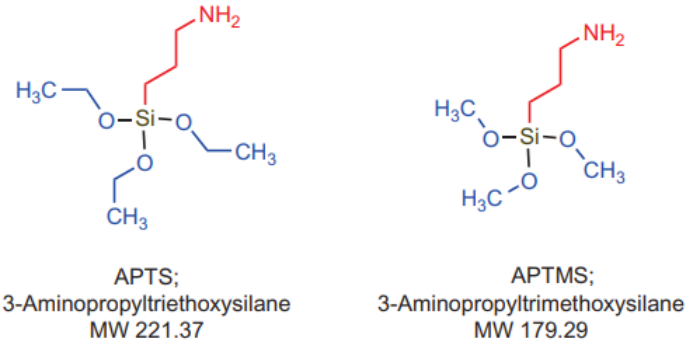

Figure 2.13: Chemical structure of APTS and APTMS. The difference lies in the silane-reactive portion that contains either a triethoxy group or a trimethoxy group.

- Trimethoxy Compound: more reactive and can be deposited on a substrate using 100% organic solvent without the presence of water to promote hydrolysis of the alkoxy groups prior to coupling. This method follows the organic solvent deposition protocol described earlier, allowing for the covalent modification of substrates with a layer of aminosilane compounds. The advantage of this process is that it enables

a thinner, more controlled deposition, creating a monolayer of aminopropyl groups on the surface.

- Triethoxy Compound: less reactive compared to the trimethoxy compound and typically requires the presence of water to hydrolyze the alkoxy groups before coupling. When using APTS, the reaction must occur in at least a partially aqueous environment because the ethoxy groups are not reactive enough to couple spontaneously with the –OH groups on an inorganic surface without prior hydrolysis to form silanols.

Once deposited on a substrate, the alkoxy groups form a covalent polymer coating with the primary amine groups extending from the surface and available for subsequent conjugation (see Figure 2.14). The choice between these two agents depends on the specific application and desired outcome for surface modification. Ethoxysilanes tend to hydrolyze more slowly compared to methoxysilanes, which can be advantageous in situations where greater control over the reaction is needed. Slower reactivity can reduce the formation of aggregates and improve the formation of a uniform monolayer. On the other hand, methoxysilanes have higher reactivity, which can be useful for applications where the reaction time needs to be minimized. Furthermore, methoxysilanes do not necessarily require hydrolysis. [18]

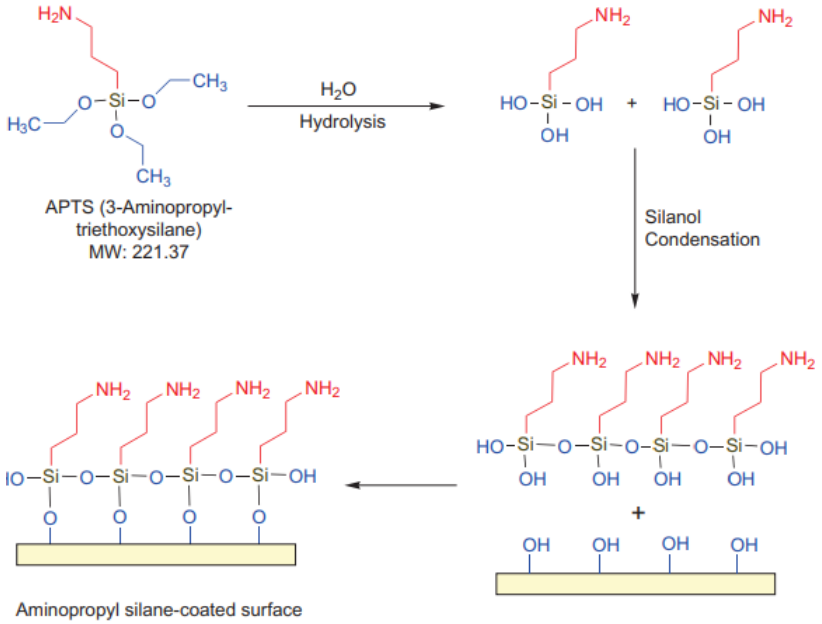

Figure 2.14: The deposition of APTS on inorganic substrates results in the formation of a covalent coating containing primary amine groups ready to be used for further bioconjugation.

GPTMS/GPTES

Two very useful silane modification agents are glycidoxy compounds containing reactive epoxy groups. Surfaces covalently coated with these silane coupling agents can be used to conjugate thiol-, amine-, or hydroxyl-containing ligands, depending on the pH of the reaction. Thus, 3-Glycidoxypropyltrimethoxysilane (GPTMS) or 3-Glycidoxypropyltriethoxysilane (GPTES) can be used to link inorganic silica or other metallic surfaces containing –OH groups with biological molecules containing any of these three major functional groups. GPTMS has been used most often in bioconjugation applications, but the triethoxysilane compound also may be used in similar protocols.

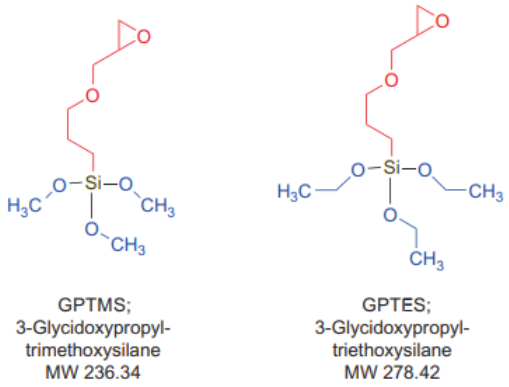

Figure 2.15: Chemical structure of GPTMS and GPTES. The difference lies in the silane-reactive portion that contains either a triethoxy group or a trimethoxy group.

Considering the functional group, there could be three possible reaction mechanisms:

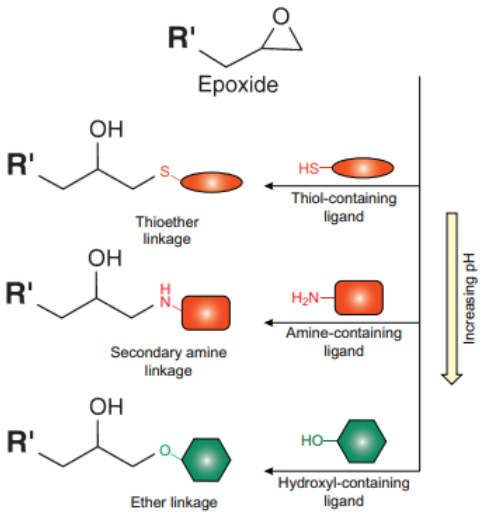

Figure 2.16: Opening of the epoxide ring due to the presence of a nucleophile agent. Epoxides can react with thiol-, amine- or hydroxyl- containing ligands leading to a thioether, a secondary amine or an ether linkage.

- Epoxide with thiol group: yields a thioether linkage and are the most highly reactive nucleophiles with epoxides, requiring a buffered system closer to the physiological pH range of 7.5 to 8.5 for efficient coupling.
- Epoxide with amine group: results in a secondary amine bond and react at more moderate alkaline pH values, typically needing buffer environments of at least pH 9.0.
- Epoxide with hydroxyl group: forms an ether and require high pH conditions, usually in the range of pH 11 to 12.

The relative reactivity of an epoxy group is thiol > amine > hydroxyl, which is reflected by the optimal pH range for each reaction. The lower the reactivity of the functional group, the higher the pH required to drive the reaction efficiently.

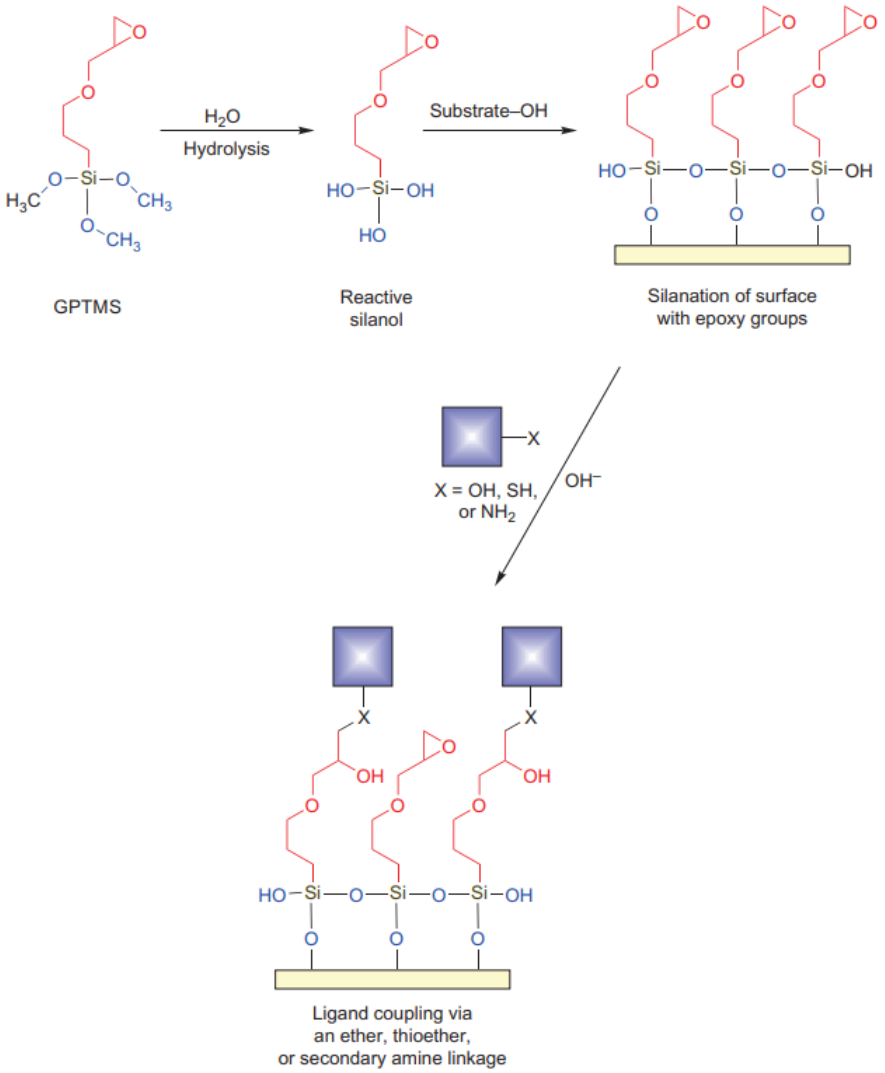

Figure 2.17: Epoxy-containing silane coupling agents form reactive surfaces that can be used to couple amine-, thiol-, or hydroxyl-containing ligands. In this case, a hydrolysis step is considered; however, especially in the case of GPTMS, this step can be skipped due to the high reactivity of methoxy grops with hydroxyl terminations of the activated surface.

Carboxyethylsilanetriol

Silane coupling agents containing carboxylate groups can be used to functionalize a surface with carboxylic acids for subsequent conjugation with amine-containing molecules. One such agent is carboxyethylsilanetriol, which contains an acetate organo group on a silanetriol inorganic reactive end. Unlike most other silanization reagents, the silanetriol component is immediately reactive with inorganic –OH substrates without requiring prior hydrolysis of alkoxy groups. This reagent has been used to add carboxylate groups to fluorescent silica nanoparticles for coupling antibodies in multiplexed bacteria monitoring.

It can similarly be used to add carboxylate functionality to various inorganic or metallic nanomaterials, which also creates negative charge repulsion to maintain particle dispersion in aqueous solutions. Covalent coupling to the carboxylated surface can then be achieved by activating the carboxylic acid groups with a carbodiimide, facilitating direct reaction with amine-containing molecules or forming intermediate NHS esters.

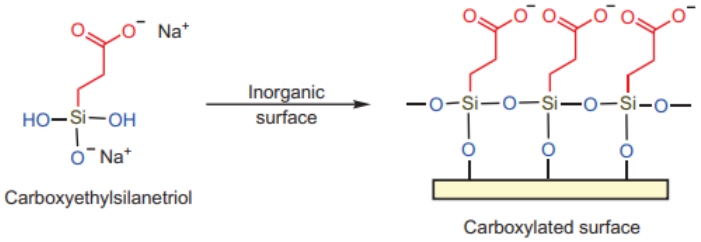

Figure 2.18: Carboxylethylsilanetriol can be used to modify an inorganic substrate to have a functionalized surface with carboxylate groups for coupling amine containing ligands.

TMS-EDTA

Another useful silanization reagent containing carboxylates is N-(Trimethoxysilylpropyl)-ethylenediamine triacetic acid (TMS–EDTA), which is an effective chelator of metal ions. TMS–EDTA contains a trimethoxy group for coupling to –OH groups on inorganic substrates and an EDTA group for coordinating metals. The EDTA group is modified to function as the linking arm attached to the silicon atom. The main applications are:

- Immobilized Metal Affinity Chromatography (IMAC): TMS–EDTA can be used to coat substrates and provide a metal-chelating functional group for IMAC. This method targets certain functional groups in proteins or other biomolecules.
- Directed Targeting: various metal ions can be chelated by EDTA affinity groups to target biological groups such as phosphate modifications or histidine-rich areas in proteins. For example, phosphorylation sites in proteins can be bound using a silane–EDTA-modified surface containing gallium.
- Proteome Analysis: preparing particles or surfaces that can specifically capture a fraction of the proteome using metal affinity separations enables the analysis of distinct protein populations by mass spectrometry.

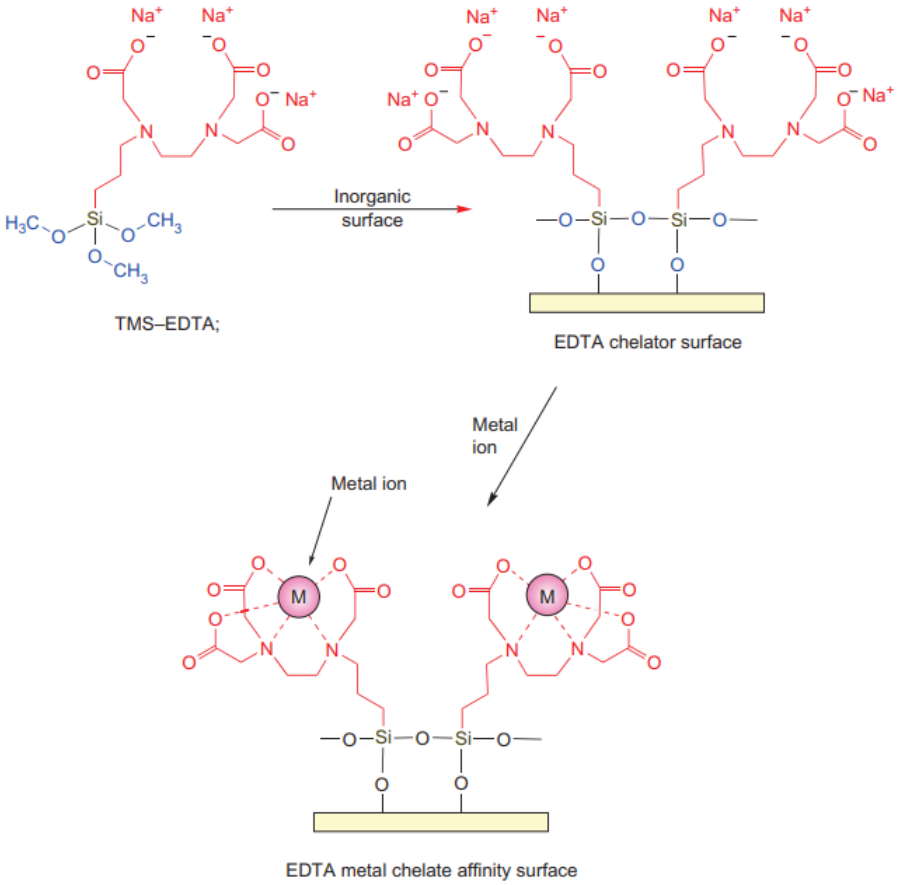

Figure 2.19: TMS–EDTA can be used to modify an inorganic substrate to contain EDTA chelating groups for complexation with metal ions.

TMS–EDTA holds metal ions through five coordination bonds, typically leaving only one remaining for interacting with other molecules. This property may result in lower affinities with biological molecules and alter the capture behavior for specific metal interaction sites on proteins. The reactions and use of TMS–EDTA in modifying inorganic surfaces and coordinating metals for affinity chromatography are shown in Figure 2.19.

ICPTES

Isocyanate groups are extremely reactive toward nucleophiles and will hydrolyze rapidly in aqueous solution. They are especially useful for covalent coupling to hydroxyl groups under nonaqueous conditions, making them suitable for conjugation to many carbohydrate ligands. Isocyanatopropyltriethoxysilane (ICPTES) contains an isocyanate group at the end of a short propyl spacer, which is connected to a triethoxysilane group that facilitates attachment to inorganic substrates.

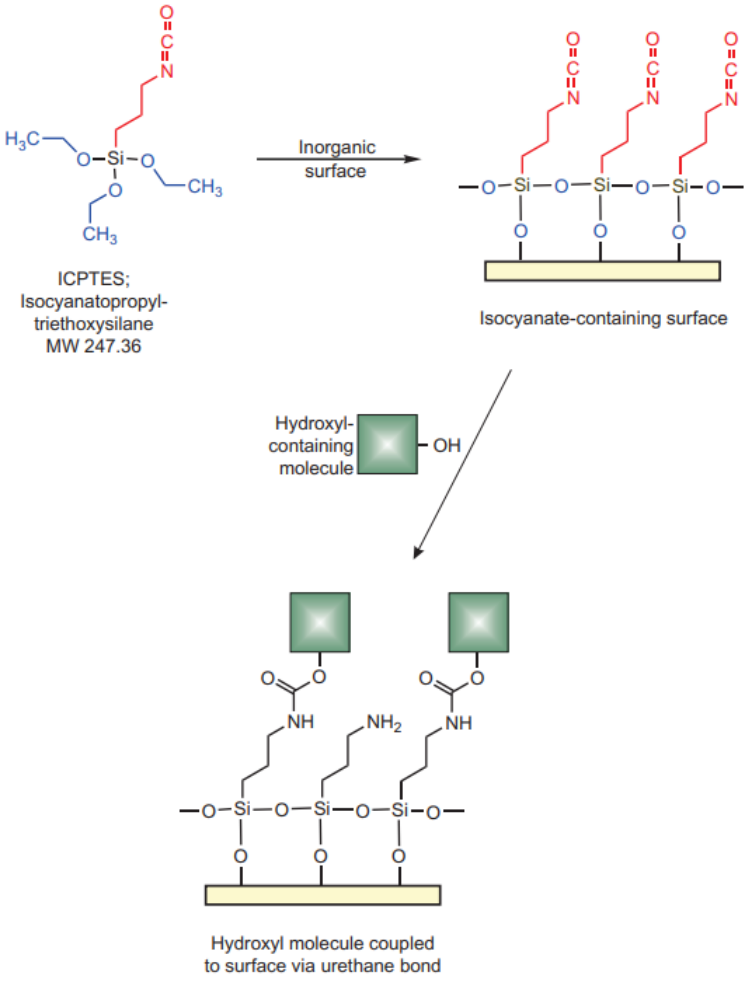

Figure 2.20: The isocyanate-containing silane coupling agent can be used to couple hydroxyl-containing molecules to inorganic surfaces.

Applications

Table 2.1 provides a brief summary of all the silanes described above, along with their main applications.

Table 2.1: In this table are reported all the silanes described in Section 2.2.5. For all of them, the main applications they are used for are reported.

Silane	Applications
APTS/APTMS	- Surface modification of glass and silica - Adhesion promoter - Coupling agent for polymers and resins - Bioconjugation - Functionalization of nanoparticles
GPTMS/GPTES	- Surface modification - Adhesion promoter - Coupling agent for epoxy resins - Coatings and sealants - Bioconjugation - Functionalization of nanoparticles
Carboxyethylsilanetriol	- Surface modification - Coupling agent for metal oxides - Functionalization of nanoparticles - Bioconjugation - Fluorescent silica nanoparticles for antibody coupling
TMS-EDTA	- Chelating agent - Surface modification - Metal ion binding and removal - IMAC - Directed targeting of biological groups - Proteome analysis
ICPTES	- Surface modification - Adhesion promoter - Coupling agent for urethane systems - Functionalization of nanoparticles - Bioconjugation - Conjugation to carbohydrate ligands

3 | Materials and methods

This chapter outlines the materials and methods utilized during my research, which was conducted over the course of a one-year internship at STMicroelectronics with the Silicon Biotech team. The materials and instruments employed were critical in achieving the objectives of this study. The primary materials and methods include various chemicals and a series of instruments used for characterization. Each of these is detailed in the following sections.

3.1. Materials

For general cleaning of all instruments, isopropanol (CMC Materials) and acetone (CMC Materials) were used. Sulfuric acid (Sigma-Aldrich) and hydrogen peroxide 30% (Carlo Erba Reagents) were used for the preparation of the piranha solution. The silane used was 3-Glycidoxypropyltrimethoxysilane 98% (Sigma-Aldrich). The solvents used for the silanization were anhydrous ethanol (Carlo Erba Reagents), acetone (CMC Materials) and anhydrous toluene 99.8% (Sigma-Aldrich).

The substrates used for the experiments are 0.6 mm thick silicon dies taken from wafers produced by STMicroelectronics. The working area measures 17.65x12.15 mm^2 with a 1 μm thermally grown silicon dioxide layer on top.

For the solvents cleaning of the substrates, a Powersonic 510 ultrasonic cleaner (HST) and a spin coater WS-650SZ-6NPP/LITE (Laurell) were used.

Two oligonucleotides were tested:

- P1 : 5'-[AmC6]TTGGACTAGAAATCTCGTGCTGA[6FAM] (Sigma-Aldrich)
- P2 : 5'-[AmC6]CAAGGTGAACGTGGATGAAG (Sigma-Aldrich)

Two buffer solutions were tested for the DNA grafting: Tris-EDTA buffer solution pH 8 (Sigma-Aldrich) and disodium hydrogen phosphate pH 9 (Sigma-Aldrich). A potassium chloride solution (Sigma-Aldrich) was used in the DNA mix to stabilize the oligonucleotides.

3.2. Surface preparation and characterization

The following instruments were employed to characterize the functionalized surfaces. A brief explanation of their working principles is provided to better understand how they will be used in the experiments.

3.2.1. Low-Pressure RF Plasma

The plasma cleaner is a system that generates plasma (an ionized gas capable of conducting electricity and absorbing energy from an electrical supply) from a neutral gas through the application of an electrical field. In an inert gas, such as argon, the excited ions can bombard a surface ("sandblast") and remove a small amount of material; in this case the process is defined as physical etching. Using an active gas, such as oxygen, both ion bombardment and chemical reactions occur, in a process defined as RIE (Reactive Ion Etching). As a result, organic compounds and residues are removed, and the surface chemistry composition can be altered depending on the material and the process parameters used. This plasma technology can be used on various materials (glass, metals, plastics, textiles, ceramics) for surface cleaning and activation without using aggressive chemicals.

The model used for this thesis is the Plasma Cleaner System, Tucano (Gambetti Kenologia Srl). This system is equipped with a 6-liter aluminum chamber, a vacuum pump to evacuate the chamber, and two gas suppliers for gas flow control. It allows automatic matching of all process parameters (vacuum, gas flow, gas pressure, power, and time). The system is equipped with a RF generator (13.56 MHz) with a maximum power of 200 W, making it flexible and useful for achieving either the cleaning or activation of the irradiated surface.

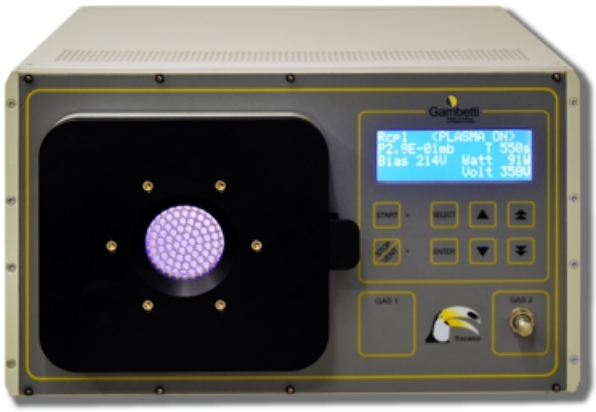

Figure 3.1: Plasma Cleaner System, Tucano (Gambetti Kenologia Srl)

3.2.2. Drop Shape Analyzer

The Drop Shape Analyzer (DSA30) is the instrument used to measure the contact angle in the experiments. It features a movable stage that can be adjusted manually along the x, y, and z axes, and a syringe that moves in the z direction; the movement and the dosing of the syringe is controlled by software. The DSA30 is equipped with a camera, allowing for the capture of videos or pictures of the drop. This enables both dynamic or static measurements of the contact angle.

Figure 3.2: Drop Shape Analyzer, DSA30S.

Contact angle

The contact angle is a fundamental parameter in surface science that provides valuable insights into the wettability and surface energy of materials. The contact angle (θ) is the angle formed at the interface where a liquid meets a solid surface, quantifying the wettability of the solid by the liquid. It is measured through the liquid at the point where the liquid, solid, and gas phases intersect.

Young's equation relates the contact angle to the interfacial tensions between the three phases:

$$\gamma_{SG} = \gamma_{SL} + \gamma_{LG} \cos\theta \tag{3.1}$$

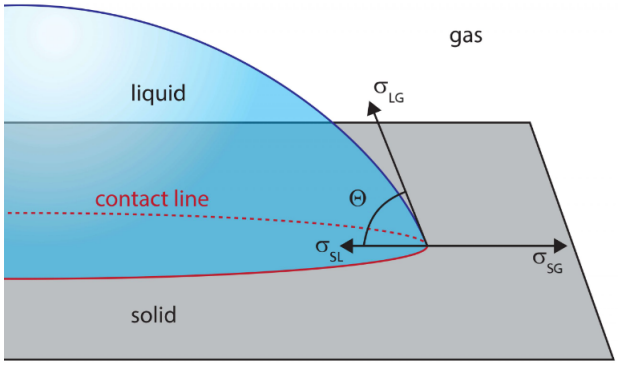

Figure 3.3: Visualization of Young's equation: The contact angle (θ) is the angle formed between the solid-liquid and liquid-gas interfaces.

where:

- γ_{sg} is the solid-gas interfacial tension.
- γ_{sl} is the solid-liquid interfacial tension.
- γ_{lg} is the liquid-gas interfacial tension.
- θ is the contact angle.

In all the experiments, the static contact angle is measured using the sessile drop method. In this method, a droplet of liquid is placed on the solid surface, and the angle formed at the liquid-solid-gas interface is measured using a goniometer. The calculation of the contact angle is performed by the software, which measures the left and right contact angles and provides a mean value between them.

Figure 3.4: This is the image provided by the software of the contact angle measured, in which the left and right contact angles can be observed.

3.2.3. TOF-SIMS

Time-of-Flight Secondary Ion Mass Spectrometry (TOF-SIMS) is one of the few techniques that can provide specific compound identification of molecules on a surface. Conceptually, TOF-SIMS is rather simple: bombardment of a surface by high-energy ions causes the emission of secondary ions, which are mass-analyzed by measuring the time required for the ions to fly from the sample to the detector.

All the measurements performed for this thesis were made at the AGR FMT Physical Lab located in STMicroelectronics, Agrate (MB). The instrument used was an Ion–ToF ToF–SIMS M6. Static SIMS conditions were employed. The ion source was a BiMn-liquid metal ion gun (LMIG) with a potential of 30 keV and a maximum current of 1.3 pA. Spot areas of 200x200 μm^2 were sampled, integrating a dose of 10^{12} $ions/cm^2$. Negative ion mode was analyzed over a mass range of 0–500 amu.

Figure 3.5: Ion–ToF ToF–SIMS M6.

Basic principles

Secondary Ion Mass Spectrometry (SIMS) methods measure charged species emitted from a surface bombarded by high-energy ions. Typically, the most used primary ions are Bi_1^+ and Bi_3^+. The choice of the primary ion is based on surface sensitivity and the type of signals one wants to prioritize. For example, Bi_1^+ has higher analysis depth and prioritize elemental signals, while Bi_3^+ is more superficial, giving higher yields of the complexes studied.

When a primary ion strikes a solid surface, its kinetic energy dissipates through collisional cascades within the near-surface region. This process results in the primary ion being buried below the surface, breaking bonds near the impact site, and ejecting atoms, molecular fragments, and molecules from the top one to three atomic layers.

Most ejected species have no net charge; however, a small fraction will be either positively or negatively charged. Only these charged species (ions) are detected by the mass spectrometer, giving rise to the term "SIMS." There are two working modes of SIMS techniques depending on the primary ion dose:

- Static Mode: If the primary ion dose is below 10^{12} $ions/cm^2$, the probability of two primary ions striking the same location is low. The surface remains unchanged (static) during the measurement, and nearly all ions emitted originate from virgin, unsputtered material, representing the original surface.
- Dynamic Mode: If the primary ion dose exceeds 10^{12} $ions/cm^2$, there is a significant probability that emitted ions will come from a previously sputtered area, not representative of the virgin surface. Dynamic SIMS provides elemental composition typically as a function of sputter depth but does not offer the chemical information that static SIMS does.

In a TOF-SIMS, ions of charge q, typically $\pm e$ (unitary charge), are subjected to an extraction field, V_e, of several thousand volts, imparting each ion with a fixed kinetic energy, E_k. Kinetic energy is given by $E_k = qV_e$, which is also equal to $\frac{1}{2}mv^2$, where m is the mass of the ion and v is the velocity of the ion. Since E_k is constant for all ions, the velocity of each ion is inversely proportional to its mass. Lighter ions reach higher velocities in the extraction field. Hence for a given flight path length, l, the flight time, t, is shorter for lighter ions ($t = \frac{l}{v}$). Heavier ions have lower velocities and travel more slowly. Thus, the mass of any ion having unit charge can be determined from the flight time.[7]

$$m = 2qV_e\frac{t^2}{l^2} \tag{3.2}$$

3.2.4. AFM

Atomic Force Microscopy (AFM), also known as Scanning Force Microscopy (SFM), is a very-high-resolution type of scanning probe microscopy (SPM) aimed at obtaining the topography of a sample with nanometer resolution. The ability to obtain high-precision maps is made possible by the use of piezoelectric positioners, typically one for each x, y, and z dimension, which can move the probe with respect to the sample with subnanometer

precision.

The topographical maps are obtained in a raster scanning fashion, where each pixel in the map is acquired sequentially. The process involves first acquiring all the pixels along a row and then proceeding to the following row. Currently, the use of computers allows for real-time reconstruction of the topographical image. All the analysis performed for this thesis were made with a Solver PRO-M at the Department of Chemistry, Materials and Chemical engineering (DCMC) of Politecnico di Milano. The instrument is provided of two different scanners with a maximum area of 50 μm^2 and 1 μm^2.

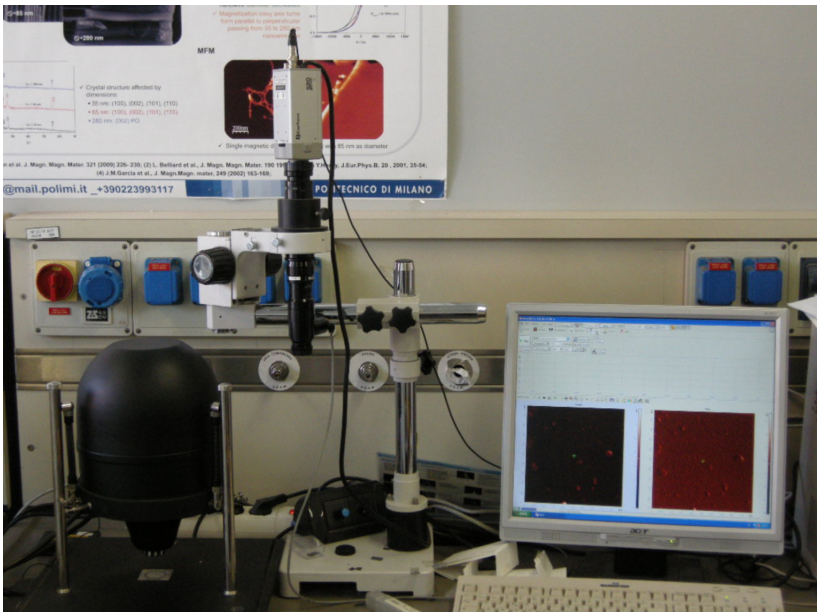

Figure 3.6: Solver PRO-M.

Basic principles

AFM operates by measuring the attractive and repulsive forces acting between the atoms of a sharp tip and those of the sample's surface. The size of the tip determines the lateral resolution of AFM, with imaging-specific tips having radii of less than 10 nm. The tip is attached to a very flexible cantilever, which bends toward or away from the sample in response to attractive or repulsive forces, respectively.

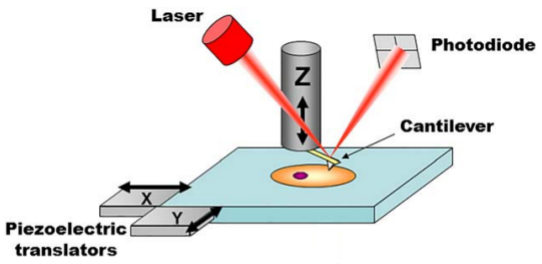

Figure 3.7: Basic scheme of an AFM setup with its most important elements. The tip interacts with the sample, causing the cantilever to bend due to attractive or repulsive forces. This bending is monitored by shining a laser onto the gold-coated backside of the cantilever and measuring the reflected light's position with a four-quadrant photodiode. Three piezoelectric positioners enable nanometer-scale movement of the tip relative to the sample, with the stage moving in the x-y axis and the cantilever in the z axis.

Cantilevers are microscopic, typically tens to hundreds of micrometers in length and width, and are etched from silicon or silicon nitride chips. The macroscopic chip can be firmly attached to a piezoelectric positioner, allowing ultra-precise vertical positioning of the cantilever. Importantly, force-induced cantilever bending and piezoelectric-based cantilever movement occur along roughly the same vertical axis, perpendicular to the sample surface.

In most AFMs, the bending of the cantilever (referred to as deflection) is detected optically. A laser light is reflected from the cantilever and detected by a quadrant photodiode. When the cantilever is undeflected (usually when far from the sample), the photodiode is manually positioned so that half of the laser spot reaches the top quadrants and the other half reaches the bottom quadrants. When properly adjusted, the difference between the photovoltage output by the top and bottom quadrants ($\Delta V = V_{top} - V_{bottom}$) is zero.

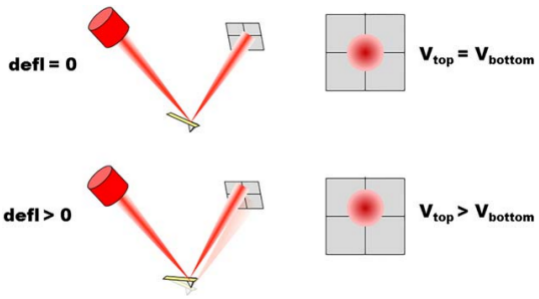

Figure 3.8: Optical-based detection of cantilever deflection. (Top) When the cantilever is undisturbed, the photodiode is manually positioned so that half of the laser spot reaches the top quadrants and the other half reaches the bottom quadrants. (Bottom) When the cantilever deflects, the laser spot shifts slightly on the photodiode, causing different output voltages for the top and bottom quadrants.

When the cantilever interacts with the sample and bends, the laser light is reflected at a slightly different angle, altering the distribution of the laser spot on the quadrants and thus changing the value of ΔV. ΔV is proportional to cantilever deflection (in the small deflections regime), and its sign indicates whether the bending is caused by attractive or repulsive forces. By measuring ΔV, the system monitors the deflection of the cantilever in real-time ($<$0.1 ms readout time) and with high precision ($<$0.01 nm accuracy).

Working modes

To obtain a topographical image using AFM, the tip is brought into contact or near-contact with the surface of interest and raster scanned over it. The AFM system continuously monitors the deflection of the cantilever and adjusts the vertical position of the cantilever in real-time to keep the deflection constant. Through this feedback mechanism, the tip of the cantilever is kept at a constant distance from the sample as it "glides" over it. Contrary to what one might assume, it is the information encoded in the vertical position of the cantilever, rather than its deflection, that is used to reconstruct the topography of the sample. When finely tuned, the deflection of the cantilever remains fairly constant during scanning. This method is widely referred to as "contact mode" imaging.

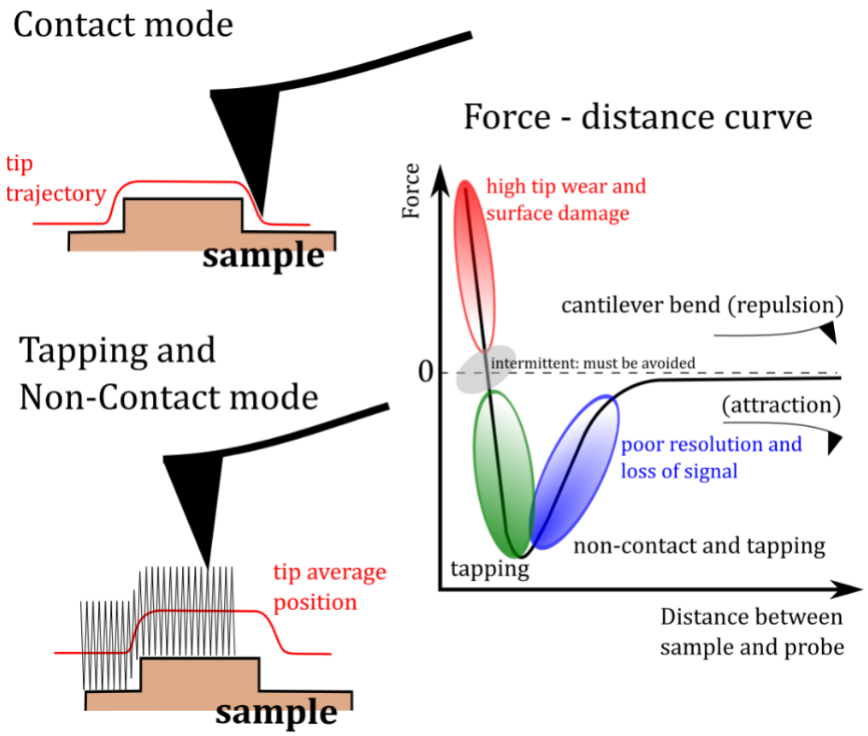

Figure 3.9: The Two Scanning Modes for AFM. (Left) The two scanning modes for AFM are contact and non-contact (tapping) mode. (Right) A force vs. distance graph shows that in contact mode, the principal forces are repulsive, while in non-contact/tapping mode, the principal forces are attractive.

A complementary approach is "tapping mode," in which the cantilever is forced to oscillate near its resonance frequency. When the tip is brought near the sample, the cantilever's resonance frequency changes slightly due to the increased forces acting between the tip and the sample. This effect is observed indirectly by monitoring changes in the amplitude of oscillation at a fixed frequency near the resonance peak. The amplitude of oscillation depends on the distance between the tip and the sample, making it a useful feedback parameter to adjust cantilever height as the topography of the sample changes. In brief, the parameter "amplitude" in tapping mode serves as the counterpart to the parameter "deflection" in contact mode, each being used to drive the feedback loop that adjusts cantilever height positioning during raster scanning.

In tapping mode, the interaction between the tip and the sample is reduced (both in duration and amount of force), making it a gentler approach preferred for imaging biological samples. All AFM imaging modes are based on raster scanning, and thus the time required to acquire an image scales with the number of pixels used.[14]

3.2.5. Q3

Q3 is a device developed by the Silicon Biotech team at STMicroelectronics. It performs time-domain PCR, meaning that all reactions and thermal cycling occur in the same chamber where conditions change over time, without the need to move the solution around the chip. The device is based on a classical implementation, including thermocycling and fluorescence-based optical read-out. The qPCR reactions take place inside a single-use Lab-on-a-Chip (LoC) with multiple wells, each with a capacity of 5 to 15 μL. The same chip hosts a printed metal heater coupled with a calibrated sensor for rapid and accurate temperature control inside the reaction mixture.

(a) Outside view. (b) Inside view. (c) LoC view.

Figure 3.10: Q3 with its LoC.

In its current version, the optical system handles up to four different detection channels, thus supporting multiplexing, i.e., amplifying and detecting multiple target sequences. For each channel, a suitable Light Emission Diode (LED) coupled with an excitation filter ensures excitation. On the sensor side, each wavelength range is detected by a dedicated Complementary Metal-Oxide Semiconductor (CMOS) image sensor, which is coupled with an emission filter.

For the purpose of this thesis, the Q3 device has been modified and simplified. Only the fluorescence-based optical read-out is necessary for the experiments, so the pads for thermal control have been removed. Consequently, the cartridge has also been modified to feature only a sliding holder for the chip, with its surface exposed for acquisitions.

Figure 3.11: Modified Q3 without the thermal control with its simplified cartidge.

Additionally, only channel 1 has been used for the experiments. In channel 1, a blue LED (wavelength: 465–485 nm) is used for excitation, coupled with a single band-pass excitation filter tuned for optimal excitation of the detectable dyes in this channel (460–490 nm). The luminous signal is read out by one CMOS image sensor (produced by STMicroelectronics) per channel. The read-out filters are tuned for optimal measurement of the dyes detectable in channel 1 (515–535 nm). During the experiments, the LED is activated, and photographs of the fluorescent emission from the sample are concurrently acquired.[4]

In the software used to acquire the images, there are three parameters that can be set:

- Exposure time: this parameter sets the duration of the light irradiated by the LED and is set in seconds. Possible values: 0.25, 0.5, 0.75, 1, 2, 4, 8 [s].
- Gain: this is a multiplier parameter that can amplify the signals obtained by the sensor. Possible values: from 1 to 16, with a step of 1.
- Power: this sets the power of the LED light in terms of intensity. Possible values: from 1 to 10, with a step of 1.

In Section 4.3.1, the parameters are reported in triplets in sequence (i.e. 0.5 5 6).

4 | Results

4.1. Overview of the work

DNA biosensors are essential tools for detecting specific genes, viruses, or bacteria, making their development critical for various applications such as medical diagnostics and environmental monitoring. The efficiency of hybridization and the overall performance of the sensor—sensitivity, selectivity, and stability—are closely tied to the quality of the biomodified surface, which involves the immobilization of DNA probes onto a solid substrate. Effective immobilization methods for probe DNA must ensure stable, covalent, and uniform attachment while being cost-effective and scalable. Consequently, the chemistry of self-assembling organosilane molecules for the covalent grafting of DNA probes onto silicon surfaces is a focal point of current research. This thesis aims to thoroughly investigate the deposition of GPTMS (or GOPS) using both liquid phase deposition (LPD) and vapor phase deposition (VPD) techniques, followed by the grafting of amino-terminated DNA onto silicon dioxide surfaces.

The goal is to establish a comprehensive protocol, encompassing the following steps:

1. Cleaning
2. Surface activation
3. Silanization (LPD or VPD)
4. Annealing
5. DNA grafting

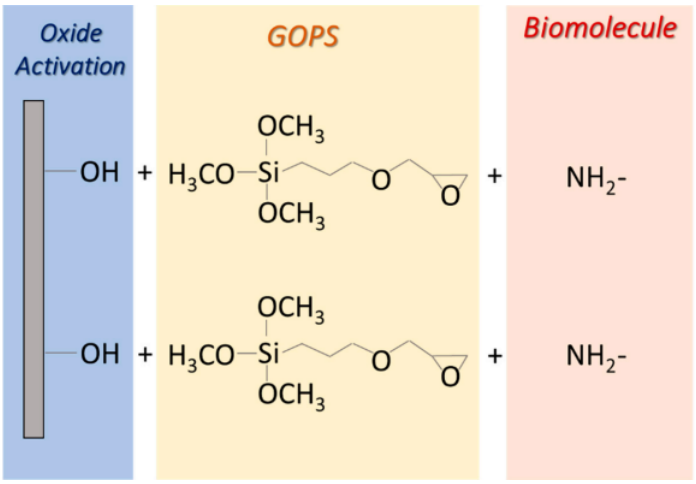

Figure 4.1: Schematic view of GOPS protocol optimized for biomolecule immobilization. The steps in the scheme are progressive, with a cleaning and activation step, silanization and biomolecule grafting.

4.2. Silanization protocol

The goal of developing this protocol is to assess the significance of each step by comparing various protocols and determining the most suitable and reliable one for this application. Literature on GOPS-based silanization protocols reveals a range of methods depending on the application and the substrate involved.

In this study, the substrate examined is a flat silicon substrate measuring 17.65x12.15 mm^2 with a 1 μm thermally grown silicon dioxide layer on top. The simple geometry of the substrate allows for versatility in the choice of deposition methods, enabling the testing of both LPD and VPD without issues. LPD is more appropriate for particles and simple geometries, whereas VPD is better suited for larger and more complex geometries.

4.2.1. Cleaning and activation

A surface cleaning step is essential to remove any contaminants and organic matter that could hinder subsequent silanization. The aggressiveness of this step must be evaluated based on the condition and type of the substrate. Various cleaning protocols are documented in the literature, including solvent immersion in an ultrasonic bath, dry etching in oxygen plasma, and immersion in aggressive media such as piranha solution or base washes.

Below are the main cleaning and activation protocols from the literature for different substrates, including silicon dioxide, silicon nitride, and glass:

- *Silicon dioxide wafers cut into 10 mm × 6 mm pieces using a dicing saw were cleaned with piranha etch solution (70% H_2SO_4 and 30% H_2O_2) for 30 min at 50°C, and then washed with copious amounts of water, followed by ethanol.[33]*
- *Silicon chips were cleaned by sonication in a series of solvents (chloroform, isopropyl alcohol, methanol, and then water). In the case of silicon nitride surfaces, the chip surfaces were activated using oxygen plasma (200W, 1 min). For silicon dioxide surfaces no such treatment was given.[33]*
- *The silicon wafers and glass slides were cut to a size of 1.0x1.0 cm^2. All samples were sonicated for 30 min in soapy water made from deionized water (Milli-Q) and Hellmanex glass cleaner. They were sonicated in deionized water again for 30 min. Samples were then treated with a base wash consisting of 1:1:5 (v/v) 30% H_2O_2 – 28–30 % NH_4OH – distilled water at 80°C for 5 min. The solution was decanted and approximately 10 mL 30% H_2O_2 was used to rinse the silicon wafers and glass slides. The silicon wafers and glass slides were then rinsed with methanol, dichloromethane, and diethyl ether, sequentially. They were stored in an oven overnight at approximately 150°C.[43]*
- *Thermally oxidized wafers were cut in chips with dimensions of 10x10 mm^2. The chips were first dry etched by oxygen plasma. The silicon wafers and glass slides were then rinsed with methanol, dichloromethane, and diethyl ether, sequentially. They were stored in an oven overnight at approximately 150°C.[27]*
- *ITO glass was cut into slides of 1x2 cm^2 in area and ultrasonically cleaned with successive washing of alcoholic KOH, ethanol, and doubly distilled water before use.[24]*
- *The process starts with a surface cleaning step (SC1), performed using an oxidizing solution (H_2O : H_2O_2 : NH_4OH, 5:1:1) at 80°C for 5 min. After rinsing with deionized water, the surface activation (increasing of Si-OH groups) was carried out by treating the substrates with acid solution (HCl : H_2O, 1:7.5) at room temperature for 10 min (SC2). Then, a drying step is carried out at 120°C for 30 min.[34, 39]*
- *Initial cleaning of slides was done in 1:1 $MeOH/HCl$ solution for 30 min with subsequent rinsing in copious amounts of deionized water. After that, the slides were heated in concentrated H_2SO_4 for 2 h and then rinsed in deionized water and boiled in it immediately prior to silanization.[21]*
- *The glass slides were precleaned for 10 min each in acetone, ethanol, and deionized water in an ultrasonic bath; and thereafter activated for 10 min in 1:1:1 hydrochloric acid, hydrogenperoxide, and deionized water. Then, a drying step is carried out at*

120°C for 10 min.[10]

- *Prepare glass slides by washing with acid (5% HCl) for several hours to remove non-binding metal ions, especially sodium, potassium, and calcium. Treatment with a mixture of 25% sulfuric acid and 15% hydrogen peroxide (piranha solution) for about 30 min is done to create a high density of hydroxyl functionalities suitable for silane modification. Glass slides also can be cleaned and washed prior to modification with a silane with DMSO, ethanol, and water, and then etched using 10% NaOH (w/w) in water for 1h.[18]*
- *The glass slides were washed in 1 M NaOH, 1 M HCl, dH_2O and methanol in turn.[45]*

Two cleaning methods were tested and evaluated in this case. The effectiveness of the cleaning step has been evaluated through contact angle measurements:

- Ultrasonic bath/spin coating in a series of solvents
- Acidic wash with piranha etch solution

Here is reported the precise protocol for both cleaning methods:

Piranha etch solution protocol

Table 4.1: The protocol described here involves an acidic wash using a piranha solution. The mixture consists of sulfuric acid and hydrogen peroxide in a 3:1 ratio. No more than 60 mL of piranha solution was used to prevent an excessively exothermic reaction, which would otherwise require a cooling system.

	Materials and methods	Time	Temperature
Immersion	$H_2SO_4 : H_2O_2(30\%)$ 3 : 1	30 min	$\sim$ 100°C
Immersion	H_2O	5 min	RT
Dehydration bake	Hot plate	5 min	135°C

Solvents cleaning protocol

Table 4.2: The protocol involves an ultrasonic bath in acetone followed by successive washes using a spin coater with isopropyl alcohol.

	Materials and methods	Time	Temperature
Ultrasonic bath	Acetone	5 min	RT
Spin coating	Isopropyl alcohol	10 s x 3	RT
Dehydration bake	Hot plate	5 min	135°C

The two cleaning protocols were conducted on identical substrates to observe changes in contact angles. In both methods, a dehydration bake was performed to remove excess water or solvent from the substrate, ensuring more accurate and reliable measurements afterward.

It's important to note that the piranha solution not only cleans the substrate of contaminants and organic matter but also activates the surface by creating hydroxyl terminations. Therefore, the activation step is included in this cleaning method. To compare the two cleaning methods using contact angle measurements, the piranha solution protocol should be compared with the solvent cleaning method integrated with its activation protocol. So, here is the activation method tested after the cleaning step with solvents:

Plasma activation protocol

Table 4.3: The protocol for plasma cleaning involves setting the parameters for time, RF power, pressure, and the composition of the gases. After surface activation, the substrates are ready for the next steps.

	Gas composition	Time	RF power	Pressure
Oxygen/Ar plasma	$90\%O_2/10\%Ar$	240 s	180 W	1 mbar

The parameters chosen for plasma etching were fairly standard for surface atomic cleaning of residual organic species and subsequent activation with hydroxyl terminations. Although 120 seconds would have been sufficient, the protocol doubles this time to ensure complete cleaning and activation.

Introducing 10% argon helps physically remove surface species through atomic collisions, while oxygen, which constitutes the majority, chemically etches the surface species. The

excited oxygen bonds with carbon or hydrogen atoms, producing CO_x and H_2O, which vaporize and are pumped out of the system. After the treatment, the surface is atomically cleaned with hydroxyl terminations. Consequently, contact angle measurements should show very low contact angles due to the high hydrophilicity. Regarding piranha cleaning and activation, the resulting contact angles were notably lower than those measured for substrates cleaned with the solvent cleaning protocol mentioned in Table 4.2. However, performing multiple cleanings with different solutions resulted in varying and inconsistent contact angles.

As shown in Figure 4.2, the piranha cleaning and activation resulted in a lower mean contact angle compared to just solvent-cleaned substrates, but with a high standard deviation. This suggests that while the cleaning effectively removed contaminants from the substrate, it may not have generated enough hydroxyl terminations on the surface. This can be inferred by comparing the contact angle values obtained after the plasma etching protocol. Substrates treated with plasma etching were so hydrophilic that measuring the contact angles was challenging.

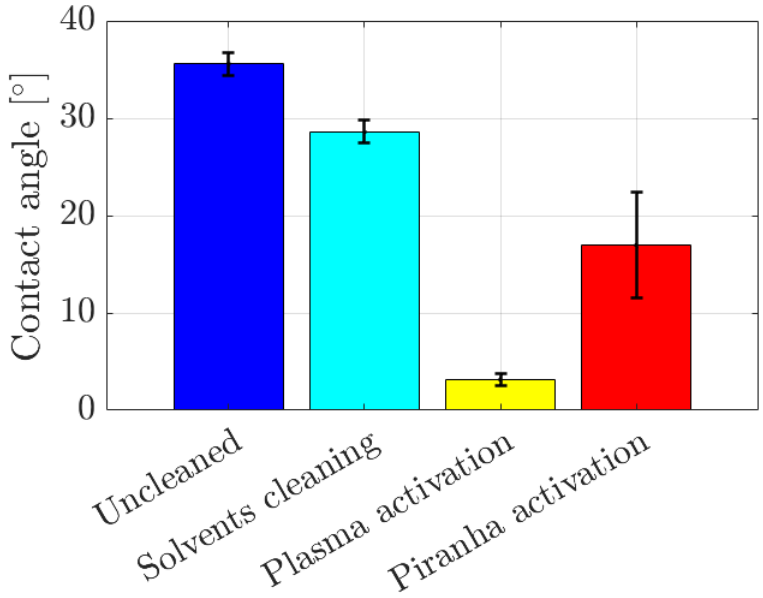

Figure 4.2: A comparison between the contact angles after each step of the silicon dioxide substrate. There is an evident decrease in the contact angle with the cleaning and activation step. The plasma activation has the strongest effect, with the surface being highly hydrophilic.

Furthermore, piranha solution is quite dangerous to use, but it can be very useful for heavily contaminated samples. However, the substrates used in the experiments were taken from a wafer and were practically clean. This is evident from the contact angle

of approximately 35°, indicating that the substrate is quite hydrophilic and requires only mild cleaning. Therefore, the chosen protocol includes solvent cleaning followed by plasma activation. This approach avoids the use of aggressive solutions like piranha solution, which can be hazardous.

4.2.2. Silanization

After the plasma treatment, the substrates are ready to be silanized. At this point, the surface is covered with hydroxyl terminations, ready to couple with GOPS molecules. This step involves many variables that should be evaluated to optimize the protocol. The controlling parameters depend on the silanization method, which can be either LPD or VPD.

The controlling parameters for LPD include:

- Silanization time:
  - Typical range: 30 minutes to several hours.
  - Longer reaction times can increase the likelihood of multilayer formation.
- Temperature:
  - Typical range: Room temperature to 80°C.
  - Higher temperatures can accelerate the reaction but may also lead to unwanted side reactions.
- Solvent used:
  - Common solvents: ethanol, toluene, chloroform, acetone.
  - The choice of solvent can affect the solubility and reactivity of the silane.
- Concentration:
  - Typical range: 0.1% to 5% (v/v).
  - Higher concentrations can lead to multilayer formation.
- pH:
  - Adjusting the pH of the solution can influence the hydrolysis and condensation reactions of the silane.
  - Slightly acidic or neutral pH is generally preferred.

- Humidity:

  - Typical range: RH $< 40\%$.

  - A certain amount of humidity could alter the silanization due to the formation of silanols that can interact with each other.

- Mixing velocity:

  - A mixing velocity that is too high could hinder the silanization process, so it should be properly tuned.

The controlling parameters for VPD include:

- Silanization time:

  - Typical range: 30 minutes to some hours

  - Longer reaction times can increase the likelihood of multilayer formation.

- Temperature:

  - Typical range: 50°C to 150°C.

  - Higher temperatures can accelerate the reaction but may also lead to unwanted side reactions.

- Volume of GOPS:

  - An higher volume of GOPS inside the chamber could lead to multilayer formation.

- Humidity:

  - Typical range: RH $< 40\%$.

  - A certain amount of humidity could alter the silanization due to the formation of silanols that can interact with each other.

- Pressure:

  - Typical range: 1 to 200 Torr.

  - Lower pressures can help in achieving a more uniform monolayer by reducing the likelihood of multilayer formation.

A small variation in any of these parameters could significantly alter the quality of the GOPS SAM, so they need to be properly tuned and maintained constant throughout the entire silanization process. For LPD, there are more controlling parameters compared to

VPD, which might suggest that LPD is more difficult to achieve. This is partially true, as silanizations are typically performed in VPD; however, both methods have pros and cons that should be evaluated.

LPD is generally simpler to implement and does not require special equipment. It can be used with a wide range of solvents and reaction conditions. However, LPD tends to favor the formation of multilayers, especially if the silane concentration is high or if the reaction time is prolonged.

On the other hand, VPD allows for more uniform coverage of the surface, as silane molecules can freely diffuse and reach all areas of the surface. VPD tends to favor the formation of monolayers because silane molecules in the vapor phase are less likely to aggregate and form multilayers compared to those in the liquid phase. However, VPD requires specific equipment such as vapor reaction chambers, which can be more expensive and complex to manage. Additionally, the reaction conditions, including temperature and pressure, must be carefully controlled to achieve optimal results.

The final objective is to coat the ISFET gate with GOPS so that when ssDNA binds with GOPS and further hybridization occurs, electrical detection is possible. Since the sensitivity of the ISFET is inversely proportional to the thickness of the GOPS layer, a thinner layer results in higher sensitivity.

4.2.3. LPD

The protocol developed for LPD is based on various protocols found in the literature. Some of the parameters have been evaluated by fixing all other parameters except the one being considered.

Below are some of the protocols found in the literature:

- *The chips were derivatized in 10% GOPS in H_2O (v/v) at 90°C for 3 h. The pH of the mixture was maintained below 3 with concentrated HCl (1 M).[33]*
- *For substrate modification with GOPS the slides were suspended in dry toluene containing 1% silane at 80°C for 4-6 h. Then they were washed thoroughly with ethylacetate and used immediately.[27]*
- *A silanization reaction (SIL) is carried out by immersion for 4 h in toluene and 1% GOPS, under a nitrogen atmosphere. This step is performed using Glovebox equipment under controlled humidity level of 0.1 ppm and oxygen level of 0.3 ppm at 20°C. The substrates were, then, rinsed with toluene and dried under vacuum. A*

final curing process at 120°C for 30 min was executed.[34, 39]

- *The silanization was performed for 6–8 hr at 70°C in 10 mM GOPS in dry toluene. After rinsing the GOPS-silanized probes in toluene, ethanol, and deionized water, the substrates were dried under a nitrogen flow and ready for further processing.[10]*
- *Prepare a GOPS solution in o-xylene or 95% ethanol at a concentration of 2% (v/v). If the organic solvent is used, add 2 mg/ml N-ethyldiisopropylamine (DIPEA) as base. Immerse the glass slides in the GOPS solution and mix by stirring. React at 37°C (for the ethanol solution) or 55°C (for the o-xylene solution) for at least 5-6h with mixing. Wash slides thoroughly with solvent and then dry in an oven at 135°C for 1h (explosion-proof oven). The slides are now ready to couple ligands through their epoxy groups.[18]*
- *A dried 500-mL two-necked round-bottomed flask containing a stir bar and the silicon wafers or glass slides was flushed with Ar gas. Dried toluene (250 mL) was then added to the flask under Ar gas. GOPS (80 mL) and Hunig's base (2.4 mL) were then transferred sequentially to the flask under Ar gas. The relative amounts of toluene, GOPS, and Hunig's base were approximately 100:30:1 (v/v). A dried condenser was flushed with Ar and was then attached to the round bottomed flask. The stopcocks and joints were sealed with Teflon tape. The reaction was stirred and heated at 110°C for 24 h. The samples were then sonicated for 15 min in methanol twice, and then were rinsed with dichloromethane and diethyl ether. The samples were stored in a desiccator under vacuum.[43]*
- *A 95% ethanol-5% water solution was adjusted to pH 4.5-5.5 with acetic acid, and GOPS was added with stirring to yield a concentration of 1% (v/v) for use in the silanization of the ITO surface. ITO glass slides were taken from storage in doubly distilled water and immediately dipped into the solution. This procedure kept hydrocarbon contamination to a minimum and ensured that the slides remained completely wettable when immersed in theaqueous silane solution. A reaction time of 30 min was used to allow for hydrolysis and silanol formation. After this period, the glass slides were removed and rinsed free of excess silane solution by dipping briefly in ethanol. Curing of the silane layer was carried out for 1 h at 100°C in an oven. The surface-modified ITO glass (GOPS-ITO) slides were then washed with copious amounts of doubly distilled water and dried under reduced pressure.[24]*
- *The samples were first immerged in 2% GOPS in ethanol at 37°C and stirred for 6 h, then annealed at 135°C for 1 h in air.[11]*

- *The cleaned slides were put into a freshly prepared solution of 1.5% GOPS and 95% ethanol for 50 min, then dipped in 95% ethanol for 1 min to remove the excessive silane and dried at 80°C in a vacuum oven.*

Based on all the protocols reported here, a new protocol has been developed by combining the most significant points. This new protocol was subsequently tested to verify the effectiveness of the silanization through contact angle measurements, AFM surface characterization, and TOF-SIMS analysis.

Here is the first protocol, to be added to the cleaning and activation steps previously discussed in section 4.2.1, put to the test:

LPD

Table 4.4: The protocol described here outlines the first LPD protocol developed. The silanization steps include immersion in a solution of 2% GOPS in ethanol with constant mixing. The samples are then washed in fresh ethanol to remove any unbound GOPS from the surface. Finally, an annealing step is performed to remove excess ethanol and humidity and to cure the GOPS SAM.

	Materials and methods	Time	Temperature
Immersion with constant mixing	2% GOPS in ethanol	6 h	37°C
Washing	Fresh ethanol	5 min	RT
Annealing	Hot plate	1 h	135°C

First LPD trials

After the initial trials, the silanized samples were first analyzed using contact angle measurements to verify an increase in contact angle due to the lower surface tension. After the activation step, the contact angle is very low due to the hydroxylated terminations of the surface. Therefore, a negative control of a substrate exposed to the same LPD protocol but without GOPS in the solution is necessary (0% GOPS in ethanol). The two samples, the silanized sample and the negative control, were then tested, and their contact angles were measured.

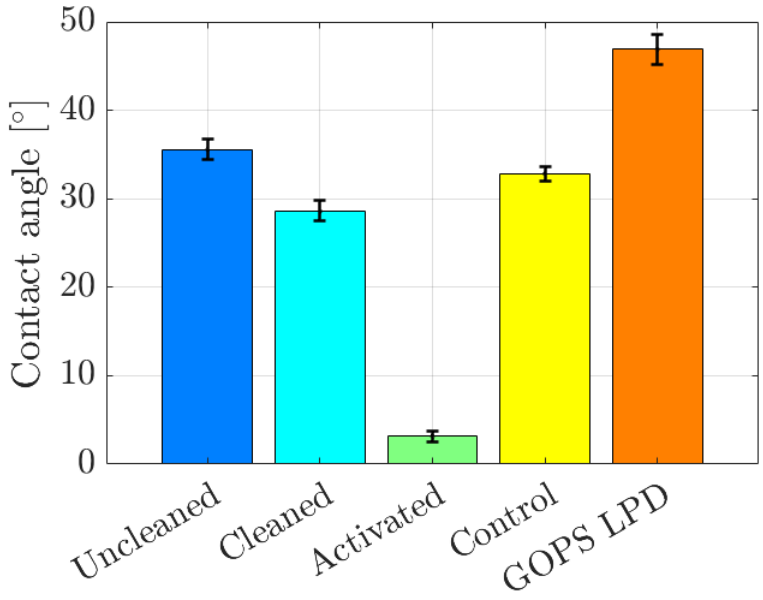

Figure 4.3: The contact angles at each step of the substrate's lifecycle were measured to observe the evolution of the contact angles. The first three bars give the contact angles of an uncleaned, cleaned and activated substrate respectively. The "GOPS LPD" sample followed the standard LPD protocol. A "Control" sample followed the LPD protocol with 0% GOPS in the solution.

In Figure 4.3, the mean contact angle from four drop measurements on a single substrate is reported for each step of the LPD protocol. Multiple drops were measured on the same substrate to verify the consistency of the values and the deviation from the mean value. This deviation is represented by the error bars on each bar in the histogram. The larger the error bar, the greater the standard deviation.

The "GOPS LPD" sample showed an higher contact angle due to the deposition of the GOPS SAM, with a mean value of 46.88°, which is consistent with values obtained in the literature using a similar protocol [11]. The "Control" sample returned to values intermediate between the uncleaned and cleaned phases.

Three additional experiments were conducted to observe how varying a single parameter, while keeping all others fixed, could alter the contact angles:

1. Variation of silanization times and annealing effect
2. Variation of GOPS concentration in the solution
3. Variation of solvent for the solution

Silanization time and annealing effect

This experiment was conducted three different times to ensure consistent results. Additionally, the effect of annealing was evaluated in these tests. Eight different substrates followed the same LPD protocol (Table 4.4) up to the activation step. Four of them continued until the annealing step, while the other four stopped at the ethanol wash phase with a quick heating step to evaporate the ethanol, skipping the annealing step. Each of the two sets of samples then followed the protocol with four different silanization times: 1, 3, 6, and 24 hours. The contact angles of all eight samples were subsequently measured.

Table 4.5: Summary of the experiment set-up.

Sample	Silanization time [h]	Annealing
1	1	Yes
2	3	Yes
3	6	Yes
4	24	Yes
5	1	No
6	3	No
7	6	No
8	24	No

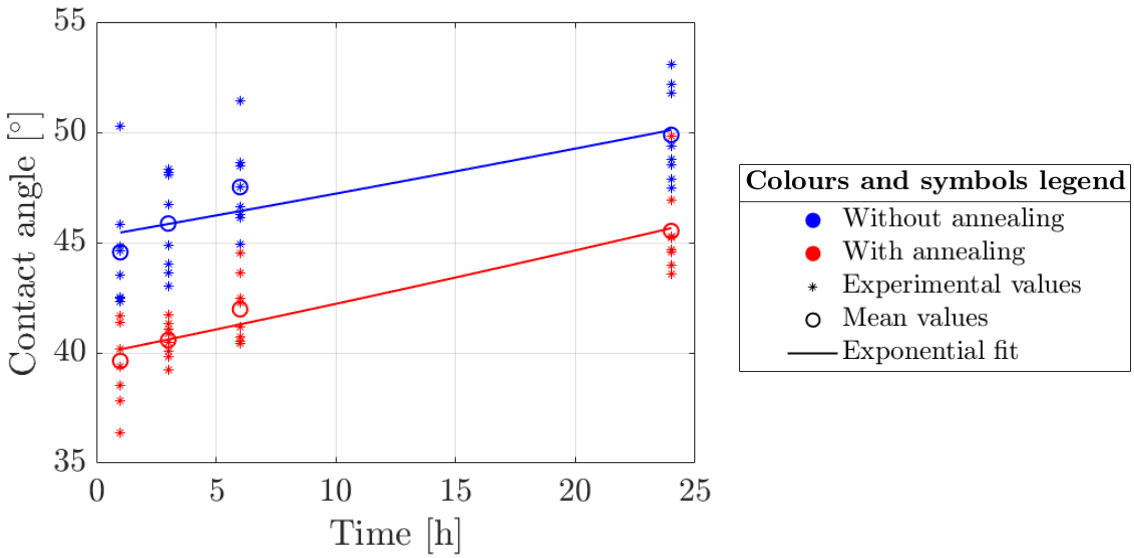

Figure 4.4: Experiment 1 - Contact angle vs silanization time with annealing effect.

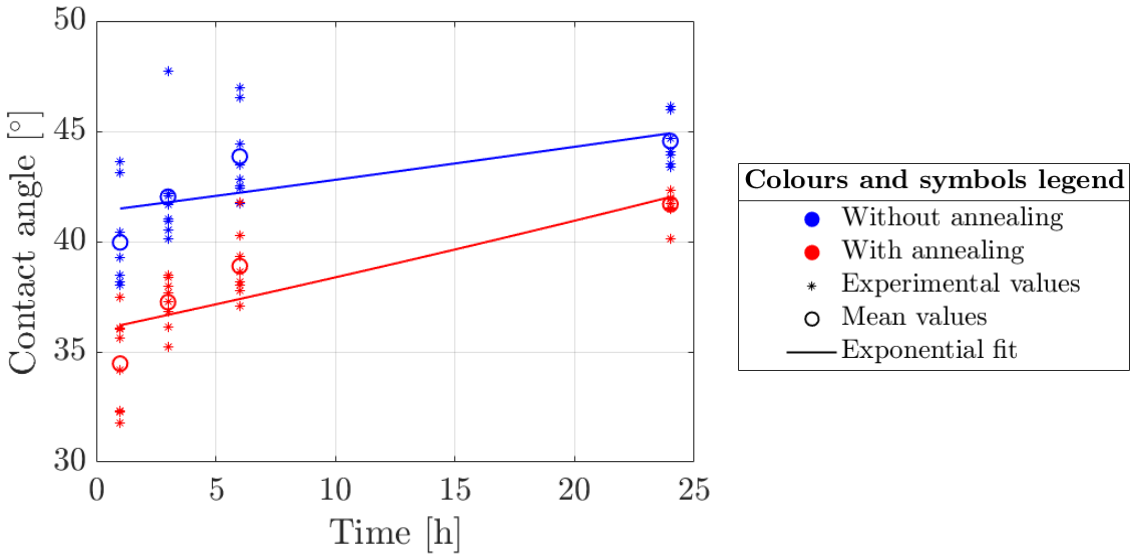

Figure 4.5: Experiment 2 - Contact angle vs silanization time with annealing effect.

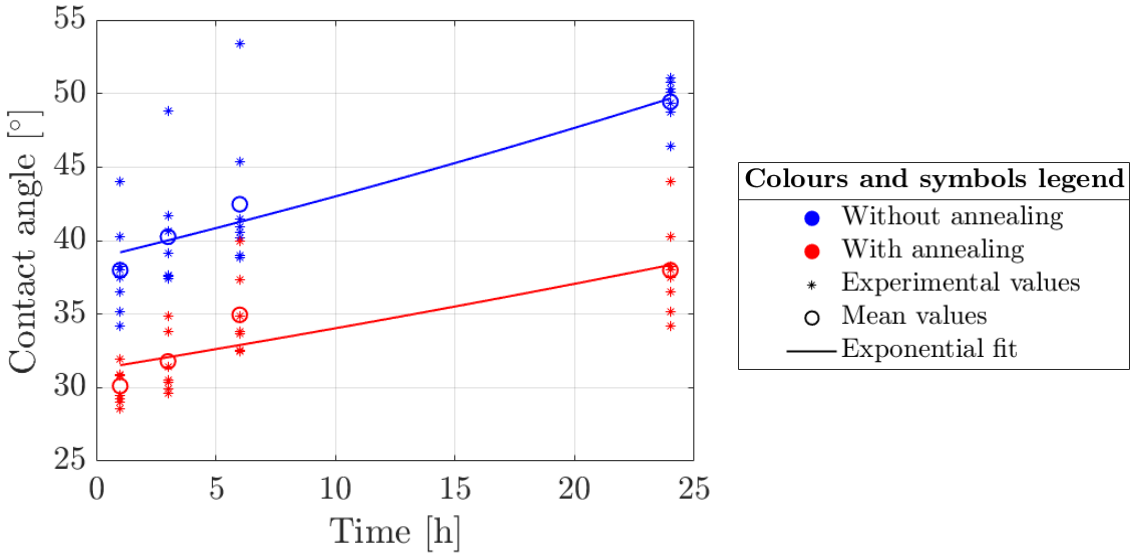

Figure 4.6: Experiment 3 - Contact angle vs silanization time with annealing effect.

Figures 4.4, 4.5, and 4.6 represent three sets of the same experiment conducted at different times. It can be seen that the curves, which are an exponential fit of the mean values of the 8 contact angles taken from a single substrate, all exhibit the same trend. This indicates good repeatability of the experiment and reliable results.

Firstly, there is an increasing trend with silanization time, indicating that longer times result in higher silane density on the surface. There is also a consistent difference in

contact angles between samples with and without annealing. This is because the annealing process enhances the cross-linking and polymerization of the silane molecules, leading to a more uniform and hydrophilic surface. The lack of thermal treatment can result in a less uniform silane layer with more surface roughness and irregularities, which can increase the contact angle. Additionally, the elevated temperature helps in the evaporation of any residual solvents, by-products, or water that might be present from the silanization process. These substances can interfere with the silane bonding process and subsequently disturb the measurements, leading to higher contact angles.

However, an important observation can be made from the three experiments. The contact angle values, in general, are not always the same. For example, taking the mean contact angle values after 6 hours of silanization time for the annealed substrates in all three experiments, they are 41.98°, 38.89°, and 34.95°, respectively. These values are progressively lower, indicating that the efficiency of the silanization decreased over time. The explanation for this behavior could lie in the solvent used, which is ethanol as reported in the protocol in Table 4.4. The solvent used for the three experiments was always the same, and it is possible that the flask became contaminated after each experiment, for example, with humidity. The presence of water or other contaminants could interfere with the silanization, hindering its efficiency and reducing the silane density on the surface. This is also confirmed by the fact that the contact angle value reported in Figure 4.3 is higher and was taken from an experiment conducted before these three experiments with the same ethanol flask. This was one of the first experiments done, and the ethanol in the flask was pure and anhydrous, resulting in higher contact angles and higher silanization efficiency.

Concentration effect

In this experiment the only parameter that is varying is the concentration while the other all are fixed and equal to the LPD protocol described in Table 4.4. The GOPS concentration taken in consideration varied from 0% to 5% with a step of 1% between each experiment. Ideally, the higher is the concentration the higher should be the density of the GOPS layer along with its efficiency and this was in fact the trend obtained with the experimental results.

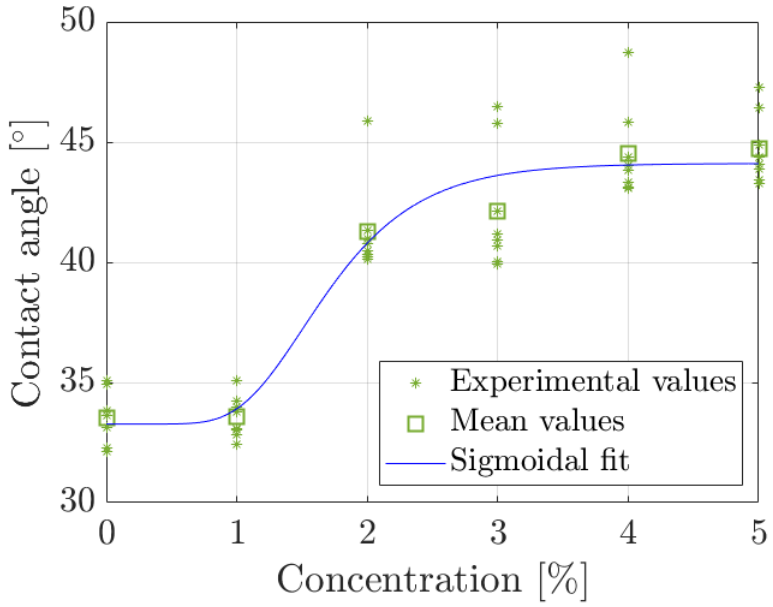

Figure 4.7: The graph shows how the contact angle varies depending on the GOPS concentration in the solution. The fitting curve is a sigmoidal fit that interpolates the mean values of the experimental results. For each concentration value, 8 experimental contact angles were measured per substrate.

The experimental results in Figure 4.7 confirm what one would expect from this experiment. There is an increased contact angle as the GOPS concentration increases. However, it can be noted that the trend remains quite constant for very low concentrations ($< 1\%$) and approaches saturation asymptotically for concentrations above 2%. There is an intermediate range, between 1% and 2%, where there is an abrupt increase in the contact angle. This is likely due to the concentration becoming high enough to ensure a good silane density on the surface, which is achieved at higher concentrations. Therefore, a too low GOPS concentration does not guarantee a sufficient density on the surface. On the other hand, higher GOPS concentrations ensure high silanization densities, but there could be the formation of GOPS multilayers, resulting in a non-homogeneous surface density.

This experiment confirms that a 2% GOPS concentration, which was already the choice in the developed LPD protocol, is a good choice from the perspective of silane density, as it guarantees a good contact angle with a lower probability of forming multilayers.

Solvents effect

For the experiments conducted in the previous sections, ethanol was always used. However, acetone and toluene were also tested to observe how the contact angle would change. For all tested samples, the GOPS concentration remained consistently at 2%.

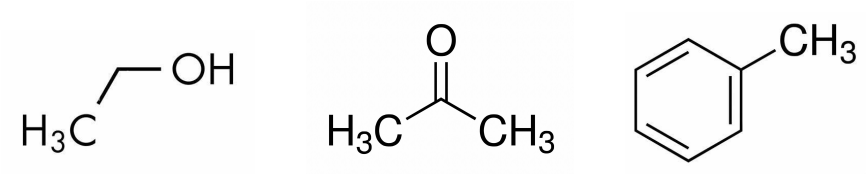

(a) Ethanol (b) Acetone (c) Toluene

Figure 4.8: Chemical formula of the three solvents used in the LPD protocol.

In all the experiments performed, the highest contact angle achieved with ethanol was 47°. With acetone, the highest contact angle reached was 51°, and with toluene, it was 56°.

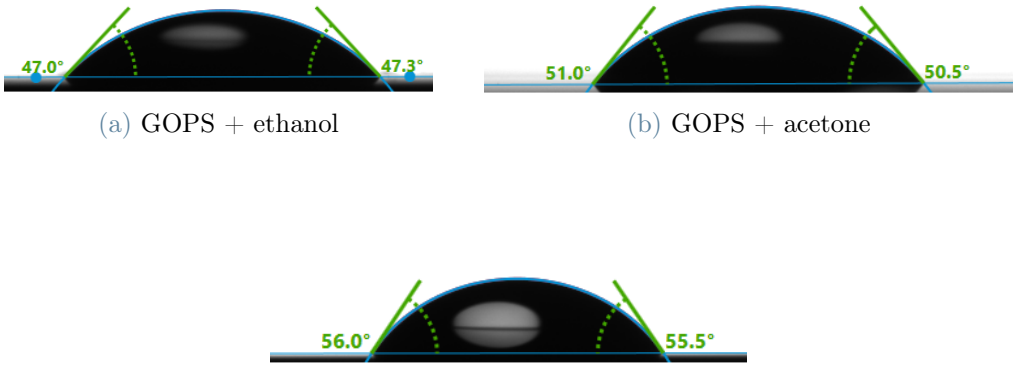

(a) GOPS + ethanol (b) GOPS + acetone

(c) GOPS + toluene

Figure 4.9: The highest contact angle measured with the three different solvents.

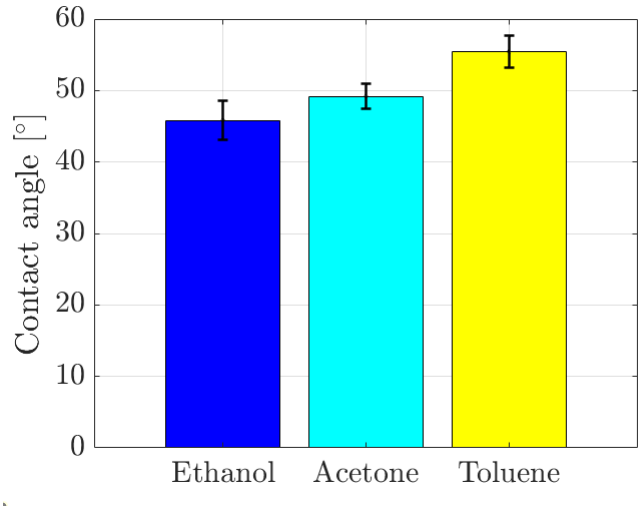

Figure 4.10: Comparison between the three solvents used for the LPD protocol. Eight drops were measured on all samples, and the mean values are displayed with relative error bars. The deviation from the mean values is fairly consistent among the three samples.

As shown in Figure 4.10, there is an impact on the silanization effectiveness based on the chosen solvent. This is because the solvent must have minimal interaction with the GOPS molecules, preventing the formation of silanols that could bind with other GOPS molecules in the solution. Consequently, the resulting contact angles are consistent with what one might expect by examining the chemical formulas of the solvents.

Toluene, being a non-polar solvent, has the least interaction among the three solvents, resulting in higher silanization densities. This minimal interaction prevents premature hydrolysis and condensation of the GOPS molecules, allowing them to react more effectively with the surface rather than with each other. Higher contact angles observed with toluene indicate more effective silanization, as a well-silanized surface is typically more hydrophobic.

TOF-SIMS analysis

A good indication to see if the surface is correctly silanized is to chemically characterize the surface. TOF-SIMS performs well in this regard, as it can detect the presence of GOPS on the surface. TOF-SIMS is one of the spectrometry techniques that excels in surface analysis. Therefore, one should first look for the characteristic footprints of the molecule being searched for, as reported in Table 4.6.

GOPS ion fragments

Table 4.6: Expected ion fragments of GOPS-modified Si wafer.[43]

Mass [m/z]	Species
1	H^-
17	OH^-
25	C_2H^-
28	$Si^-/C_2H_4^-$
31	CH_3O^-
41	C_2HO^-
43	$C_2H_3O^-$
59	$C_2H_3O_2^-$

In Figure 4.11, the results of the analysis are presented. Two samples were tested: a GOPS-treated sample, which fully followed the LPD protocol reported in Table 4.4, and a control sample, which followed the protocol up to the activation step. For each sample, two primary ions were used to determine if there were any differences in the resulting spectrum.

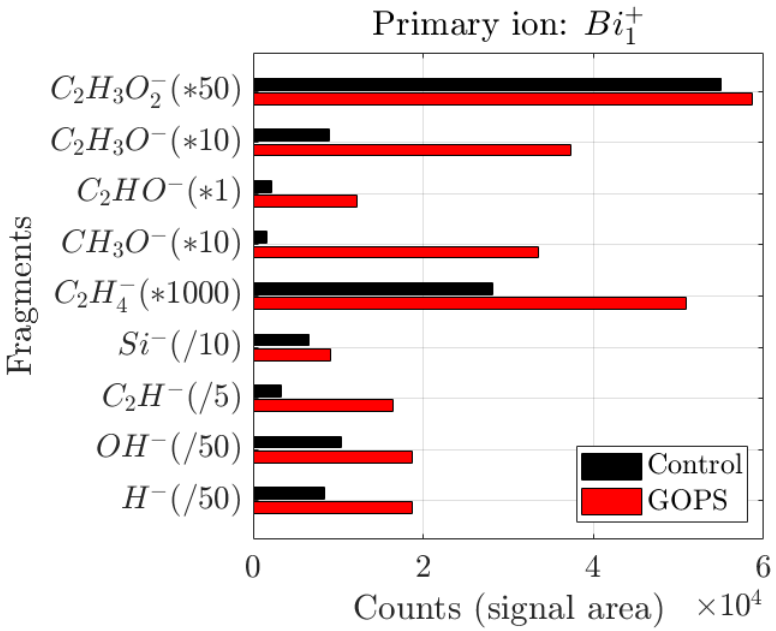

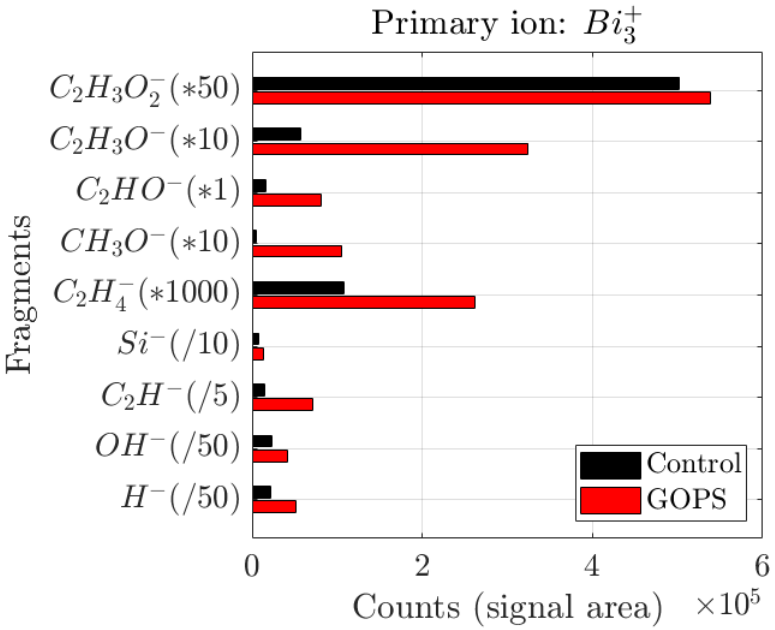

Figure 4.11: Comparison between the two primary ion sources on the same samples. Each fragment has been normalized to produce a more readable and comprehensible histogram.

The results of the experiments indicate that both Bi_1^+ and Bi_3^+ gave similar results in terms of the counts of each fragment. As stated in Section 3.2.3, Bi_1^+ has a higher analysis depth and prioritizes elemental signals, while Bi_3^+ is more superficial, providing higher yields of the complexes studied. Although the counts per signal area differed in magnitude between the two primary ions, the ratio of GOPS to the control sample remained consistent.

Moreover, there is an evident abundance of the fragments typical for GOPS in the GOPS sample, indicating the effectiveness of the silanization protocol.

AFM analysis

AFM is a powerful technique used to analyze the topography and surface properties of materials at the nanometer scale. This capability is particularly useful for comparing a silanized surface to a control sample without any treatment. In an ideal scenario, where a perfect monolayer is formed, the surface roughness of the silanized sample should be comparable to that of the untreated sample, or at most, slightly higher. This is because GOPS molecules arrange themselves on the surface with their functional groups exposed to the environment, forming an orderly arrangement. The steric hindrance in the x and y planes is typically around 1 nm, while in the z direction, it should be even less than 1 nm.

AFM can provide detailed insights into the uniformity and consistency of the silane layer. By measuring the surface roughness and morphology, we can assess the quality of the silanization process. Any significant deviations in roughness could indicate incomplete or uneven coverage, which might affect the surface's intended properties.

The parameters taken into account for the AFM analysis are:

Table 4.7: AFM parameters considered, along with a brief explanation of each parameter.

Parameter	Explanation
Average roughness, Sa	This is the arithmetic mean of the absolute values of the surface height deviations measured from the mean plane. It is a common measure of surface roughness.
Root mean square, Sq	This is the root mean square of the surface height deviations from the mean plane. It is another measure of surface roughness that gives more weight to larger deviations.
Surface skewness, Ssk	This is a measure of the asymmetry of the surface height distribution. A positive value indicates a surface with more peaks than valleys, while a negative value indicates more valleys than peaks.
Coefficient of kurtosis, Ska	This is a measure of the "peakedness" of the surface height distribution. A value greater than 3 indicates a distribution with sharper peaks and deeper valleys than a normal distribution.
Entropy	This is a measure of the randomness or complexity of the surface texture. Higher entropy values indicate more complex surface structures.

A GOPS-treated sample, silanized using the LPD protocol described in Table 4.4 with acetone as the solvent, and a control sample (untreated) were tested with AFM. The results of the AFM analysis revealed significant differences in surface topography and roughness between the two samples.

Table 4.8: The AFM results of an untreaded sample (Control) and a GOPS LPD-treated sample.

Parameter	Control	GOPS LPD
Sa	0,0919823 nm	0,457242 nm
Sq	0,132599 nm	0,575694 nm
Ssk	1,03	0,341978
Ska	5,71842	2,79143
Entropy	2,08528	4,25117

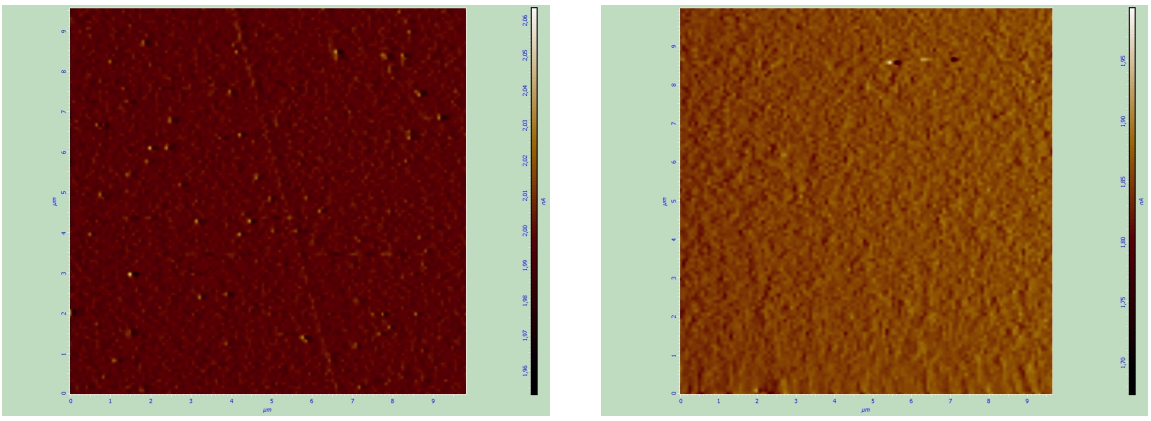

(a) Control (b) GOPS LPD

Figure 4.12: The AFM topographic images of the two surfaces.

In Table 4.8 are reported the values of AFM results of the two samples. The two most important values are the first twos; the average roughness and the root mean square. The values for both average roughness and root mean square increased for the GOPS-treated sample, indicating that the GOPS layer has increased the surface roughness, which is an indication of successful silanization. The lower value of surface skewness indicates that the GOPS-treated sample has more valleys than peaks. In contrast, the control sample revealed sharp peaks due to impurities and surface scratches. The reduction in skewness is another indication of successful silanization. Regarding the coefficient of kurtosis, the GOPS-treated sample exhibited fewer pronounced peaks and valleys, indicating a sufficient GOPS layer density. Finally, the higher entropy in the GOPS-treated sample indicates increased surface complexity, suggesting the presence of an additional molecular layer that was absent in the control sample.

In addition to this experiment, three other GOPS-treated samples were analyzed to observe how silanization progresses over time. Specifically, three silanization durations were

studied: 1 hour, 3 hours, and 6 hours. The results obtained from the AFM analysis are as follows.

Table 4.9: The AFM results of an untreaded sample (Control) and a GOPS LPD-treated sample with different silanization times.

Parameter	Control	GOPS 1 hour	GOPS 3 hour	GOPS 6 hour
Sa	0,0919823 nm	0,802579 nm	0,729417 nm	0,457242 nm
Sq	0,132599 nm	0,933414 nm	0,919311 nm	0,575694 nm
Ssk	1,03	0,0822667	0,375017	0,341978
Ska	5,71842	-0,980332	3,96344	2,79143
Entropy	2,08528	4,88397	4,904	4,25117

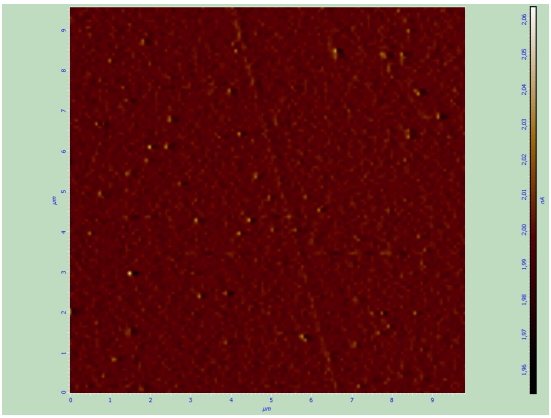

(a) Control

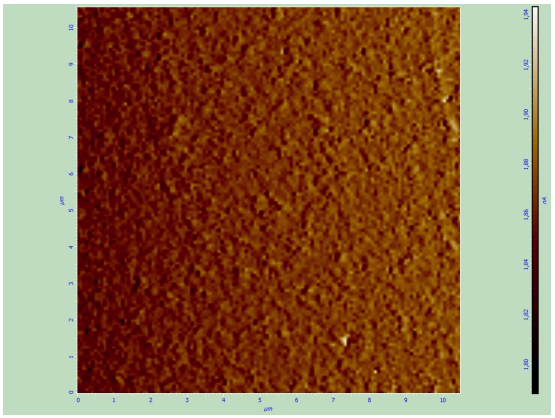

(b) GOPS 1 hour

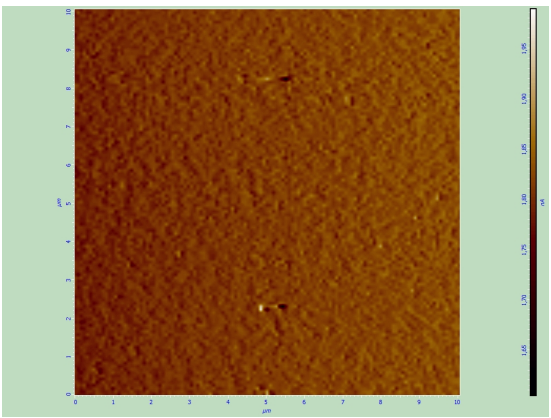

(c) GOPS 3 hours

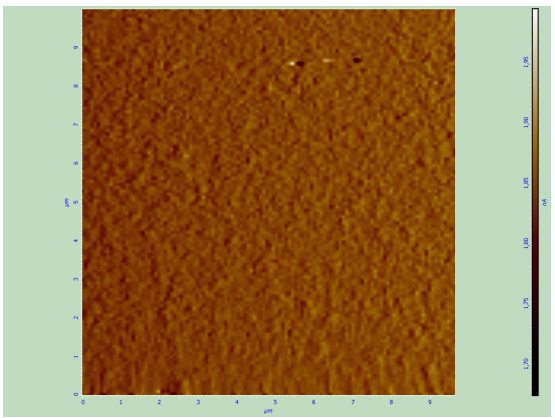

(d) GOPS 6 hours

Figure 4.13: The AFM topographic images of the four surfaces.

Similar assumptions can be made for this experiment. Generally, for Sa and Sq, there is

an increased value for the GOPS 1-hour sample compared to the control, and progressively lower values for the GOPS 3 hour and 6 hour samples, indicating that silanization progresses over time. This is because surface roughness decreases as the GOPS density increases. Regarding Ssk and Ska, the GOPS 1 hour sample showed low values, indicating the presence of many valleys; this is because, at this silanization time, the GOPS molecules are depositing as islands, making the surface more full of valleys than sharp peaks. Finally, for entropy, there is a decreasing trend with silanization time, suggesting that the surface complexity decreases and a uniform layer forms.

4.2.4. VPD

VPD has also been tested to observe any differences in the results compared to LPD. The VPD protocol was developed by comparing various protocols found in the literature. Below are some of the protocols found in the literature:

- *Silanization is carried out by depositing GOPS in vapor phase and in anhydrous conditions at 100°C for 1 h, followed by an ethanol rinsing and a heat treatment at 135°C for 1 h in order to remove the remaining water, giving rise to a SAM on the surface of the samples.[12]*
- *The vapor phase silanization was realized under two different conditions, either at reduced pressure or at elevated temperature (and ambient pressure). In a desiccator under a primary vacuum, the samples were placed above a container with 1 mL of GOPS in such a way that their surface was exposed to vaporized molecules for 1 h at room temperature. Then the samples were annealed at 135°C for 1 h in air. In these cases, the annealing was followed by a rinsing using ethanol. At elevated temperatures, the samples were placed close to a container with 150 mL of GOPS inside a sealed chamber under nitrogen atmosphere (humidity rate: 1%). Then the sealed chamber was placed in an oven at the desired temperature to allow GOPS evaporation. Two deposition temperatures were tested: 100°C and 130°C for 1 hour. Then in all cases, after rinsing and drying, the samples were annealed at 135°C for 1 h under air.[11]*

Based on these protocols, and considering the same cleaning and activation step of the LPD protocol, the following is the one that has been tested:

VPD

Table 4.10: The protocol described here outlines the first VPD protocol developed. During the silanization step, the substrates are positioned inside a closed chamber with a small container next to the substrates with 2 mL of pure GOPS per substrate. The closed chamber is then positioned in a explosion-proof oven for 1 hour at 130°C. The samples are then washed in fresh acetone to remove any unbound GOPS from the surface. Finally, an annealing step is performed to remove excess acetone and humidity and to cure the GOPS SAM.

	Materials and methods	Time	Temperature
Oven	2 mL GOPS/substrate	1 h	130°C
Washing	Fresh acetone	5 min	RT
Annealing	Hot plate	1 h	135°C

This protocol allows for a much faster process for silanization. The experiments conducted are quite similar to those for LPD, including contact angle measurements, TOF-SIMS, and AFM analysis.

First VPD trials

The first VPD experiments gave contact angles comparable to LPD with toluene as solvent, which means that the silanization efficiency was good. Figure 4.14 reports the mean contact angle measured after the first trials.

Figure 4.14: A picture of the drop shape with its relative contact angle of a sample silanized with VPD protocol.

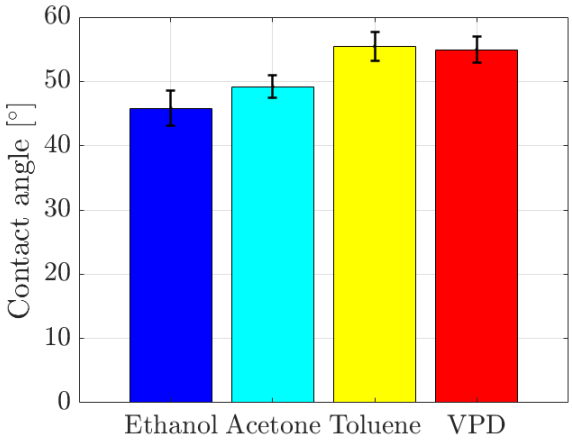

Figure 4.15: Comparison between the initial trials with the VPD and LPD protocols using three different solvents. As the LPD samples, eight drops were measured, and the mean value is displayed. The error bar represents the dispersion of the values compared to the mean value.

Silanization time effect

Similar to the three LPD experiments reported in Section 4.2.3, six silanization times were tested with VPD, ranging from 15 minutes to 90 minutes with 15 minute intervals for each substrate. All other parameters remained fixed as reported in the VPD protocol in Table 4.10. After silanization, eight drops were measured for each substrate, and the trend of the mean contact angle was analyzed.

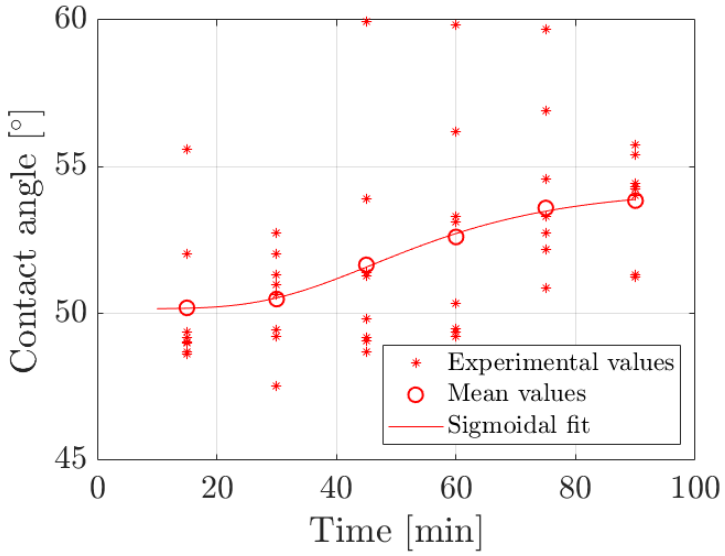

Figure 4.16: Effect of silanization time on the contact angle. Six different times were tested, ranging from 15 minutes to 90 minutes, with 15-minute intervals between each sample.

Unlike the experiments conducted for LPD, the annealing effect was not tested along with the silanization times for VPD. However, the contact angles of a sample without the annealing treatment were measured.

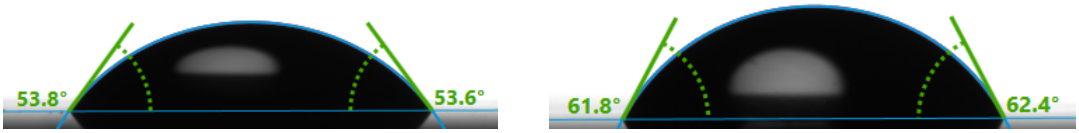

(a) VPD with annealing (b) VPD without annealing

Figure 4.17: The contact angles of two drops taken from two substrates, one treated fully with VPD protol while the other without the annealing step.

As shown in Figure 4.17(b), the sample without the annealing step exhibited higher contact angles, following a trend similar to the one observed in the LPD experiments.

AFM analysis

AFM measurements were also conducted for VPD samples. Similar to the TOF-SIMS analysis, these measurements were done in parallel with an LPD sample to observe any differences in the results. Thus, three samples were tested: one control sample, an LPD sample, and a VPD sample.[1]

Table 4.11: The AFM results of an untreaded sample (Control), a GOPS LPD-treated sample and a GOPS VPD-treated sample.

Parameter	Control	GOPS LPD	GOPS VPD
Sa	0,0919823 nm	0,457242 nm	0,145468 nm
Sq	0,132599 nm	0,575694 nm	0,199424 nm
Ssk	1,03	0,341978	0,527683
Ska	5,71842	2,79143	3,80462
Entropy	2,08528	4,25117	2,69241

[1]The control and LPD samples are the same as those in Table 4.9.

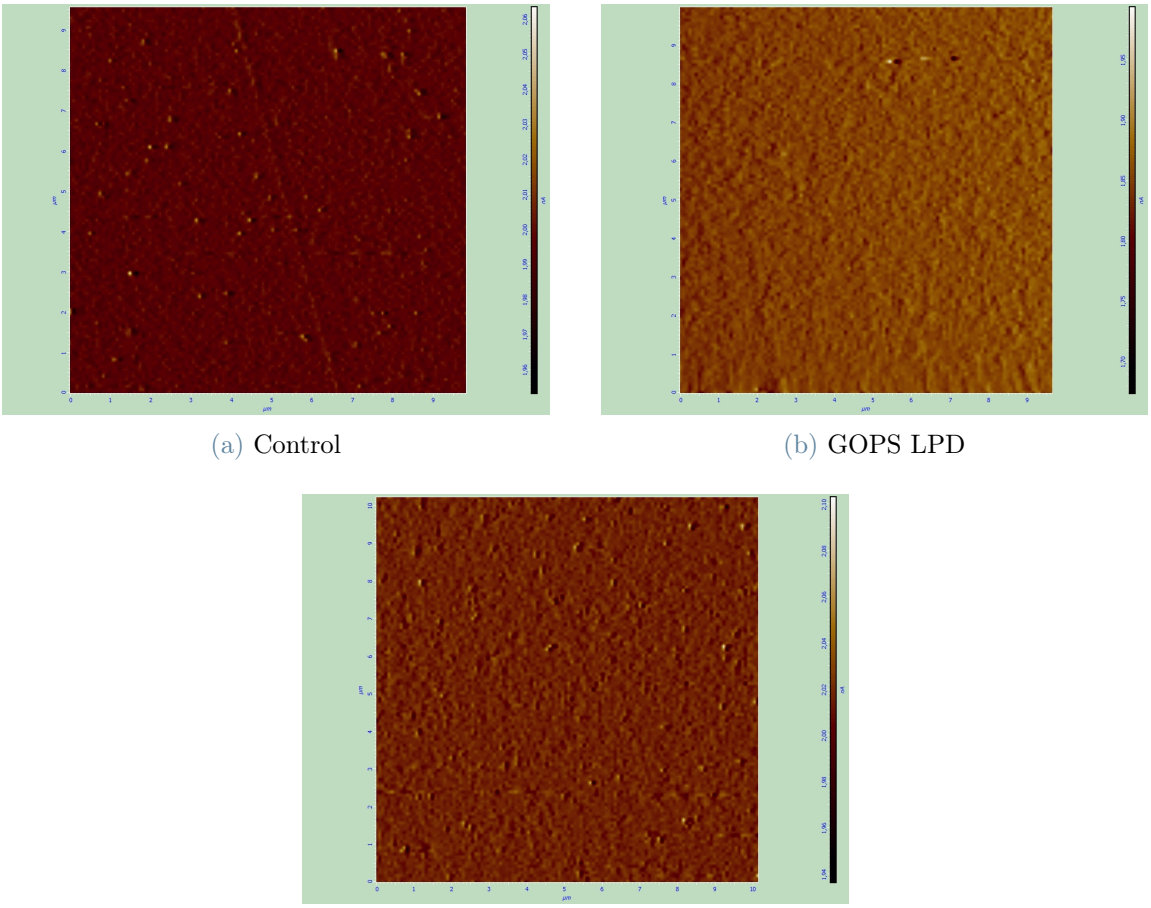

(a) Control

(b) GOPS LPD

(c) GOPS VPD

Figure 4.18: The AFM topographic images of the three surfaces.

From Table 4.11, it can be noted that the values of each parameter for the VPD sample are more similar to those of the control sample. Specifically, the Sa and Sq values are only slightly higher, indicating that the surface is just a bit rougher. The Ssk and Ska values are intermediate between those of the control sample and the LPD sample, suggesting that the surface has fewer peaks than the control sample and a higher number of valleys. Regarding entropy, the VPD sample again occupies an intermediate position between the other two samples. These results suggest that the density of the GOPS layer is high, with good homogeneity and distribution of the molecules on the surface. Visually, Figure 4.18(c) shows that the topographic image of the VPD sample lies between the other two samples, indicating surface modification compared to the control and a smoother, more homogeneous surface compared to the LPD one.

TOF-SIMS analysis

A TOF-SIMS analysis was also carried out for VPD. In this experiment, five samples were tested: a VPD sample, three LPD samples silanized with three different solvents, and a control untreated sample (up to the activation step). The primary ion used was Bi_3^+. In this case, since there are five samples to be compared, the data were area-normalized by the total ion intensity. This normalization process helps to account for variations in total ion yield and ensures that the data are comparable across different samples or regions.

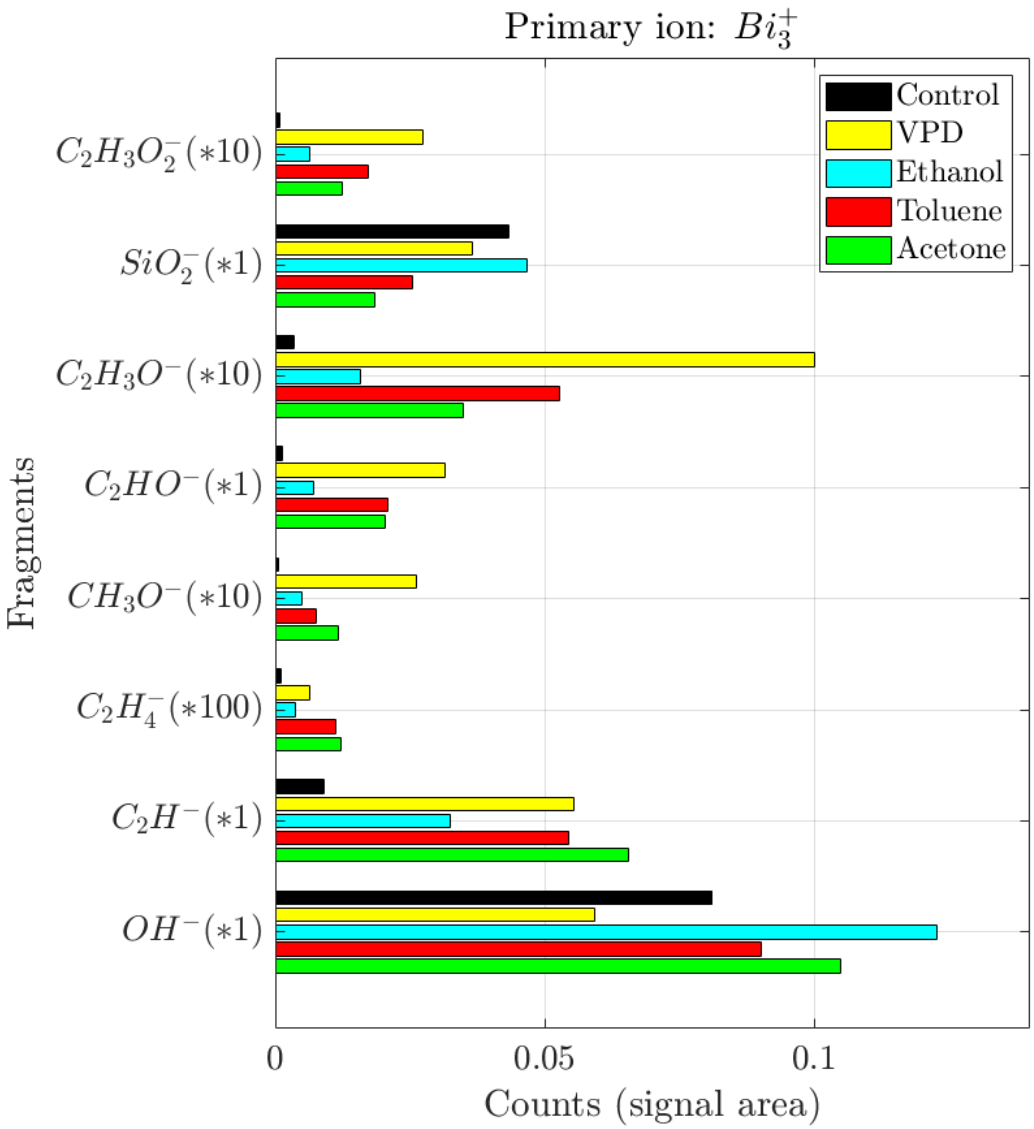

Figure 4.19: TOF-SIMS results of a comparison between five samples, three silanized with LPD with different solvents, one with VPD and the last one is an untreated sample (control).

From Figure 4.19, it can be noted that VPD gave the best results for most of the peaks, while LPD with ethanol gave the worst results. LPD with toluene performed quite similarly to LPD with acetone, except for some peaks where the sample silanized with toluene performed slightly better. An interesting observation can be made for the SiO_2^- and OH^- peaks. The SiO_2^- peak should be high if the silanization did not perform well, because these ion fragments are highly present on the silicon dioxide surface, but it could also be low if the GOPS layer formed is a multilayer. For these reasons, VPD performed the best because its results are in the middle between LPD and the control sample. For the OH^- peak, VPD is again the best, as it has the lowest value, indicating a low amount of silanols formed and good homogeneity of the silane on the surface.

Based on these results, a ranking of the silanization methods can be made:

1. VPD
2. LPD with toluene
3. LPD with acetone
4. LPD with ethanol

4.3. DNA grafting

After the silanization, DNA grafting experiments were conducted using a protocol developed based on existing methods. Below are some of the relevant methods from the literature:

- *All sequences were diluted to 3 $\mu mol\ L^{-1}$ in 1X phosphate-buffered saline (PBS) (1.0 mol L^{-1} NaCl, 50 mmol L^{-1} Na_2HPO_4, pH 7.0) hybridization buffer. H_2SO_4 (0.017 mol L^{-1}) was added to the solution containing sequence 1 to catalyze the opening of the epoxide ring. The DNA samples were vortex-mixed. The samples were spotted with a micropipette tip on a 3-mm diameter area. They were placed on top of a moist towel inside a well-sealed Petri dish to provide a humid environment to prevent the spots from drying. The slides were stored in the dark at room temperature (RT) for 5 hours. The slides were then washed with 1X Tris-SDS (diluted from 10X, 0.1 mol L^{-1} Tris-HCl, 0.1% SDS, pH 7.5) washing buffer for 1 min twice, and then doubly-distilled H_2O for 1 min twice. The slides were then scanned using the ChipReader.[43]*

- *For the bioconjugation procedure, a 10 μM solution of amino-modified nucleotides in a 2X saline sodium citrate (SSC) buffer was prepared. Silanized glass powder/microspheres were placed in the solution at 4°C overnight. After bioconjugation, the glass was washed once in Milli-Q water, dried, and characterized using fluorescence microscopy and scanning electron microscopy.[32]*

- *In view of DNA grafting on Si surface, the DNA probes were diluted at 10 μM in a phosphate buffer (pH 8.5). 1 μL drops of this solution were deposited on all samples. After 1h drying in ambient conditions, the samples were cured at 60°C for 30 min in humid atmosphere. Then a rinsing step for 5 min with deionized water was performed to remove the salts.[11]*

- *Avidin solution (5.6 unit mL^{-1} in phosphate buffer) was dropped onto the surface of each chip and incubated at room temperature for 1 h. Chips were thoroughly rinsed with deionized water and buffer to remove any loosely bound avidin, and used immediately for immobilization of oligonucleotides.[2][33]*

- *The amino-oligonucleotides were dissolved at a concentration of 50 μM in 0.1 KOH. Droplets of the solution were applied to the epoxy-silanized surface of the chips and incubated at 37°C for 6h in a covered Petri dish containing a small amount of water.*

[2]The grafting here is not of an oligonucleotide, but it is completely analogous since the grafting mechanism is the same.

After removal of the droplets, the chips were washed with di-ionized water at 50°C for 15 min with constant shaking, prior to air-drying.[27]

- *For fluorescence measurements, a small microarray (4 columns X 3 rows) was printed on GOPS silanised substrates by Perking Elmer PiezoArray. Spotting volumes of 333 pl of solutions containing 10 μM of ssDNA probe (P1, P2, P3 and P4) in 150 mM of phosphate buffer (pH : 9.5) were spotted on Si_3N_4 and SiO_2 substrates surfaces.[34]*
- *Different concentrations of the oligonucleotide solutions (0.5–100 μM) were manually spotted on the silanized surfaces (1 μL per spot) and incubated overnight at 37°C in a humidity chamber. After DNA immobilization, the substrates were rinsed in different washing solutions: 0.1% Triton 100X, hydrochloric acid (pH : 4), 0.1 M potassium chloride and deionized water.[10]*
- *The sample is left to react for 1 h at room temperature and ambient conditions, subsequently it is placed in a humidity chamber at 60°C for 30 min and then kept overnight at room temperature and ambient conditions. Finally, the samples are rinsed with a 0.2% sodium dodecyl sulphate aqueous solution and deionized water.[12]*

Based on these, the protocol in Table 4.12 has been developed.

DNA grafting

Table 4.12: The protocol described here outlines the first DNA grafting protocol developed. A DNA mix is prepared and 3 μL of the mix are spotted on the substrate. Then, the substrates are put in a closed chamber with RH>90%, provided by putting a wet wipe below the substrates. After 4 hours at RT, the samples are then washed with distilled water to remove any unbound DNA from the surface.

	Materials and methods	Time	Temperature
DNA mix	- Oligonucleotides - Buffer - Fluorophores (optional) - Salt (optional)	-	RT
Grafting	3 μL DNA mix spotted in a closed and humid chamber	4 hours	RT
Washing	Distilled H_2O	2 min	RT
Drying	Air	2 min	RT

The first step is the preparation of the DNA primer solutions. Two oligonucleotides were tested: P1 and P2 (the sequences are reported in Section 3.1). Both of them have an amine group on the 5' end that will open the epoxide ring and bind to it. P1 has a fluorophore (6FAM) on the 3' end, while P2 does not have any fluorophore. Therefore, as described in Table 4.14, SG II was introduced in the preparations of the P2 mixes to ensure detection through fluorescence.

Table 4.13: P1 mix 1 & 2 solutions.

	Materials
P1 mix 1	- 1 μL P1 (100 μM) - 9 μL Na_2HPO_4 (pH : 9.2)
P1 mix 2	- 1 μL P1 (100 μM) - 8 μL Na_2HPO_4 (pH : 9.2) - 1 μL KCl (1 M)

Table 4.14: P2 mix 1 & 2 solutions.

	Materials
P2 mix 1	- 1 μL P2 (100 μM) - 7 μL TE (pH : 8) - 1 μL SG II (10X) - 1 μL KCl (1 M)
P2 mix 2	- 1 μL P2 (100 μM) - 8 μL TE (pH : 8) - 1 μL KCl (1 M)

All the mixes were prepared to have a final solution volume of 10 μL with the following final concentrations[3]:

- Final concentration of P1 and P2 primers: 100 μM $\rightarrow$ 10 μM
- Final concentration of SG II: 10 X $\rightarrow$ 1 X
- Final concentration of KCl: 1 M $\rightarrow$ 0.1 M

After preparing the mixes, the grafting procedure was followed, and fluorescence was evaluated using the Q3 device. Pictures in fluorescence are captured to visually evaluate

[3]The arrow "$\rightarrow$" indicates that after adding these elements to the final solution, they will have a diluted concentration in the final mixture.

the presence of the grafted primers on the surface. P1 has the most direct method of detection because the fluorophore is intrinsic to the primer. For P2, since SG II is an independent molecule, the measurement could be more indirect. However, both methods were tested to observe the differences.

4.3.1. P2 mix tests

The first experiments (see Figure 4.20) were conducted with the P2 mixes to determine if fluorescence indicating the presence of bound oligos could be observed after the grafting step. After performing several tests, all the experiments yielded similar results. After washing with distilled water, the signal decreased compared to the signal acquired with a liquid drop right after the grafting protocol, but it remained present on the surface. However, fluorescence signals were observed even outside the drop area, even after two washes.

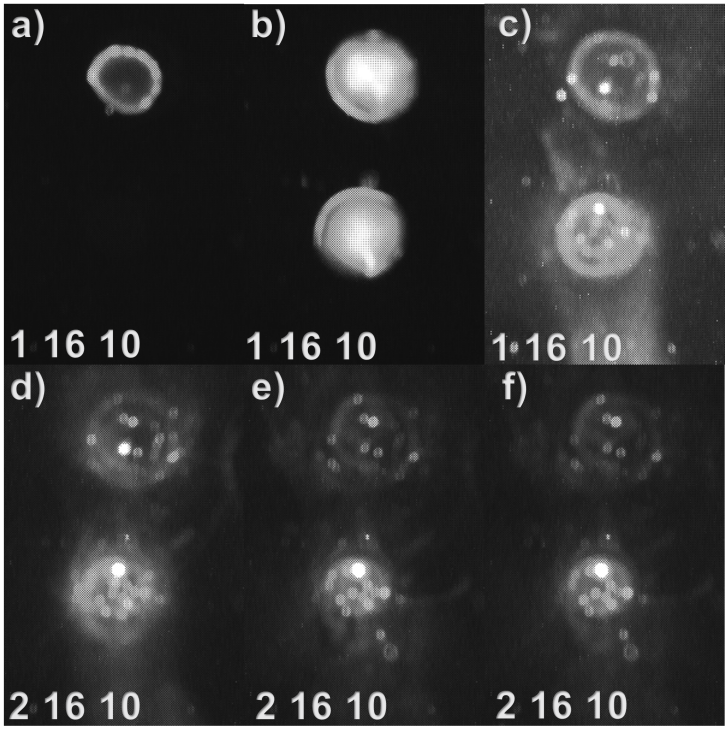

Figure 4.20: This experiment was performed on a sample where P2 mix 1 (top) and P2 mix 2 (bottom) were spotted. (a) This is the sample after the grafting step where the drops were left to dry. (b) Two drops of SG II 1X were spotted on both dried spots. (c) The sample was washed with distilled water and left to dry. (d), (e), and (f) are iterations of spotting SG II 1X, washing with distilled water, and drying.

In this experiment, Figure 4.20(a) shows that after the grafting step, the bottom drop

gave no fluorescence signal due to the absence of SG II in the initial mix, while the top drop, which initially contained SG II, gave a fluorescence signal. In Figure 4.20(b), both drops are visible because 2 μL of SG II 1X were added to the grafting spots and the image was acquired. Then, in Figure 4.20(c), the sample was washed and dried to observe any differences from the previous image; interestingly, the signal did not decrease significantly, but fluorescence signals were observed even outside the spots. Figures 4.20(d), (e), and (f) are iterations of steps (b) and (c), and the same observations apply to all of them.

These initial experiments reveal an inherent problem with SG II. It appears that SG II intercalates into the GOPS molecules and remains trapped inside them, giving false indications of possible probe grafting.

A confirmation of this issue is provided by the experiment shown in Figure 4.21.

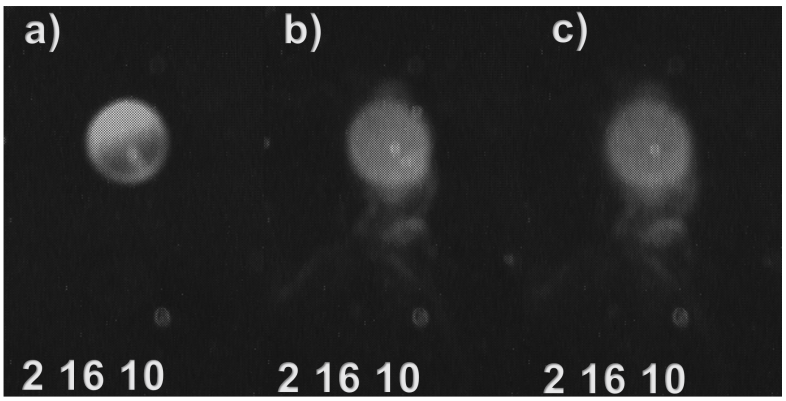

Figure 4.21: This experiment was performed on a sample where 2 μL of SG II 1X were spotted. (a) This image shows the sample with the liquid drop of SG II 1X. (b) This image shows the same sample after washing with water and drying. (c) Another wash was performed to observe any changes in fluorescence.

This provides clear evidence that SG II is not reliable for this type of experiment, as it disturbs the signal of the grafted probes and gives false indications of the efficiency of the process.

4.3.2. P1 mix tests

P1 overcomes the limitations of the P2 mixes, as the fluorophore is directly integrated into the probe itself. This ensures that any observed fluorescence signals come necessarily from the grafted probe. Initial experiments were performed using P1 mix 1 and 2, but instead of Na_2HPO_4, TE buffer solution was used. These experiments yielded poor

results, as the fluorescence signals disappeared completely after washing the substrates, indicating that the grafting procedure was not efficient. To address this, three factors were considered. According to the literature, as reported in Section 2.2.5, the grafting efficiency strongly depends on the pH of the mix solution. Amine groups react with the epoxide ring at an alkaline pH of around 9. Additionally, the influence of grafting time was tested, even extending to several days, but no significant changes were observed. Therefore, a grafting time of 4 hours was deemed sufficient. Temperature was also considered during the grafting step, specifically at room temperature (RT), 30°C, and 37°C. Increasing the temperature appeared to enhance fluorescence signals after the washing step.

Based on these tests, the following considerations were made:

- Na_2HPO_4 was chosen as buffer solution to mantain a pH of 9.2.
- The grafting time was set to 4 hours, as in the initial protocol.
- The temperature of the grafting step was increased to 37°C.

Table 4.15 presents the updated grafting protocol, including all modifications.

DNA grafting

Table 4.15: The protocol described here outlines the final DNA grafting protocol developed. A P1 mix is prepared, and then 3 μL of the mix are spotted on the substrate. The substrates are placed in a closed chamber with a humid atmosphere, provided by placing a wet wipe below the substrates. The closed chamber is then positioned in an explosion-proof oven for 4 hours at 37°C. After the grafting step, the samples are washed with distilled water to remove any unbound DNA from the surface.

	Materials and methods	Time	Temperature
DNA mix	P1 mix 1 or 2	-	RT
Grafting	3 μL DNA mix spotted in a closed and humid chamber	4 hours	37°C
Washing	Distilled H_2O	2 min	RT
Drying	Air	2 min	RT

Figure 4.22 shows the results obtained with P1 mixes 1 and 2 using the updated grafting protocol.

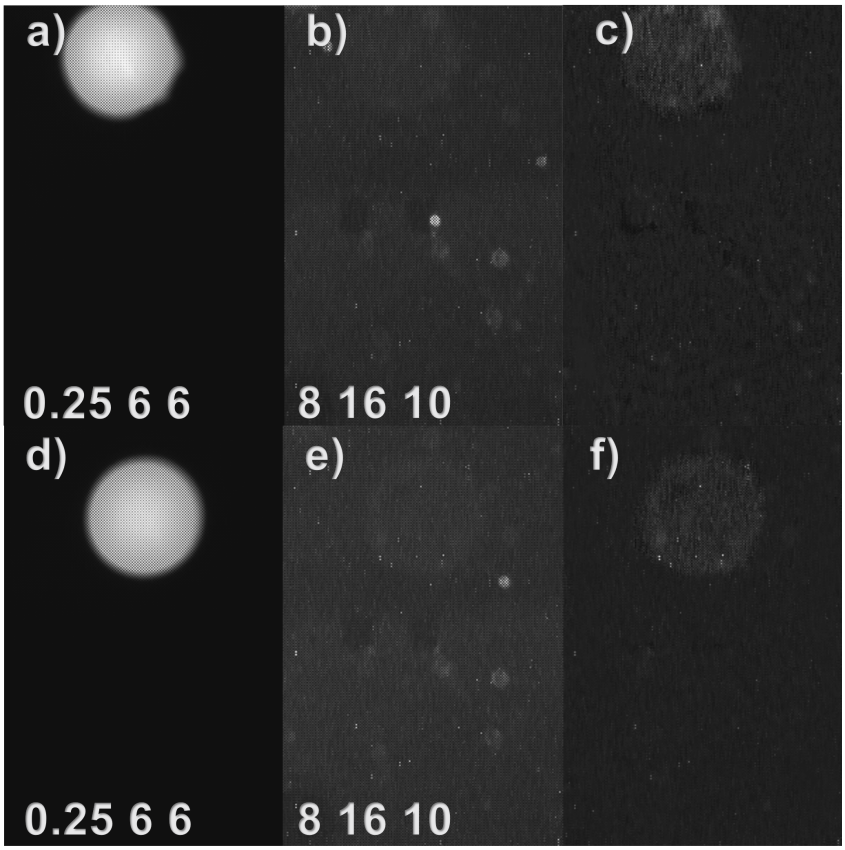

Figure 4.22: This experiment was performed on a sample where P1 mix 1 [(a), (b), (c)] and P1 mix 2 [(d), (e), (f)] were spotted. Images (a) and (d) show the samples after the grafting step, with the drops still present. Images (b) and (e) were taken after the washing step. Images (c) and (f) are the post-processed versions of (b) and (e), respectively, to enhance the fluorescence signal of the grafted probes.

As shown, after the washing step, there was still a fluorescence signal in the same spot as the liquid drop. However, the intensity was significantly decreased compared to the original signal. Figures 4.22(c) and (f) are post-processed images using ImageJ to better highlight the fluorescence signal of the grafted probes in the spot, while also decreasing the intensity of the background signal. The need for such high tuning of the optical parameters can be hypothesized by considering an ideal case of two spots: one with a liquid drop containing P1 mix 1 and the other with grafted P1 after the washing step. A rough estimate of how much the fluorescence signal could decrease can be made by considering simple geometrical aspects and the number of probes in the solution. If each probe has one fluorophore, then the output fluorescence could be comparable to the number of probes in the two spots. A ratio of the number of probes in the two spots can roughly indicate how the fluorescence intensity could change after the washing step

compared to a liquid drop.

Let's set up an idealized model to calculate the ratio of the number of probes in volume to the number of probes on the surface spot. The initial data for the problem are:

- $[P1]_{solution} = 10\ \mu$M
- $MW_{P1} = 7829$ g/mol
- $V_{drop} = 3\ \mu$L

The number of probes in the volume of the liquid drop is calculated as follows:

$$n_{P1,drop} = [P1]_{solution} * 10^{-12} * V_{drop} = 10 * 10^{-12} \frac{mol}{\mu L} * 3\ \mu L = 3 * 10^{-11}\ mol \tag{4.1}$$

$$\begin{aligned} \#P1_{drop} &= n_{P1,drop} * N_A = 3 * 10^{-11}\ mol * 6.022 * 10^{-23}\ mol^{-1} = \\ &= 1.8 * 10^{13}\ molecules \end{aligned} \tag{4.2}$$

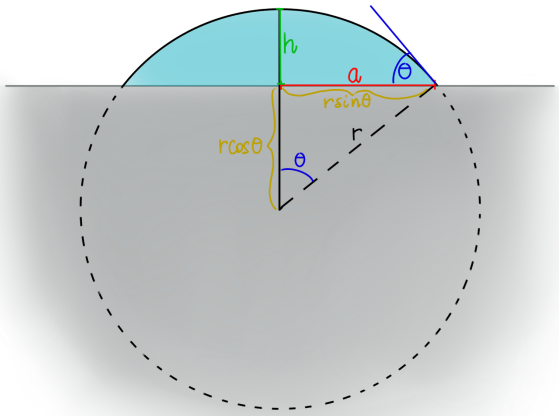

Figure 4.23: Representation of the parameters used for the calculations of the radius a of a spherical cap.

In Figure 4.23, the calculation of the radius of a spherical cap is schematized based on the contact angle of a drop. Since the substrates used for the last tests were silanized with LPD using acetone as the solvent, the contact angle considered is 51°, as reported in Section 4.2.3.

The volume of a spherical cap is defined as:

$$V = \frac{\pi}{6} * h(3a^2 + h^2) \tag{4.3}$$

with $a = r\sin\theta$ and $h = r(1 - \cos\theta)$. So, using the definitions of a and h, one can reorganize Equation 4.3 to obtain the dependence of the radius of the drop with respect to the contact angle.

$$a = \sin\theta\sqrt{\frac{6V}{\pi(1-\cos\theta)[3\sin^2\theta + (1-\cos\theta)]}} \tag{4.4}$$

If the contact angle is 51°, the same angle in radiants is $\frac{51°}{1800} * \pi = 0.89\ rad$. Then:

$$a = \sin(0.89)\sqrt{\frac{6 * 3 * 10^{-9}\ m^3}{\pi(1-\cos(0.89))[3\sin^2(0.89) + (1-\cos(0.89))]}} = 0.00155\ m = 1.55\ mm \tag{4.5}$$

The calculated radius is quite consistent with the experimentally measured values. Therefore, the surface area of a spot is:

$$A_{spot} = \pi a^2 = \pi * 1.55^2\ mm^2 = 7.545\ mm^2 = 7.545 * 10^{12}\ nm^2 \tag{4.6}$$

To determine the number of probes present on the spotted surface, one should model how the probes graft onto the surface, along with their efficiency. According to literature, there are studies with simulations of probe grafting. First, let us define σ_{P1} as the radius of the steric hindrance of a probe in the x-y plane. Based on literature simulations, a good estimation of the distance between each grafted molecule is 7σ, with $\sigma_{P1} = 5$ nm [25]. Then, the occupied area of a single probe on the surface is:

$$A_{P1} = \pi * r_{P1}^2 = \pi\left(\frac{7\sigma}{2}\right)^2 = \pi * \left(\frac{7 * 5\ nm}{2}\right)^2 = 962.11\ nm^2 \tag{4.7}$$

Then, the number of probes on the spotted area can be calculated:

$$\#P1_{spot} = \frac{A_{spot}}{A_{P1}} = \frac{7.545 * 10^{12}\ nm^2}{962.11\ nm^2} = 7.84 * 10^9\ molecules \tag{4.8}$$

Finally, the ratio between the amount of P1 probes is found:

$$\frac{\#P1_{drop}}{\#P1_{spot}} \simeq 2304 \tag{4.9}$$

This provides a rough indication of how the fluorescence signal should decrease compared to the one captured in volume. The numbers here should not be taken precisely, but they give an indication of how significantly the signal should decrease, which is consistent with the results obtained. To observe the fluorescence signal after the washing step, the optical parameters had to be maximized to ensure sufficient detection.

5 | Conclusions and future developments

In this thesis, a protocol for the surface functionalization of silicon dioxide using GOPS was developed, followed by the subsequent grafting of oligonucleotides. This is of particular interest for biomolecular diagnosis of diseases and general biodiagnostics. Section 2.1.2 provides a detailed description of the working principle of a sensor capable of detecting small changes in the electrical charge of a medium near the sensing membrane with high precision. Considering that DNA has an intrinsic negative electrical charge, surface functionalization and bioconjugation could be highly beneficial in developing a novel method for DNA detection based on electrical charges.

Typical detection methods, such as PCR, qPCR, and others (detailed descriptions of these techniques are provided in Chapter 1), rely on optical and electrical apparatuses, along with fluorescent dyes that must be included in the solution mix. Using a sensor could simplify and streamline the detection process. The optical components of these devices, along with the fluorescent dyes, constitute a significant portion of the costs and contribute to the increased size of the device. In contrast, a sensor would only require the electrical components, as the sensing elements and the electrical charge are intrinsic to the DNA, allowing for a more compact device due to the absence of optical parts.

Before realizing an ISFET, proper characterization and analysis of the functionalization of the sensing membrane are necessary to ensure reliability in detecting the target elements. Without proper functionalization and grafting on the sensing membrane, the target DNA may not interact with the sensor, rendering the instrument ineffective.

For these reasons, the functionalization of the sensing membrane studied in this thesis involves the following steps: silanization of a silicon dioxide surface with GOPS and subsequent grafting of oligonucleotides. The primary aim was to create a reliable platform for DNA-based biosensing, which could significantly enhance the sensitivity and specificity of genetic material detection. Through a series of experiments, various methods for cleaning and activating SiO_2 surfaces were explored, silanization protocols using both LPD and

VPD were optimized, and the effectiveness of these methods was evaluated using contact angle measurements, AFM, and TOF-SIMS. Additionally, different DNA mixtures for grafting were tested and the attachment was validated through fluorescence measurements. The following sections provide a detailed discussion of the results, conclusions, and future developments based on these investigations.

5.1. Cleaning and Activation of Silicon Dioxide Surfaces

The initial step in the protocol involved cleaning and activating SiO_2 surfaces to ensure they were properly prepared for silanization. Various cleaning treatments, including piranha solution, solvent cleaning, and oxygen/argon plasma treatment, were evaluated. Plasma treatment proved to be the most effective, providing a clean and highly reactive surface, as confirmed by contact angle measurements showing very low values, indicating the high hydrophilicity of the treated surface. Solvent cleaning, using acetone and isopropyl alcohol, was preferred over piranha cleaning due to its versatility, simplicity, and safety. Piranha cleaning, while effective, is dangerous and harmful due to its highly corrosive nature, posing significant risks during handling. In contrast, solvents like acetone and isopropyl alcohol are less dangerous and easier to handle, making them a safer alternative for cleaning. Although piranha cleaning includes both cleaning and activation, achieving a high density of hydroxyl terminations is necessary for this application, and the contact angles suggested that plasma treatment gave better results in these terms. Piranha treatment could be more useful if the surfaces to be treated are highly contaminated, but since the substrates used were taken from wafers processed by STMicroelectronics in the industrial line, the contamination level was already low. This step was crucial for achieving uniform and dense silane layers during subsequent silanization.

5.2. Silanization with Liquid and Vapor Phase Deposition

Two silanization methods were explored: LPD and VPD. For LPD, experiments assessed the effects of silanization time, annealing, concentration of the silane solution, and different solvents. The silanization time, as expected, has the effect to provide higher silane densities as the time goes on; based on the results obtained the evolution of the silanization appeared to linearly progress over time. The annealing, lowered the contact angles in general, this is because high temperatures cure the silane layer, giving more homogene-

ity of the molecules, rearreaning them. Its function is also to remove any contaminants or solvents left on the surface. Among the solvents tested, toluene yielded the best results, achieving contact angles comparable to VPD, then acetone was good enough, while ethanol gave the worst results in terms of silanization quality. A reason behind this fact, rely on the fact that during silanization, a formation of flakes of GOPS were observed, hindering a proper and sufficient silanization. VPD was similarly studied for its silanization time and annealing effects. The results demonstrated that VPD outperformed LPD in terms of silane density, homogeneity, and functional groups orientation.

5.2.1. Evaluation of the Best Silanization Methods

To determine the most effective silanization method, comprehensive surface characterization was performed using contact angle measurements, AFM, and TOF-SIMS.

- Contact Angle Measurements: higher contact angles were observed for VPD-treated surfaces compared to LPD, indicating a more effective silanization process. Toluene was identified as the optimal solvent for LPD, achieving contact angles comparable to VPD.
- AFM: the analysis revealed that VPD provided a more uniform and dense silane layer compared to LPD. The surface roughness measurements confirmed the homogeneity of the silane layer. Measures performed on substrates silanized with LPD in different times suggested the progression of the silanization in time, giving proof of the contact angle measurements increasing trend.
- TOF-SIMS: the analysis showed that VPD resulted in a higher density of silane molecules and a more favorable chemical profile of surface ion fragments compared to LPD. This results confirmed all the other studies performed and gave informations again on the best solvent for LPD. Toluene was the best, while ethanol was the worst; acetone was in an intermediate situation.

5.3. Grafting test with different DNA mixtures

Various DNA mixtures were tested for grafting onto the GOPS-functionalized SiO_2 surfaces. The grafting process was fine-tuned by adjusting parameters such as time, temperature, and pH of the DNA mixture. Fluorescence measurements were used to evaluate the efficiency of DNA grafting. Firstly, a DNA mix with SG II was tested, where the fluorophores are independent molecules and not integrated into the probes themselves. These mixes did not give reliable results because SG II was interacting with the GOPS

molecules on the surface, giving false indications of whether the grafting was successful or not. Therefore, three other mixes were tested, where the oligonucleotides were already marked on the 3' end with a fluorophore. The first mix gave poor results because the TE buffer solution was not in the optimal pH range to favor the ring opening of the epoxide ring of GOPS. Consequently, another buffer solution, disodium hydrogen phosphate, was used to ensure a higher pH of 9.2. In this case, even though the repeatability was not good enough, a fluorescence signal was present even after subsequent washing of the substrates. The presence of salt, such as potassium chloride, was introduced in the solution to provide more stability to the probes. Salts can help stabilize DNA structures and reduce electrostatic repulsion between negatively charged DNA strands, promoting better attachment to the surface. However, the results did not provide sufficient information to determine if the addition of salt significantly improved the grafting process. Finally, these results confirmed the successful attachment and stability of the grafted oligonucleotides, validating the effectiveness of the overall functionalization and grafting protocols.

5.4. Complete protocol

Based on the characterization results, the updated protocol for silanization and grafting is outlined in Table 5.1. This protocol encompasses all steps, starting from the cleaning and activation of the substrates, proceeding with the optimal silanization method identified from the results, and concluding with the grafting procedure.

Table 5.1: The protocol described here outlines the final and complete procedure, integrating all the steps from cleaning and activation of the substrates to silanization and final grafting.

Cleaning

	Materials and methods	Time	Temperature
Ultrasonic bath	Acetone	5 min	RT
Spin coating	Isopropyl alcohol	10 s x 3	RT
Dehydration bake	Hot plate	5 min	135°C

Activation

	Gas composition	Time	RF power	Pressure
Oxygen/Ar plasma	$90\%O_2/10\%Ar$	240 s	180 W	1 mbar

VPD silanization

	Materials and methods	Time	Temperature
Explosion-proof oven	2 mL GOPS/substrate in a closed chamber	1 h	130°C
Washing	Fresh acetone	5 min	RT
Annealing	Hot plate	1 h	135°C

DNA grafting

	Materials and methods	Time	Temperature
DNA mix	P1 mix 1 or 2	-	RT
Grafting	3 μL DNA mix spotted in a closed and humid chamber	4 hours	37°C
Washing	Distilled H_2O	2 min	RT
Drying	Air	2 min	RT

5.5. Future developments

The work presented in this thesis has successfully demonstrated the silanization of silicon dioxide surfaces with GOPS and the subsequent grafting of oligonucleotides. However, several key developments are needed to enhance the reliability, efficiency, and application scope of the developed platform. These future developments focus on improving process parameters, surface characterization, functionalization optimization, and integration with sensing systems.

Detailed characterization of process parameters

To optimize the silanization and grafting protocols, a more extensive study of the process parameters is required. Factors such as GOPS concentration, reaction time, temperature, and environmental conditions during silanization should be systematically analyzed.

Precise control and fine-tuning of these parameters will allow for a more consistent and reproducible grafting process, providing a robust and scalable platform. The development of a "perfect setting" for the protocol will ensure the repeatability of the results, which is critical for industrial-scale applications and high-throughput manufacturing.

Surface characterization post-grafting

While the initial surface characterization provides valuable insights, further analysis of the surface after the oligonucleotide grafting step is essential to confirm the successful functionalization and uniformity of the modification. Advanced characterization techniques such as AFM can provide topographical and mechanical property data, while TOF-SIMS will offer molecular-level insight into the surface composition. Furthermore, the integration of Fourier Transform Infrared Spectroscopy (FT-IR) and X-ray Photoelectron Spectroscopy (XPS) will complement the surface analysis by identifying functional groups and chemical bonding, providing a holistic understanding of the grafting efficiency and oligonucleotide density across the surface.

Development of protocols for hybridization and optimization of parameters

Following oligonucleotide grafting, the next critical step is the hybridization of complementary strands. A detailed protocol for this hybridization process must be developed, focusing on key parameters such as reaction time, temperature, and buffer composition. Each parameter should be optimized to ensure maximum hybridization efficiency. Fluorescence-based detection methods will be employed to evaluate and quantify the hybridization yield, ensuring high sensitivity and specificity of the functionalized surface.

Protocol integration with ISFET sensing membrane

The next phase of development will involve transferring the optimized silanization, grafting and hybridization protocols onto the sensing membrane of an ISFET. This will allow for real-time electrical detection of hybridization events, enabling label-free sensing. The performance of the ISFET will be evaluated based on parameters such as signal-to-noise ratio, sensitivity, and detection limits. Extensive testing will be conducted to assess the robustness and reproducibility of the electrical signals generated by the grafted oligonucleotides in response to hybridization events.

Design of a microfluidic system for reagent handling and SP-PCR

To automate the hybridization process and enable the system to handle complex biological samples, a microfluidic system will be designed. This system will efficiently deliver reagents necessary for the hybridization and SP-PCR reactions, minimizing reagent consumption and enhancing reaction kinetics. The microfluidic design will focus on precise control of fluid flow, temperature regulation, and integration with the ISFET platform for seamless hybridization and detection. Optimizing the microfluidic system will also allow for parallelization of experiments, paving the way for high-throughput analysis.

Development of packaging for optimal sealing and system integration

A critical aspect of implementing this system in real-world applications is ensuring proper packaging of the ISFET chip with the microfluidic system. Packaging development will focus on achieving perfect sealing between the chip and the microfluidic channels to prevent leaks, contamination, and reagent evaporation. Additionally, the system must guarantee a reliable electrical connection between the ISFET and external components to ensure accurate signal transmission. The packaging design will also need to ensure compatibility with standard lab instrumentation and allow for easy handling and scalability. Careful attention will be paid to material selection, thermal management, and long-term stability, ensuring that the system remains functional over extended usage periods.

A | Appendix A

Whenever a material aborbs a photon, it absorbs energy and the system moves from the so-called **ground state** to an **excited state**.

$$System: \ A \xrightarrow{h\nu} A^* \tag{A.1}$$

One useful way to represent this transition is by looking at the Perrin-Jablonski diagram:

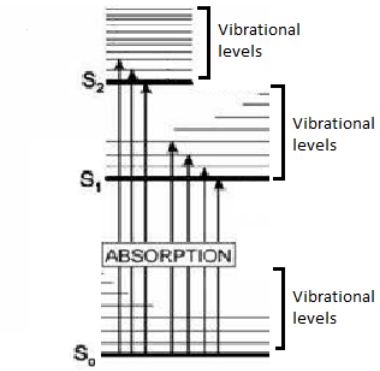

Figure A.1: This is a Perrin-Jablonski diagram with its energy states where S_0 is the ground state and S_i are the excited states. For each energy states there are multiple vibrational levels.

The vertical arrows correspond to transitions between energy levels. In Figure A.1, these arrows represent the absorption of a photon and start from the lowest vibrational state of the ground state $S_0(\nu_0)$ to one of the vibrational levels of the excited states $S_i(\nu_i)$. The arrow is vertical because the transition is so fast that the system has no time during the absorption to have a concomitant nuclei displacement. This means that the system reaches an excited state that relaxes onto a specific equilibrium geometry. So, in a P-J diagram, the transition can be represented in a simpler way considering only the difference in energy.

Once the system reaches an excited state, after some time, it will come back to the ground state through a de-excitation process: $A^* \rightarrow A$.

A.1. Fluorescence

There could be different de-excitation processes, but in this Appendix only the fluorescence process is described.

It is the most probable de-excitation process if the excited state is S_1 and it is a radiative process, which occurs by the release of a photon. Let's look first at the case where the excited state is S_1 (Figure A.2).

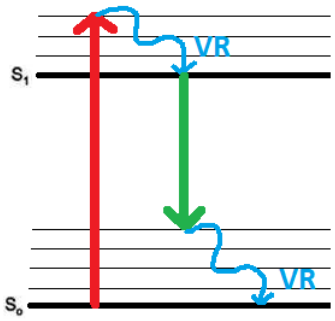

Figure A.2: Fluorescence mechanism if the excited state is S_1.

The red arrow indicates that there is an absorption of a photon (with energy $h\nu$) from the ground state S_0 to the excited state S_1: $S_0(\nu_0) \rightarrow S_1(\nu_i)$.

Then a non-radiative process occurs, where there is a transition, inside the same energy state, between vibrational levels: $S_1(\nu_i) \rightarrow S_1(\nu_0)$.

This process is called **vibrational relaxation** (VR) and happens in a very short time ($\sim 10^{-12} - 10^{-10}$ s).

After VR there is a radiative de-excitation phenomenon, the **fluorescence**, which occurs by the release of a photon: $S_1(\nu_0) \rightarrow S_0(\nu_i)$.

The photon emitted has a longer wavelength compared to the absorbed one because there is an energy loss that occured in the excited state due to VR ($h\nu' < h\nu$).[1] After fluorescence, another VR can occur relaxing the system to the ground state: $S_0(\nu_i) \rightarrow S_0(\nu_0)$.

If the excited state is S_n a similar radiative process would happen (see Figure A.3).

[1] $E = h\nu = \frac{hc}{\lambda} \quad \Rightarrow \quad \frac{hc}{\lambda'} < \frac{hc}{\lambda} \quad \Rightarrow \quad \lambda' > \lambda$

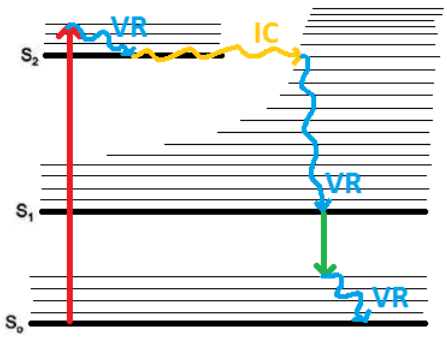

Figure A.3: Fluorescence mechanism if the excited state is S_2.

The red arrow is the absorption phenomenon (a photon is absorbed by the material) bringing the system to the excited state S_2: $S_0(\nu_0) \rightarrow S_2(\nu_i)$.

Then VR and **internal conversion** (IC) occurs. The last phenomenon is a non-radiative process, similar to VR, but in this case, the system moves from the lowest vibrational level of an excited state to an higher vibrational level of the lower energetic state: $S_2(\nu_0) \rightarrow S_1(\nu_i)$.

The characteristic time of an IC process is slightly slower than VR, around $\sim 10^{-11} - 10^{-9}$ s. Then VR brings the system to the lowest vibrational state of S_1: $S_1(\nu_i) \rightarrow S_1(\nu_0)$.

And again fluorescence occurs, emitting a photon with longer wavelength compared to the absorbed one ($h\nu' < h\nu$): $S_1(\nu_0) \rightarrow S_0(\nu_i)$.

After fluorescence the system can return to the ground state through VR: $S_0(\nu_i) \rightarrow S_0(\nu_0)$.

B | Appendix B

Semiconductors like Silicon (Si) or Germanium (Ge), which are commonly used, are also referred to as metalloids because they exhibit properties between those of insulators and conductors. In metals, electrons are free to move within an 'electron cloud' due to the overlap of the valence and conduction bands, allowing outer shell electrons to move freely. In contrast, insulators have a wide band gap between the valence and conduction bands, preventing valence electrons from being excited into the conduction band to move freely. Semiconductors, however, occupy an intermediate position; with a smaller band gap, valence electrons can be promoted to the conduction band when a certain amount of energy, corresponding to the band gap, is supplied. This characteristic is extensively exploited in microelectronics, and doping can further narrow the band gap, enhancing the conductivity of semiconductors.

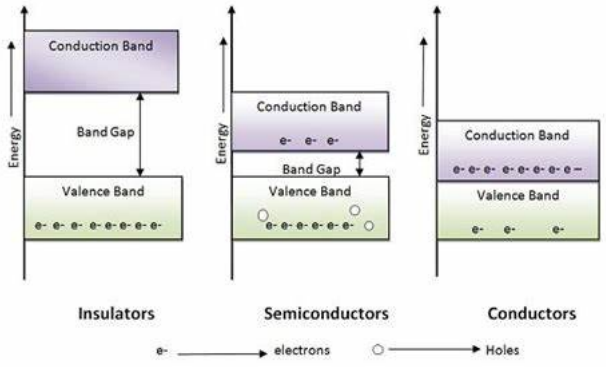

Figure B.1: Band gap for insulators, semiconductors and metals. In the case of metals, conduction and valence band are overlapping, while in the other two cases there is a non negligible band gap.

B.1. Doping

B.1.1. Intrinsic semiconductors

An intrinsic semiconductor is a perfect semiconductor crystal with no impurities or lattice detects. At absolute zero temperature (T = 0 K), all electrons are bound in covalent

bonds, leaving no free carriers for conduction: the valence band is completely filled with electrons, and the conduction band is empty. However, at temperatures above absolute zero (T > 0 K), thermal energy can excite electrons, creating electron-hole pairs (EHPs). Both holes in the valence band and free electrons in the conduction band contribute to current conduction. One method to promote electrons from the valence band (E_V) to the conduction band (E_C) is by illuminating the material with light of sufficient energy to overcome the band gap. The energy E provided by the light must be at least equal to the band gap energy, calculated as ($E = h\nu \geq E_G$), where h is Planck's constant and ν is the frequency. Since EHPs are generated simultaneously, the concentration of electrons n in the conduction band is equal to the concentration of holes p in the valence band, expressed in units of ($electrons/cm^3$) and ($holes/cm^3$), respectively.

Thus, for intrinsic semiconductors: $n = p = n_i \rightarrow n * p = n_i^2$

The conductivity of semiconductor materials increases with temperature. This is because heat enables some electrons in the valence band to acquire enough energy to transition to the conduction band, becoming available for conduction. The greater the heat applied, the more electrons can gain the necessary energy for this transition, thus increasing the number of charge carriers. Another method to increase charge carriers is through the introduction of atoms from an external source. Doping, or implantation, is the process by which atoms of a different element are introduced into a semiconductor to alter its properties. Semiconductors are commonly doped with elements like boron (B), arsenic (As), and phosphorus (P) to modify and improve their electrical characteristics.

B.1.2. Extrinsic semiconductors

Doping a crystal can create an abundance of either electrons or holes, resulting in two types of doped semiconductors: n-type, with a majority of electrons, and p-type, with a majority of holes. When a crystal is doped to alter the equilibrium carrier concentrations n_0 and p_0 from the intrinsic carrier concentration n_i, the material becomes extrinsic. The introduction of impurities or lattice defects adds new energy levels within the band gap of the energy band structure. For effective doping of silicon, which belongs to the 4^{th} group of the periodic table, atoms that can form stable covalent bonds are selected. Atoms from the 3^{rd} group, known as acceptors (like B, Ga, etc.), and 5^{th} group, known as donors (like P, As, etc.), are typically used for doping silicon.

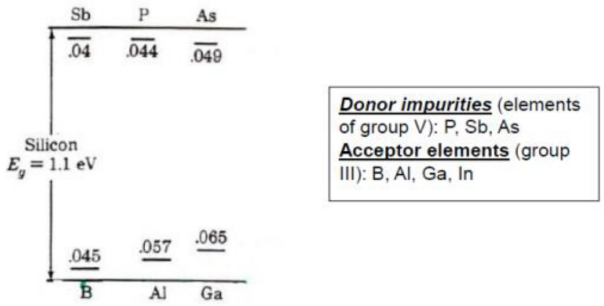

Figure B.2: Modification of the band gap by doping with different elements. Donors add an other energy level below the conduction band, while acceptors above the valence band.

Depending on the element used to dope Si, there are two types of doping:

- n-type doping: P is an element with 5 electrons in the outer shell, one more than Si. This introduces extra electrons into the lattice which can be released through the application of heat, producing an electron current.
- p-type doping: B is an element with 3 electrons in the outer shell, one less than Si. This introduces holes into the lattice which can be made mobile by applying heat. This gives birth to a hole current.

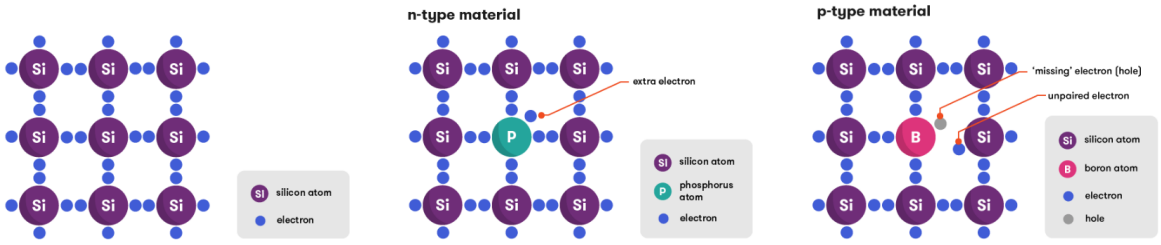

(a) Intrinsic Silicon (b) P doping (c) B doping

Figure B.3: Doping by introduction of external elements as impurities in the lattice crystal.

B.2. P-n junction

When a p-type semiconductor is joined to an n-type semiconductor, a p-n junction is formed, which can act as a rectifier. A rectifier is a component that permits current to flow predominantly in one direction. At the junction, electrons from the n-type region diffuse into the p-type region, leaving behind a region with a net positive charge in the n-type layer. Conversely, holes from the p-type region diffuse into the n-type region, creating a region with a net negative charge in the p-type layer. This diffusion of charge

carriers results in the formation of an electric field at the junction, which influences the direction of electric current flow. The region where recombination of charges happen, is called depletion zone or depletion region.

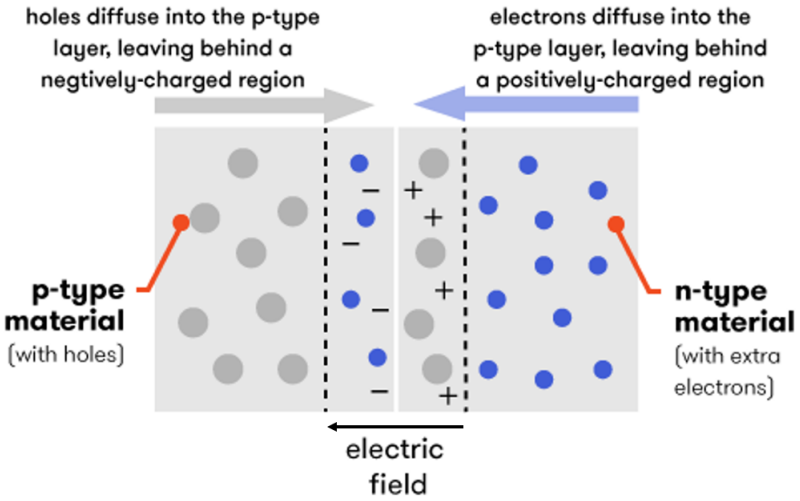

Figure B.4: Scheme of the charge movements in a p-n junction. In the depletion zone there is a built-in field that is caused by the presence of the majority carriers in the two interfacing materials.

Then a voltage can be applied to a p-n junction and two effects can be observed depending on the voltage applied.

B.2.1. Forward bias

Whenever an outer voltage (V_F) that exceeds the built-in field (V_0) is applied, the majority carriers are drawn towards the external charges at the poles, which push them towards, reducing the width of the depletion zone. The electric field within the depletion zone is then given by: $V = V_F - V_0$.

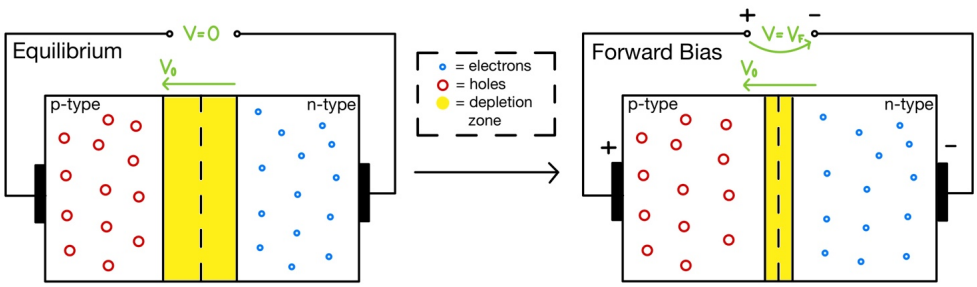

Figure B.5: Shrinkage of the depletion zone caused by the presence of a forward bias.

B.2.2. Reversed bias

Conversely, when an external reversed voltage (V_R) is applied in the same direction as the built-in potential (V_0), the majority carriers are attracted towards the poles, moving them away from the junction and increasing the depletion zone's width. The resulting electric field within the depletion zone is: $V = V_R + V_0$.

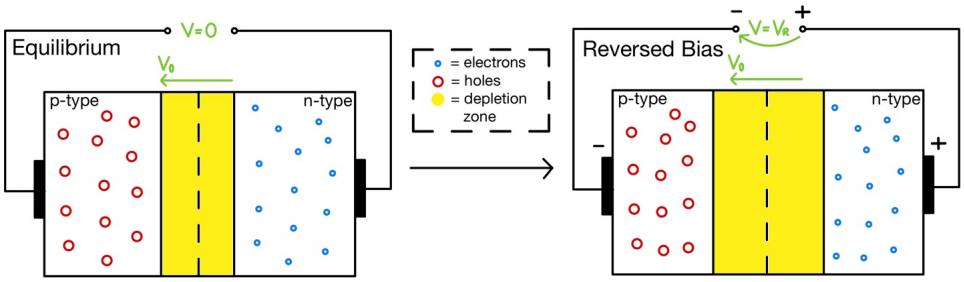

Figure B.6: Dilatation of the depletion zone caused by the presence of a reversed bias.

List of Symbols

Variable	Description
Sa	Average Roughness
E_G	Band gap
μ	Carrier mobility
$\frac{W}{L}$	Channel width-to-length ratio
ρ_0	Charge carrier density
Ska	Coefficient of kurtosis
E_C	Conduction band
θ	Contact angle
I_{DS}	Drain current
V_{DS}	Drain voltage
q	Elementary charge
$\emptyset_f$	Fermi potential of the silicon substrate
ν	Frequency
C_{ox}	Gate capacitance per unit area
Q_{ox}	Gate charge density
V_{GS}	Gate voltage
t_{ox}	Insulator thickness
γ_{lg}	Liquid-gas interfacial tension
h	Planck's constant
x	Polarization potential
E_{ref}	Reference electrode potential
Sq	Root mean square
γ_{sl}	Solid-liquid interfacial tension
γ_{sg}	Solid-gas interfacial tension

Variable	Description
φ_{eo}	Surface potential
Ssk	Surface skewness
C_T	Threshold cycle
V_{TH}	Threshold voltage
E_V	Valence band
$\emptyset_{si}$	Work function of the silicon substrate

List of Abbreviations and Acronyms

Acronym	Description
AFM	Atomic Force Microscopy
APTMS	3-Aminopropyltrimethoxysilane
APTS	3-Aminopropyltriethoxysilane
CVD	Chemical Vapour Deposition
CMOS	Complementary Metal-Oxide Semiconductor
DNA	Deoxyribonucleic Acid
dsDNA	Double Stranded Deoxyribonucleic Acid
EHP	Electron Hole Pair
FRET	Fluorescence Resonance Energy Transfer
GPTES	3-Glycidoxypropyltriethoxysilane
GPTMS/GOPS	3-Glycidoxypropyltrimethoxysilane
IC	Internal Conversion
ICPTES	Isocyanatopropyltriethoxysilane
IMAC	Immobilized Metal Affinity Chromatography
ISFET	Ion Sensitive Field Effect Transistor
LED	Light Emission Diode
LMIG	Liquid Metal Ion Gun
LoC	Lab-on-a-Chip
LPD	Liquid Phase Deposition
MOSFET	Metal Oxide Semiconductor Field Effect Transistor
PCR	Polymerase Chain Reaction
P-J	Perrin-Jablonski
qPCR	Quantitative Polymerase Chain Reaction
RE	Reference Electrode

Acronym	Description
RIE	Reactive Ion Etching
RF	Radio Frequency
RH	Relative Humidity
RT	Room Temperature
SAM	Self Assembled Monolayer
SFM	Scanning Force Microscopy
SG I	SYBR Green I
SG II	SYBR Green II
SPA	Solid Phase Amplification
SPM	Scanning Probe Microscopy
SP-PCR	Solid Phase - Polymerase Chain Reaction
ssDNA	Single Stranded Deoxyribonucleic Acid
TE	Tris-EDTA buffer
THF	Tetrahydrofuran
TMS-EDTA	N-(Trimethoxysilylpropyl)ethylenediamine Triacetic Acid
TOF-SIMS	Time-Of-Flight Secondary Ion Mass Spectrometry
VPD	Vapor Phase Deposition
VR	Vibrational Relaxation

List of Figures

List of Tables

Bibliography

[1] C. Adessi, G. Matton, G. Ayala, G. Turcatti, J. Mermod, P. Mayer, and E. Kawashima. Solid phase dna amplification: characterisation of primer attachment and amplification mechanisms. *Nucleic Acids Reasearch*, 28, 2000.

[2] S. Cao, P. Sun, G. Xiao, Q. Tang, X. Sun, H. Zhao, S. Zhao, H. Lu, and Z. Yue. Isfet-based sensors for (bio)chemical applications: A review. *Electrochemical Science Advances*, 2022.

[3] M. Cereda. Sviluppo e applicazioni diagnostiche di un sistema point-of-care basato su real-time pcr. Master's thesis, Università degli Studi di Milano-Bicocca, 2007.

[4] M. Cereda, A. Cocci, D. Cucchi, L. Raia, D. Pirola, L. Bruno, P. Ferrari, V. Pavanati, G. Calisti, F. Ferrara, A. Bramanti, and M. Bianchessi. Q3: A compact device for quick high precision qpcr. *Sensors*, 18, 2018.

[5] D. Chandler, L. Bryant, S. Griesemer, R. Gu, C. Knickerbocker, A. Kukhtin, J. Parker, C. Zimmerman, K. George, and C. Cooney. Integrated amplification microarrays for infectious disease diagnostics. *Microarrays*, 1:107–124, 2012.

[6] W. Chin, Y. Sun, J. Hogberg, T. Hung, A. Wolff, and D. Bang. Solid-phase pcr for rapid multiplex detection of salmonella spp. at the subspecies level, with amplification efficiency comparable to conventional pcr. *Anal Bioanal Chem*, 2017.

[7] D. Cole, S. Attavar, and L. Zhang. Surface analysis methods for contaminant identification. *Developments in Surface Contamination and Cleaning*, 1:333–394, 2016.

[8] V. Didenko. Dna probes using fluorescence resonance energy transfer (fret): Designs and applications. *Biotechniques*, 31:1106—-1121, 2001.

[9] A. Dragan, J. Pavlovic, J. McGivney, J. Casas-Finet, E. Bishop, R. Strouse, M. Schenerman, and C. Geddes. Sybr green i: Fluorescence properties and interaction with dna. *J Fluorescence*, 22:1189–1199, 2012.

[10] G. Festag, A. Steinbruck, A. Wolff, A. Csaki, R. Moller, and W. Fritzsche. Opti-

mization of gold nanoparticle-based dna detection for microarrays. *Journal of Fluorescence*, 15:161–170, 2005.

[11] G. Festag, A. Steinbruck, A. Wolff, A. Csaki, R. Moller, and W. Fritzsche. Dna grafting on silicon nanonets using an eco-friendly functionalization process based on epoxy silane. *Materials Today: Proceedings*, 6:333–339, 2019.

[12] G. Festag, A. Steinbruck, A. Wolff, A. Csaki, R. Moller, and W. Fritzsche. Optimization of gops-based functionalization process and impact of aptamer grafting on the si nanonet fet electrical properties as first steps towards thrombin electrical detection. *Nanomaterials*, 10, 2020.

[13] L. Garibyan and N. Avashia. Research techniques made simple: Polymerase chain reaction (pcr). *J Invest Dermatol.*, 2013.

[14] N. Gavara. A beginner's guide to atomic force microscopy probing for cell mechanics. *Microsc. Res. Tech.*, 80:75–84, 2017.

[15] S. Giglio, P. Monis, and C. Saint. Demonstration of preferential binding of sybr green i to specic dna fragments in real-time multiplex pcr. *Nucleic Acids Research*, 31, 2003.

[16] M. Green and J. Sambrook. Polymerase chain reaction. *Cold Spring Harbor Protocols*, 2019.

[17] H. Gudnason, M. Dufva, D. Bang, and A. Wolff. Comparison of multiple dna dyes for real-time pcr: effects of dye concentration and sequence composition on dna amplification and melting temperature. *Nucleic Acids Research*, 35, 2007.

[18] G. T. Hermanson. *Bioconjugate Techniques*. Elsevier Inc., 3 edition, 2013.

[19] M. Kahieshesfandiari and M. Sabri. Streptococcosis in oreochromis sp.: is feed-based biofilm vaccine of streptococcus agalactiae effective? *Aquaculture International*, 2019.

[20] C. Kokkula, N. Palanisamy, M. Ericstam, and J. Lennerstrand. Sybr green ii dye-based real-time assay for measuring inhibitor activity against hiv-1 reverse transcriptase. *Mol Biotechnol*, 2016.

[21] A. Krasnoslobodtsev and S. Smirnov. Effect of water on silanization of silica by trimethoxysilanes. *Langmuir*, 18:3181–3184, 2002.

[22] C. Lee, S. K. Kim, and M. Kim. Ion-sensitive field-effect transistor for biological sensing. *Sensors*, 9:7111–7131, 2009.

[23] M. Lessel, O. Bäumchen, M. Klos, H. Hähl, R. Fetzer, M. Paulus, R. Seemanna, and K. Jacobs. Self-assembled silane monolayers: an efficient step-by-step recipe for high-quality, low energy surfaces. *Surface and Interface Analysis*, 47:557—-564, 2015.

[24] X. Liu, K. Neoh, and E. Kang. Viologen-functionalized conductive surfaces: Physicochemical and electrochemical characteristics, and stability. *Langmuir*, 18:9041–9047, 2002.

[25] J. Mercier and G. Slater. Solid phase dna amplification: A brownian dynamics study of crowding effects. *Biophysical Journal*, 89:32–42, 2005.

[26] A. Methods. Pcr - the polymerase chain reaction. Technical report, The Royal Society of Chemistry, 2014.

[27] R. Moller, A. Csaki, J. Kohler, and W. Fritzsche. Dna probes on chip surfaces studied by scanning force microscopy using specific binding of colloidal gold. *Nucleic Acid Research*, 2000.

[28] K. Mullis. The unusual origin of the polymerase chain reaction. *Scientific American*, 1990.

[29] K. Mullis and F. Faloona. Specific synthesis of dna in vitro via a polymerase-catalyzed chain reaction. *Methods in Enzymology*, 155:335–350, 1987.

[30] K. Mullis, F. Faloona, S. Scharf, R. Saiki, G. Horn, and H. Erlich. Specific enzymatic amplification of dna in vitro: The polymerase chain reaction. *Cold Spring Harbor Symposia on Quantitative Biology*, 51:263–273, 1986.

[31] K. Nath, J. Sarosy, J. Hahn, and C. Di Como. Effects of ethidium bromide and sybr green i on different polymerase chain reaction systems. *J. Biochem. Biophys. Methods*, 42:15–19, 2000.

[32] R. Nowaczyński, P. Paszke, A. Csaki, J. Mazuryk, K. Rożniatowski, P. Piotrowski, and D. Pawlak. Functionalization of phosphate and tellurite glasses and spherical whispering gallery mode microresonators. *ACS Omega*, 8:48159–48165, 2023.

[33] S. Pal, M. Kim, and J. Song. Quantitation of surface coverage of oligonucleotides bound to chip surfaces: a fluorescence-based approach using alkaline phosphatase digestion. *The Royal Society of Chemistry*, 8:1332—-1341, 2008.

[34] S. Petralia, T. Cosentino, F. Sinatra, M. Favetta, P. Fiorenza, V. Bongiorno, S. Sciuto, E. anc Conoci, and S. Libertino. Silicon nitride surfaces as active substrate for electrical dna biosensors. *Sensors and Actuators B: Chemical*, 252:492—-502, 2017.

[35] K. Ririe, R. Rasmussen, and C. Wittwer. Product differentiation by analysis of dna melting curves during the polymerase chain reaction. *Analytical Biochemistry*, 254: 154–160, 1997.

[36] V. Saarnio, K. Salorinne, V. Ruokolainen, J. Nilsson, T. Tero, S. Oikarinen, L. Wilhelmsson, T. Lahtinen, and V. Marjomaki. Development of functionalized sybr green ii related cyanine dyes for viral rna detection. *Dyes and Pigments*, 2020.

[37] S. Santermans, F. Schanovsky, M. Gupta, G. Hellings, M. Heyns, W. Van Roy, and K. Martens. The significance of nonlinear screening and the ph interference mechanism in field-effect transistor molecular sensors. *ACS Sensors*, 6:1049–1056, 2021.

[38] D. K. Schwartz. Mechanims and kinetics of self-assembled monolayer formation. *Annu. Rev. Phys. Chem.*, 52:107—-37, 2001.

[39] E. Sciuto, V. Bongiorno, A. Scandurra, S. Petralia, T. Cosentino, S. Conoci, F. Sinatra, and S. Libertino. Functionalization of bulk sio2 surface with biomolecules for sensing applications: Structural and functional characterizations. *Chemosensors*, 2018.

[40] C. Seidel. Strongly stretched polyelectrolyte brushes. *Macromolecules*, 36:2536–2543, 2003.

[41] O. Sonmezoglu and K. Ozkay. A new organic dye-based staining for the detection of plant dna in agarose gels. *Nucleosides, Nucleotides & Nucleic Acids*, 2015.

[42] Y. Sun, R. Dhumpa, D. Bang, J. Hogberg, J. Handberg, and A. Wolff. A lab-on-a-chip device for rapid identification of avian influenza viral rna by solid-phase pcr. *Lab Chip*, 11:1457–1463, 2011.

[43] A. Wong and U. Krull. Surface characterization of 3-glycidoxypropyltrimethoxysilane films on silicon-based substrates. *Anal Bioanal Chem*, 383:187—200, 2005.

[44] L. Wu, C. Huang, B. Emery, A. Sedgwick, S. Bull, X. He, H. Tian, J. Yoon, J. Sessler, and T. James. Forster resonance energy transfer (fret)-based small-molecule sensors and imaging agents. *Chem Soc Rev*, 49:5110–5139, 2020.

[45] Q. Wu, W. Ma, R. Shi, B. Zhang, X. Mao, and W. Zheng. An activated gops-poly-l-lysine-coated glass surface for the immobilization of 60mer oligonucleotides. *Eng. Life Sci.*, 5:466–470, 2005.

[46] H. Zipper, H. Brunner, J. Bernhagen, and F. Vitzthum. Investigations on dna inter-

calation and surface binding by sybr green i, its structure determination and methodological implications. *Nucleic Acids Research*, 32, 2004.